Chemical Process Alternatives for Radioactive Waste

Principal Investigator:

Leonel E. Lagos, Ph.D., PMP®

Florida International University Collaborators:

Dwayne McDaniel, Ph.D., P.E. (Project Manager)
Anthony Abrahao, M.S.
Aparna Aravelli, Ph.D.
Amer Awwad, M.S., P.E.
Mayren Echeverria Boan, Ph.D.
Shervin Tashakori, Ph.D.
Mackenson Telusma, M.S.
DOE Fellows

FIU | **Applied Research Center**
FLORIDA INTERNATIONAL UNIVERSITY

Addendum:

This document represents one (1) of five (5) reports that comprise the Year End Reports for the period of September 29, 2019 to September 28, 2020 prepared by the Applied Research Center at Florida International University for the U.S. Department of Energy Office of Environmental Management (DOE-EM) under Cooperative Agreement No. DE-EM0000598. Incremental funding under this cooperative agreement resulted in FIU having to execute carryover scope, which was completed in November 2019. The technical information for the carryover scope from FIU Performance Year 9 has therefore also been included in these reports.

The complete set of FIU's Year End Reports for this reporting period includes the following documents:

Project 1: Chemical Process Alternatives for Radioactive Waste
    Document number: FIU-ARC-2019-800006470-04b-270

Project 2: Environmental Remediation Science and Technology
    Document number: FIU-ARC-2019-800006471-04b-267

Project 3: Waste and D&D Engineering and Technology Development
    Document number: FIU-ARC-2019-800006472-04b-256

Project 4: DOE-FIU Science & Technology Workforce Development Initiative
    Document number: FIU-ARC-2019-800006473-04b-306

Project 5: DOE-FIU Science & Technology Workforce Development Initiative for Office of Legacy Management
    Document number: FIU-ARC-2019-800012253-04b-003

Each document will be submitted to OSTI separately under the respective project title and document number as shown above. In addition, the documents are available at the DOE Research website for the Cooperative Agreement between the U.S. Department of Energy Office of Environmental Management and the Applied Research Center at Florida International University: https://doeresearch.fiu.edu

TABLE OF CONTENTS

LIST OF FIGURES

LIST OF TABLES

PROJECT 1 OVERVIEW

The Department of Energy's (DOE's) Office of Environmental Management (EM) has a mission to clean up the contaminated soils, groundwater, buildings and wastes generated over the past 60 years by the R&D and production of nuclear weapons. The nation's nuclear weapons complex generated complex radioactive and chemical wastes. This project is focused on tasks to support the safe and effective storage, retrieval and treatment of high-level waste (HLW) from tanks at Hanford and Savannah River sites. The objective of this project is to provide the sites with modeling, pilot-scale studies on simulated wastes, technology assessment and testing, and technology development to support critical issues related to HLW retrieval and processing. Florida International University (FIU) engineers work directly with site engineers to plan, execute and analyze results of applied research and development.

Although a number of tasks have been initiated and completed over the course of the cooperative agreement, at the end of this past year, there were 3 active tasks. These tasks are listed below and this report contains a detailed summary of the work accomplished for FIU's Performance Year 10.

Task 17: Advanced Topics for HLW Mixing and Processes

The objective of this task is to develop a test loop that can bridge technical gaps associated with the flushing of HLW within the transfer and processing lines at Hanford and Savannah River. This loop will aid in implementing optimal flush operations with minimized water usage and the possibility of water hammer and plug formations. These practices will aim to develop a correlation for flush parameters based on characteristics of the system at the start of flushing. The data and correlations will be useful for improving existing guidelines. Characterization of post-flush pipeline cleanliness is an additional objective of the task, which will be implemented using various elements of the loop. With discussions between FIU and engineers from Hanford and SRNL, these evaluations will help to establish criterion for flushing operations.

Task 18: Technology Development and Instrumentation Evaluation

The objective of this task is to develop inspection tools that will assist engineers in evaluating the structural integrity of the primary and secondary tank floors in the double shell tanks (DSTs) at the Hanford Site. This effort has led to the development of multiple inspection tools that are able to provide live visual feedback. These include a magnetic wheeled miniature motorized rover that can travel through the refractory cooling channels under the primary tank and a pneumatic pipe crawler that can inspect tank ventilation pipes and its central plenum. In addition, FIU is developing a marsupial robotic system that can navigate through the drain lines and inspect the secondary liner via the drain slots.

An additional objective is to investigate coatings or fixatives that can be used to mitigate and prevent further degradation of concrete walls exposed to adverse environments in the HCAEX tunnel. Efforts will focus on defining important aspects regarding the concrete specimens such as configuration (cylindrical, square, etc.), dimensions (length, thickness), exposure mode to the aggressive environment (e.g. full immersion), etc. The effort will also cover the design and development of new test setups, the experimental design (potential variables definition, number of samples), concrete samples preparation, as well as the selection of measurements to evaluate the performance of the concrete. Initial bench-scale testing will be performed including the

aforementioned considerations. An additional aspect of this task is to investigate the development of a platform that can navigate on the walls of the tunnel and potentially apply a coating that can assist in preventing further degradation. A review was conducted of adhesion mechanisms and a platform is being developed to assist in validating the design concepts.

Task 19: Pipeline Corrosion and Erosion Evaluation

The objective of this task is to provide the sites with a means to evaluate the structural integrity of waste transfer pipeline components. This has involved the evaluation of potential sensors and the viability of utilizing them to provide real time data for long durations of time. The sensors can be installed and provide thickness measurements of pipeline components and fittings found in jumper pits, evaporators, and valve boxes.

The objective of this task is also to provide the Hanford Site with data obtained from experimental testing of the hose-in-hose transfer lines, Teflon® gaskets, EPDM O-rings, and other nonmetallic components used in their tank farm waste transfer system under simultaneous stressor exposures. The experiments will be limited to various combinations of simultaneous stressor exposure to caustic solutions, high temperatures and high pressure. Evaluation of baseline materials will be conducted for comparison to materials that have been conditioned with the various simultaneous stressors.

MAJOR TECHNICAL ACCOMPLISHMENTS

Task 17: Advanced Topics for HLW Mixing and Processes

- Testing was completed for 10, 15 and 20% Kaolin/water slurries for both fully-flooded and gravity drained conditions. Results indicate that a maximum volume of 1.5 of the line volume is needed to completely flush the line.
- Additional efforts focused on optimizing processes for the flushing testbed. This includes adding a water level sensor for automating the volume of water used in the flushing operation, evaluating different approaches to quantify sediment height in the pipe using UT sensors and improving the process of recapturing used Kaolin.

Task 18: Technology Development and Instrumentation Evaluation

- A marsupial crawler system is being developed for the inspection of the secondary liner of DSTs at Hanford. The crawler has been optimized after testing in a 6-inch bench scale mockup. A rover is also being finalized that can traverse on the bottom of the tank or on with the drain slot underneath the secondary liner. The rover will be deployed from the 6-inch crawler when the system traverses through the drain line and reaches the foundation drain slots.
- A final prototype was completed for the miniature rover and a test plan was developed for the evaluation of the rover in the FIU mockup at elevated temperatures. The test plan was successfully completed and a live demonstration conducted for DOE-EM, national laboratories and contractors.
- A similar miniature rover has been developed that improves the functionality of the previous system by incorporating a UT sensor for measuring tank floor thickness at various locations from within the refractory slots of DSTs at Hanford.
- A small inspection rover has been designed and developed that has potential to navigate through the refractory slots of Tank AY-101 at Hanford. The unit can incorporate a camera for video feedback and make 90-degree turns in the concentric refractory slots of AY-101.
- Aging of concrete specimens with similar materials to the H-Canyon tunnel walls were created. These specimens are being aged in acidic conditions with and without erosion. Approximately a ¼ inch of exposed aggregate has been generated from the aging, which is similar to the conditions seen in the tunnel. The aging process will be used to evaluate potential coatings.
- Dr. Mayren Echeverria Boan was awarded ASME Best Poster/Paper Award at the WM2020 Conference, for Paper # 20301 "Aging of Concrete for the Evaluation of Repair Materials to Protect the Walls of the HCAEX Tunnel at Savannah River".
- A literature review of potential adhesion mechanisms has been conducted that can be used to develop a platform that could potentially deploy protective coatings to the H-Canyon tunnel walls. An initial prototype has been developed that utilizes a ducted fan to adhere to aged concrete and demonstrates the potential of the concept.

Task 19: Pipeline Corrosion and Erosion Evaluation

- A customized radiation test method has been developed for low and medium level radiation exposure of the Permasense UT sensors. The test plan has been approved by WRPS and is ready to be implemented.
- Testing with SRNL mass loss coupons demonstrated the potential for use in the DOE's waste transfer system. The coupons are capable of detecting very small changes in pipes due to erosion or corrosion.
- Fiber optics sensors from Cleveland Electric Limited (CEL) have been successfully tested for leak and fault detection in pipe systems. They can be deployed at various waste transfer systems for signature event detection and localization.
- An aging loop with 3 concentrations (6.25, 12.5 and 25%) of NAOH solution was designed and developed. The loop is designed to age hose-in-hose transfer line coupons as well as EPDM specimens.
- Began initial aging of the transfer line and material coupons. A number of issues arose during the initial period that required the repair of a number of pumps and sensors due to the caustic solution.

TASK 17: ADVANCED TOPICS FOR HLW MIXING AND PROCESSES

Task 17: Executive Summary

In U.S. Department of Energy (US DOE) complexes, pipelines that carry high-level radioactive waste must be properly flushed to prevent stationary or moving beds of solid sediment and address lines that are prone to hydrogen gas buildup. Currently, there exist guidelines that establish a minimum flush volume and velocity of water that is used for post-transfer flushing operations to achieve a satisfactory cleaning of pipelines. However, the Defense Nuclear Facilities Safety Board (DNFSB/TECH-40, 2016) has indicated a necessity for vigorous investigations on the technical basis for prescribing flush velocity and flush volumes in pipelines. Consequently, further studies are being investigated that will significantly assist the US DOE in waste remediation by optimizing the operational conditions that will assist in minimizing the flush volume and consequent downstream waste, which will in turn assist these DOE waste remediation sites by preserving tank storage, preventing additional waste processing, and minimizing dilutions and changes to waste chemistry.

To investigate, a 165-foot, 3-inch carbon steel experimental pipe loop was developed and constructed at Florida International University (FIU) to study non-Newtonian slurry flushing. This test bed was designed to create sediment beds of various materials and bed heights and investigate parameters that affect the efficiency of flushing operations. The objective is to find flush velocity values/modes via repeatable sediment beds inside the pipeline in both fully flooded (no pre-flush drainage) and gravity-drained (pre-flush drained) systems in various pumping modes (rotational ramp and oscillatory sweep) which lead to satisfactory cleaning of transport lines with a minimum amount of water usage.

This article presents efforts associated with flushing of kaolin-water mixtures at different concentrations and with various flush volume and flush velocity values/modes. Testing of various kaolin-water slurry simulant concentrations in fully-flooded and gravity-drained conditions. Efforts also focused on improvements to the present flushing system by introducing new equipment that automates the process of determining flush-line volume, simulant recapturing and reuse, and ultrasonic investigations to determine sedimentation of height in fully flooded and gravity-drained conditions.

Subtask 17.2: Evaluation of Pipeline Flushing Requirements for HLW at Hanford and Savannah River

Subtask 17.2: Introduction

Recently, the Defense Nuclear Facilities Safety Board (DNFSB/TECH-40, 2016) has indicated needs for vigorous investigations on the technical basis for prescribing flush velocity in pipelines. For optimal performance at the Department of Energy sites, pipelines that transfer radioactive waste must be operated above the critical velocity of fluid flow to prevent sedimentation of the sludge, which form stationary or moving beds of solids within the pipeline. These formations result in partial line plugging, leading to excessive pumping loads and erosion, or even full line plugging, which could result in a rupture at the pump or pipeline. The pretreatment facility design strategy

requires that each slurry transfer in the process lines be followed by a flush with water to minimize the chances of a partial or full line plug.

Previous reports related to pipeline flushing of several simulants (WTP-RPT-175 Rev. 0 and WTP-RPT-178 Rev. 0) were noted. Our study revealed that, in several tests, the minimum required flush volumes were more than minimum required values provided by the design guidelines in 24590-WTP-GPG-M-0058, Rev. 0 (Hall 2006). In addition, flush velocities in the pipeline exceeded the maximum velocity stated in the flushing guidelines (RPP-RPT-59600, Rev. 0). Assessment of flushing effectiveness (post-flush pipeline cleanness) were also not reported.

This research effort is intended to determine effective flushing operations using a minimal amount of water usage and provide additional guidelines in support of recently developed flushing standards (TFC-ENG-STD-26). Successful execution requires creation and characterization of sediment beds, flushing in different modes, and evaluation of operation effectiveness through measurement of post-flush pipeline residues. To extend previous flushing studies, our strategy will be creating different case studies targeting different materials and pipe lengths. In addition, existing ultrasonic and visualization methods inspired by the work conducted at PNNL (PNNL-20350 FINAL and PNNL-19441 Rev. 0) will be used in the collection and assessment of data. In each round of testing, focus will be on influential parameters set for one simulant in a fixed pipe length. These parameters are flush velocity mode (continuous one-step and pulsing) and initial conditions.

Subtask 17.2: Objectives

The objective of this effort is to provide a technical basis for flush volume used in the waste transfer process. This includes:

- Implementing optimal flush operations that minimizes waste production, pipeline erosion, and ensures satisfactory cleaning of pipelines based on an established criterion for thorough discussions between FIU and personnel at the waste sites and national laboratories.

- Developing a correlation for flush parameters based on characteristics of the system at the start of flushing (initial conditions). Data and correlations will be useful for determination of pumping requirements improving existing guidelines.

Subtask 17.2: Methodology

Test Loop

To conduct these investigations, a 165-foot (50.3m) test loop made of 3-inch schedule 40 carbon steel pipes and fittings was completed (Figure 1 and Figure 2) in the previous period of performance year. This experimental loop can perform various functions such as slurry circulation, pump cleaning, flushing, sediment and water retrieval, filtration, and post-flush circulation. The pipeline was sloped at the rate of 0.15% (3-inch height difference 100 feet of pipe length) to emulate conditions at Hanford site and facilitate gravity draining.
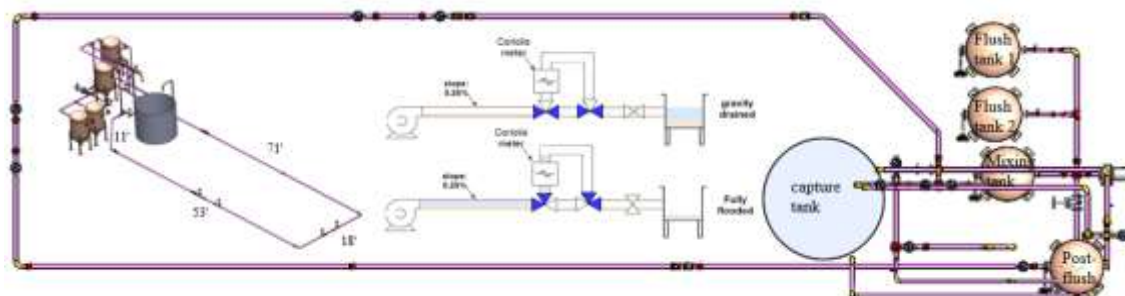
Figure 1. Schematic of a pipeline for flushing experiments.

Figure 2. Pipeline constructed for flushing experiments.

To circulate, flush, and conduct post-flush analyses, a 15 HP slurry pump (AMT 427B-95) capable of delivering 0.87 m^3/s (230 GPM) of water at 2.74 atm (40.3 psi or 93 feet of head), was used. The pump was controlled through a HopeWind variable frequency drive (VFD) to reduce ramp-up and ramp-down times to 0.5 seconds, which is the time to reach 1,750 RPM and vice-versa. Various safety features such as relief valves and burst disks protect the loop from situations where over-pressurization may occur such as when plugs form or there is pumping against a closed valve. The loop is also equipped with three clear sections in the beginning, middle, and end locations for visualization purposes. These sections assist with characterization of initial conditions and monitoring of bed variations during flushing operations. Kaolin-water simulants using EPK kaolin of 2.65 specific gravity are prepared inside a mixing tank that is equipped with a ½ HP Dayton 32V136 mixer and 6-inch propeller. To achieve the required concentrations, kaolin or water was adjusted accordingly using data obtained from a Krohne Optimass 1000 Coriolis meter in the loop. During flushing operations, the density and mass flow rate of the fluid is measured from the Coriolis meter.

Tests were performed using two flushing methods: a fully-flooded condition and a gravity-drained condition. In the fully-flooded condition, the test loop was flooded with a simulant of a specified concentration and left to settle for some time after stopping the slurry pump and without changing any configurations or system environment. After the amount of time had passed, water from a set of two flush tanks was flushed through the system using the 15HP pump and into a 500-gallon collection tank. In the gravity-drained condition, similar to the fully-flooded condition, the test loop was flooded with a simulant of specified concentration and left to settle for some time. After the amount of time has passed, a drain valve was opened to remove the water from the settled

kaolin, leaving behind a layer of sediment exposed to air within the pipeline. Water was then flushed through the system back into the collection tank.

After each test, there was a dilute mixture of kaolin-water simulant inside of the collection tank. Due to the flushing, the simulants were no longer the same solids concentration as they were pre-flush. To alleviate this issue, the dilute mixture was left to settle for some days. After settling, the water was pumped out of the collection tank via a Tsurumi HSD2.55 ¾ HP submersible pump (sump), leaving behind a layer of kaolin sludge. The submersible pump was then used to pump the sludge to the mixing tank, and the process could then be repeated.

Improvements to the Test Loop

The first improvement to the existing loop was the addition of a level sensor capable of automating the process to determine the flush-line volume by measuring the height of the water within the water flush tanks. A water level sensor was down selected from the three options considered. Of three potential sensors, the radar sensor was selected as a suitable level sensor for continuous measurement of the flushing tank. The sensor will allow automated shut-off of the pump after a designated volume has been achieved. VEGAPULS 11 is a radar sensor for non-contact, continuous level measurement and is suitable for both liquids and solids. The instrument emits a continuous, frequency-modulated radar signal through its antenna. The emitted signal is reflected by the medium and received by the antenna as an echo with modified frequency. The frequency change is proportional to the distance and is converted into the level. This sensor was procured, and initial testing was conducted which produced accurate reading of the water level.

Figure 3. Water level measurement sensor attached to the tank.

To evaluate the performance of the VEGAPULS11, the radar sensor was attached to the top of the main water flush tank during both fully flooded and gravity-drained flush operations. Before commencing the operations, the initial height was captured manually. During the operation, the VEGAPULS11's 4-20 mA output was captured by both the Bluetooth function on the VEGA mobile app and the data acquisition device (DAQ). As the operation was completed, the final level was captured. Then, linear interpolation graphs were created to convert the 4-20mA output to a fluid level output. On the gravity-drain condition, the fluid level was also measured. During this process, a random intermediate value was selected to determine how accurately the level sensor matches to this value. The result is a total of three curves: one curve with the intermediate value,

one without the intermediate value, and one with just the intermediate value. The result was an accurate reading that proved to be reliable to determine flush-line volume.
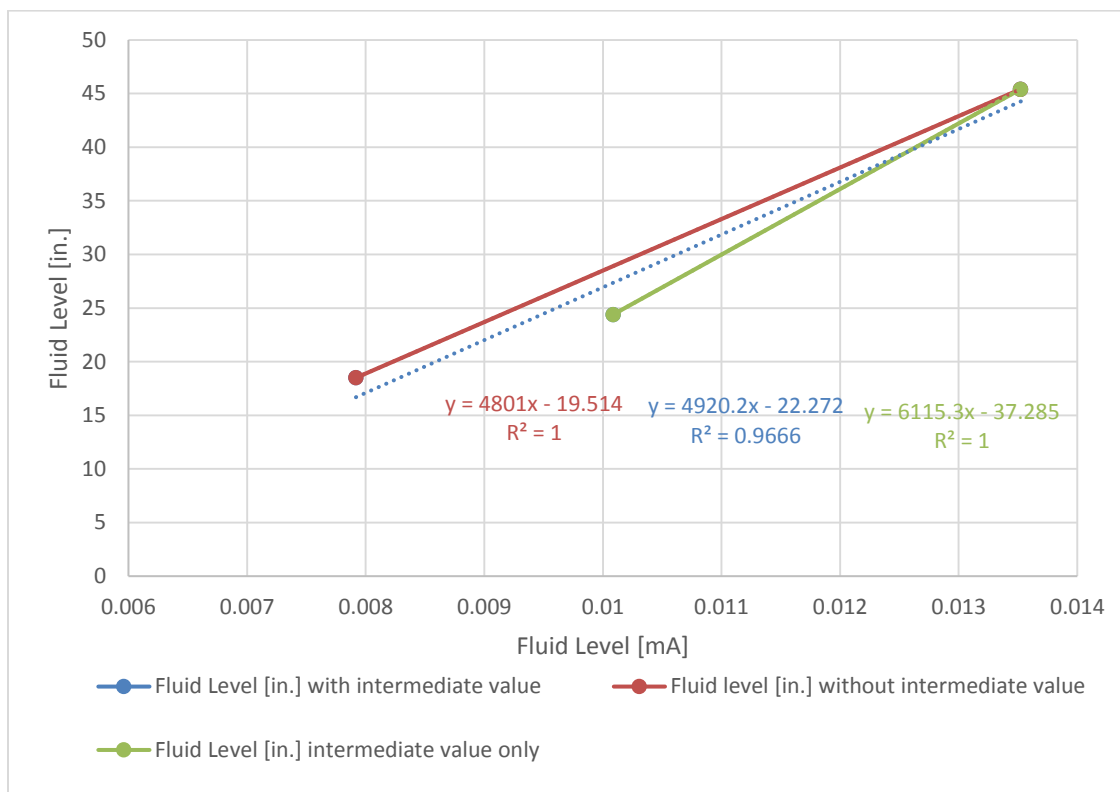
Figure 4. Water level measurement calibration curves to convert mA output to fluid level in inches. Equations shown are the linear trend equations and statistical relevancy (R2).

In addition, efforts were also focused on investigating the recycling of the kaolin after flushing evaluations. This is critical because, in its current state, the loop utilizes around 600 pounds (12 50-pound bags) for each run at 15 vol % of simulant concentration. In every flush, the settled solids are flushed to a 500-gallon tank. When left in the tank, the simulant settles, leaving behind a separated layer of kaolin solids and water. While the water can then be removed from the tank, the settled kaolin layer left behind is difficult to remove. Previous efforts of removing the settlement have been through methods of agitation by stirring the kaolin and water using a rod. However, this method has shown to be inefficient, as it still leaves a fair amount of sediment at the bottom of the tank for kaolin that has been settling over long periods of time.

Another approach utilizes a 0.75 HP Tsurumi HSD2.55 submersible pump (sump) capable of 58 gallons per minute and a maximum head of 43 feet. The pump is used to transport recaptured slurry into the mixing tank, allowing mixtures to settle out, between flushing operations. One notable issue with utilizing this solution is that while it can transport a mixture with solids that are suspended with ease, once there is long-term settling, the sludge layer that forms at the bottom of the tank becomes difficult to remove, even with the agitation apparatus attached to the base of the sump. As a result, other methods were investigated, such as agitation nozzles that pump the slurry and water in a small vertical segment of pipeline to ensure that the contents of the tank stay mixed, or using a propeller mixer and motor that stirs the contents.

The Dayton 3BB75 Submersible Pump is a cast-iron ¾ HP sump capable of 113 GPM that will be added to the waste tank as a second submersible pump dedicated to agitation of the sludge layer. The pump will agitate the sludge layer in two ways: when the sediment is vacuumed into the pump, the cast-iron impeller will act as a shredder, breaking apart any large sediment into finer particles. When the sediment is discharged, it will then be reduced to a set of two nozzles that act as an oscillating jet to agitate the sediment that surrounds the submersible pump.

Lastly, ultrasonic investigations using a UT sensor and Tektronix Oscilloscope MSO44 were done to determine the bed height of the sediment within the pipe. Figure 5 shows the experimental setup for a fully flooded system with the oscilloscope waveforms. The data was captured by placing the sensor at the top of the pipe (empty condition) as shown in Figure 6. The first echo appeared at 18 microseconds, which indicates the time of travel through the pipe wall thickness. The experiment was then repeated for the pipe filled with water and sediment at the bottom. As can be seen in Figure 6, new peaks appeared at about 115 microseconds indicating the signal travel through the liquid followed by the sediment. The changes in the thickness of the sediment can be estimated by using the velocity of the wave travel through the different media.

Figure 5. (Left) Tektronix MSO44 Mixed-Signal Oscilloscope (Right) Experimental Setup of settled kaolin in a mock 3-inch PVC pipe for fully-flooded conditions.
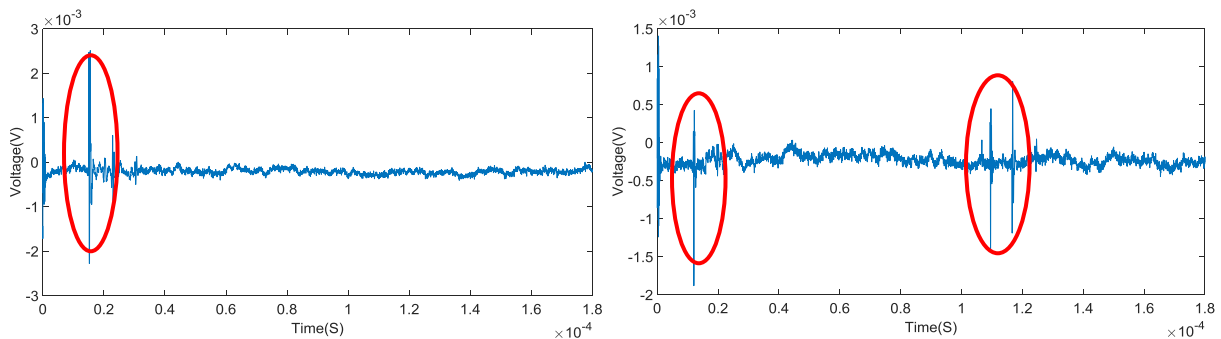
Figure 6. Oscilloscope waveforms that show (left) echoes in an empty PVC pipe and (right) fully flooded pipe with sediment.

In addition, a 5 MHz dual element transducer and 2.26 MHz single element transducer were utilized for determination of the sediment bed height in a gravity-drained system. The data was captured from the bottom of an empty pipe using the 5 MHz dual element transducer and the thickness of the pipe wall was detected as 21.03 mm. The experiment was then repeated by adding

sediment to the system. Results of the thickness changes obtained using the sensor probe and an oscilloscope are shown in Figure 1-3. It is evident that the sensor system is successful in detecting minute changes in thickness due to the sediment bed height. The same process was repeated for the 2.25 MHz single element transducer. The lower frequency transducer was also able to detect the change in the thickness, but inaccuracy in the thickness values is evident from the results. This could be due to calibration issues in the low frequency transducer.

Figure 7. Experimental setup of settled kaolin in a mock PVC pipe cut in half to simulate gravity-drained conditions.
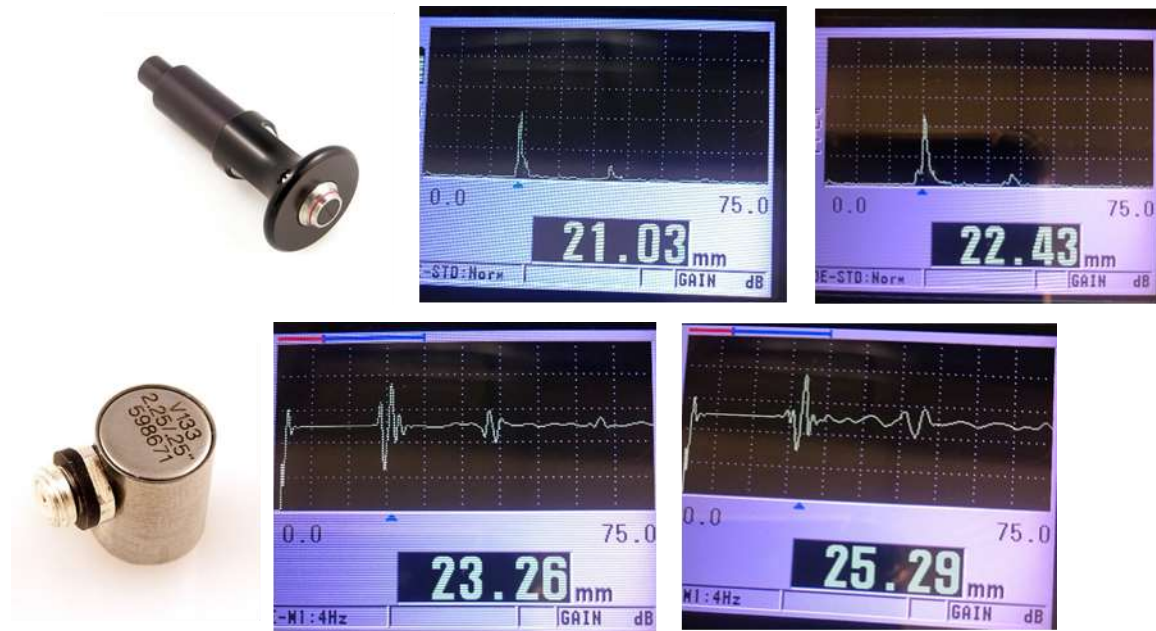
Figure 8. (Top) Oscilloscope waveform using a 5 MHz dual element transducer (bottom) and using a 2.25 MHz single element transducer.

Subtask 17.2: Results and Discussion

EPK Kaolin with a 2.65 SG was used in tests with both the gravity drained and fully flooded conditions. For the fully flooded condition, kaolin was circulated through the system and left to settle for one day. Flushing tests were done with system loads of 10, 15, and 20 vol.% of kaolin-water mixture. In the gravity drain condition, 15 vol.% and 20 vol.% kaolin was circulated through the system and left for a period of time (one week for the 15 vol.% and one day for the 20 vol.%), and the water within the line was drained before each gravity drained test. In the flush operations, the slurry pump was ceased when it was determined that the system was fully-cleaned systems

(when the Coriolis meter's density reading is the density of water). Flow quantities such as mass flow rate and density were also recorded using a FieldPoint 2010 data acquisition module and a PRO-FLO200 totalizer.

Figures 9 and 10 show data from the Coriolis meter during flushing of both the fully-flooded and gravity-drained pipes. It can be seen during the flow, for the fully flooded condition, density begins at a value of 990 kg/m³. Data sets that show this value elevated above 990 kg/m³ is likely due to suspended solids. For the gravity drained conditions, it can be seen that this value begins at approximately 1 kg/m³ (the density of air), as the contents within the vertical section of the loop (where the Coriolis meter is located) was drained prior to flushing. At the moment the slurry pump is activated, a sudden rise of fluid flow can be noticed as water flushes through the system; in the fully flooded case, an increase in density to the approximate expected density for the solid concentration as the slurry is agitated by the flush operation. This can also be similarly stated for the gravity drain condition, with the notable exception that density rises to the expected density value from near-zero. As the slurry is flushed, it can be seen that the fluid eventually plateaus to the density of water, indicating a fully cleaned pipe loop. At this moment, the slurry pump is stopped.
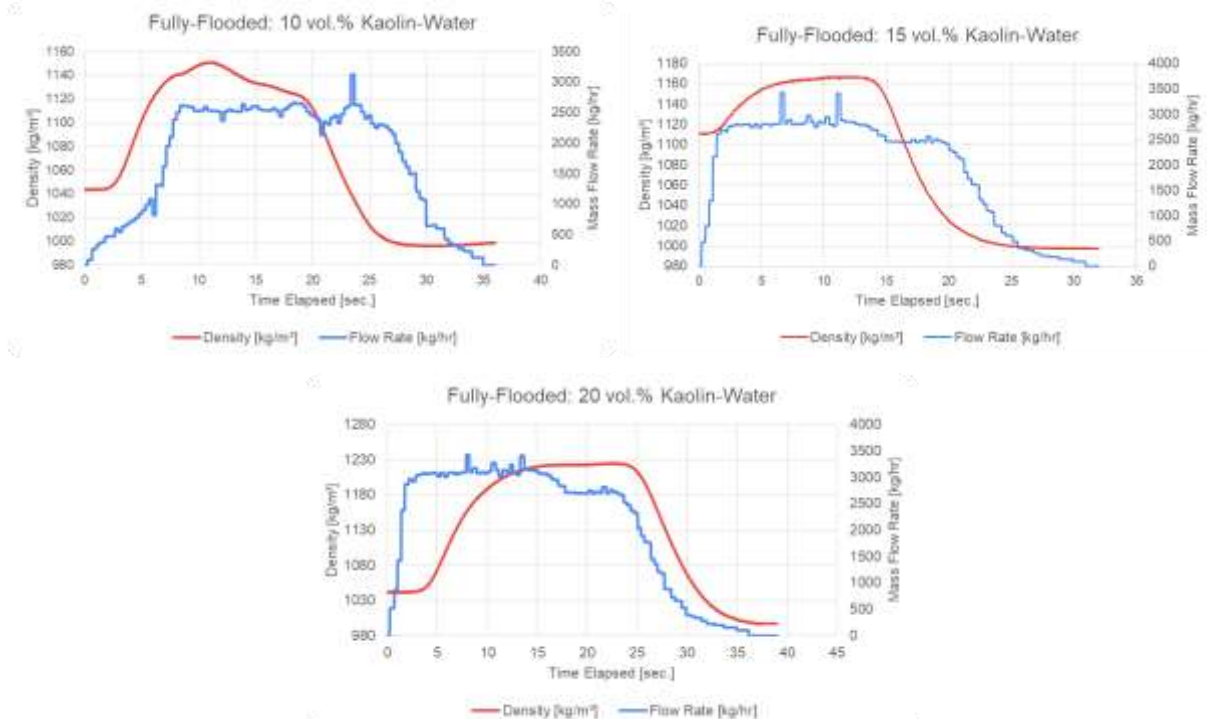
Figure 9. Density-Mass Flow Plots for 10 vol.%, 15 vol.%, and 20 vol.% kaolin-water simulants in the fully-flooded test condition.
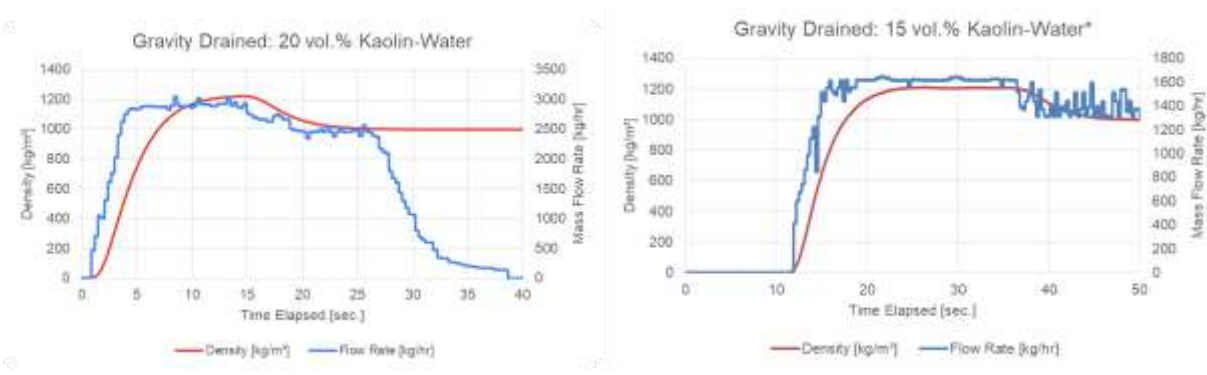
Figure 10. Density-Mass Flow Plots for 15 vol.% and 20 vol.% kaolin-water simulants in the Gravity-Drained test condition.

For the fully flooded conditions, flush-to-line volume (FTLV) was calculated manually since intermediate fluid level data was not available at the time of testing. However, for the gravity drain condition at 15 vol %, the density-mass flow plot was compared to fluid level data obtained by the level sensor during the flush operation to determine the FTLV. As can be seen, the mixture plateaus at ~0.3 FTLV until 0.75 FTLV, where the fluid density gradually decreases to water, indicating that the sediment has been fully flushed. This occurs at approximately 1 FTLV. Exact values can be determined based on specific values for the acceptable density level defined by site engineers.
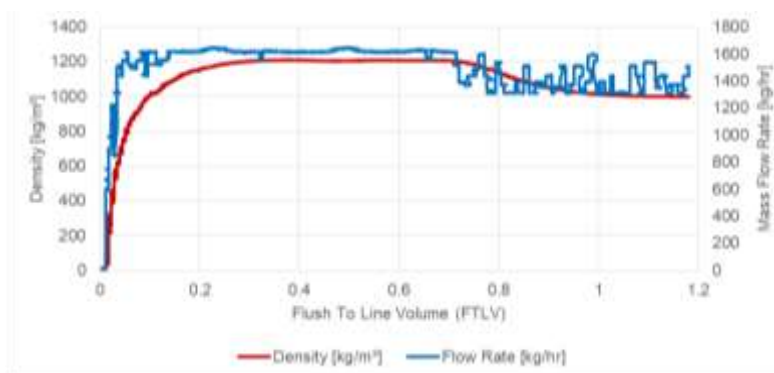
Figure 11. Density and Mass Flow Rate against FTLV of pipeline for 15 vol.% kaolin-water in the gravity-drained test condition.

Subtask 17.2: Conclusions

Results were presented that demonstrate flushing of 10 vol.%, 15 vol.%, and 20 vol.% concentrations of kaolin-water slurry sediments within a 3-inch, 165-foot carbon steel pipe loop in the fully-flooded and gravity-drained evaluation modes. Results demonstrated that flushing in these concentrations is plausible within a target flush-line volume of 1.0 – 1.5 FTLV. This plausibility was determined by plotting the density and mass flow rate against time and seeing the density behavior as it was flushed. Then, using data from the level sensor, flush-line volume was determined.

Efforts demonstrating improvements to the pipeline were also presented. These improvements assist in automation of determining the flush-line volume for flushing via the addition of a level sensor that is atop of one of the two water flush tanks; increased efficiency for simulant recapture

and reuse by implementing a set of submersible pumps dedicated to slurry agitation at the base of the collection tank; and bench-scale analyses using ultrasonic technologies to characterize sedimentation height within the pipe bed.

Subtask 17.2: References

J. R. Bontha, H. E. Adkins, K. M. Denslow, J. J. Jenks, C. A. Burns, P. P. Schonewill, G. P. Morgen, M. S. Greenwood, J. Blanchard, T. J. Peters, P. J. MacFarlan, E. B. Baer, W. A. Wilcox, "Test Loop Demonstration and Evaluation of Slurry Transfer Line Critical Velocity Measurement Instruments", PNNL-19441 Rev. 0 (2010)

K.M. Denslow, J. J. Jenks, J. R. Bontha, H. E. Adkins, C. A. Burns, P. P. Schonewill, N. N. Bauman, D. F. Hopkins, "Hanford Tank Farms Waste Certification Flow Loop Phase IV: PulseEcho Sensor Evaluation", PNNL-20350 FINAL (2011)

M. N. Hall, "Minimum Flow Velocity for Slurry Lines", 24590-WTP-GPG-M-0058, Rev 0 (2006)

E. K. Hansen, "WTP Pretreatment Facility Potential Design Deficiencies - Sliding Bed and Sliding Bed Erosion Assessment", SRNL-STI-2015-00014, Revision 0 (2015)

R. Kazban, A., "Plugging and Wear of Process Piping at The Waste Treatment and Immobilization Plant", DNFSB/TECH-40 (2016)

K. Lee, "Ultrasonic Technique for Measuring the Thickness of Scale on the Inner Surfaces of Pipes", Journal of the Korean Physical Society, Vol. 56, No. 2, p. 558-561 (2010)

V. C. Nguyen, M. S. Fountain, C. W. Enderlin, A. J. L. Fuher, L. F. Pease, "One System River Protection Project Integrated Flowsheet-Slurry Waste Transfer Line Flushing Study", RPP-RPT-59600, Rev.0 (2016)

A. P. Poloski, M. L. Bonebrake, A. M. Casella, M. D. Johnson, P. J. MacFarlan, J. J. Toth, H. E. Adkins, J. Chun, K. M. Denslow, M. L. Luna, J. M. Tingey, "Deposition Velocities of Newtonian and Non-Newtonian Slurries in Pipelines", PNNL-17639, WTP-RPT-175 Rev. 0, (2009)

S. T. Yokuda, A. P. Poloski, H. E. Adkins, A. M. Casella, R. E. Hohimer, N. K. Karri, M. Luna, M. J. Minette, J. M. Tingey, "A Qualitative Investigation of Deposition Velocities of a Non-Newtonian Slurry in Complex Pipeline Geometries", PNNL-17973, WTP-RPT-178 Rev. 0, (2009)

TASK 18: TECHNOLOGY DEVELOPMENT AND INSTRUMENTATION EVALUATION

Task 18: Executive Summary

Integrity issues in the double-shell tanks (DST) at Hanford have motivated the need for developing innovative tools that can provide information regarding the health of the tanks. These issues include the primary linear failure of AY-102 and recent concerns of thinning in the DST secondary liners. Other concerns include erosion or corrosion on transfer lines and processing pipes. In recent years, FIU has supported DOE-EM by developing tools that can assist in understanding the health of tanks and the waste transport system at Hanford.

FIU has developed a miniature rover that can be deployed through small risers and gain access to refractory slots in the Hanford DSTs. The rover traverses through the slots on the primary liner, via magnets to avoid debris in the slots. The redesigned rover uses bevel gears in order to create right angle motors which allows for side-by-side motorized wheels that give the unit enough clearance height in its middle so that it can traverse over weld seams on the liner. Using bevel gears to make right angle motors make is possible to utilize micro motors with higher stall torques (140 oz.in). In addition, the design of the control box of the rover was finalized and assembled. The new control system makes it possible to utilize stronger DC motors and allows for the use of a longer tether cable.

Prior to deploying the mini rover at Hanford, FIU worked with engineers at Washington River Protection Solution (WRPS) to develop a test plan that introduces the rover to harsh and strenuous environments in FIU's DST mockup. The test plan is comprised of four tests that include a durability test, emergency retrieval test, weld seam test, and corrosion test. Each test is designed to challenge the rover in conditions that could be encountered onsite during the actual deployment.

A UT sensor rover has also been developed based on the design of the miniature rover. This unit incorporates an ultrasonic sensor that can obtain thickness measurements using a dual element ultrasonic sensor. Prior to taking the thickness measurement, the surface can be cleaned with a motorized brush that has been added to the system.

FIU has also developed a rover that could potentially navigate in the refractory slots of AY-101. This rover can traverse through multiple 90° turns that are found in slots of AY-101. The current system includes a single rigid body that is 1/3rd the size of the current miniature rover, which allows the tool to make the hard turns. Testing has shown that the system's pull force allows the unit to navigate through multiple 90° turns and straight sections. Future work will include adding a camera and making modifications to increase its pull force strength.

To address the secondary liner issue of the DSTs, FIU has continued to develop a marsupial robotic system. It includes a 6-inch peristaltic pipe crawler that operates similar to the previous pipe crawlers developed at FIU that houses a small rover. The objective for this system is to navigate through the 6-inch drain lines, and deploy the rover at the entrance of the drain slots. The rover is designed with a scissor lift chassis that allows it to navigate on the tank floor or in the slots. A deployment module has also been developed to house the rover until the crawler reaches the tank foundation from the drain line. The module sits at the front of the crawler and provides the means for the rover to enter into the drain slots.

In addition, FIU is supporting the Savannah River Site (SRS) facility by investigating technologies to evaluate the H-Canyon exhaust tunnel for degradation and potentially assist in avoiding further degradation. Robotic inspections of the tunnel revealed significant degradation of the reinforced concrete structure that was primarily associated with acid attack, and could compromise the structural stability of the tunnel. Thus, the identification and evaluation of potential coatings that could be applied on the degraded walls to mitigate and prevent further degradation is of significant interest to the Department of Energy and the Savannah River representatives. The investigation has been divided into different phases: 1) Development and evaluation of aged concrete under accelerated aging conditions (preliminary results included in this report) and, 2) Evaluation of potential coatings applied on aged and non-aged concrete under accelerated aging conditions. In order to develop and evaluate concrete samples exposed to accelerated aging conditions, efforts were focused on defining important aspects regarding the concrete specimens, such as configuration, dimensions, exposure mode to the aggressive environment, the design and development of new test setups, the experimental design (potential variables definition, number of samples), concrete samples preparation, as well as the selection of measurements to evaluate the performance of the aged and non-aged developed concrete surfaces. In addition, based on findings and lessons learned during the initial testing (previous yearly period), a test plan was developed, discussed and finally approved by the Savannah River collaborators, including the research scope, the experimental design, data collection approaches (measurements), etc. The execution of the test plan was initiated, and preliminary results are presented in this report, including major findings of the preliminary results. The enhanced aging tests were demonstrated to be an adequate and feasible method to perform accelerated aging of concrete, providing valuable insights regarding the aging process. The combined action of the 0.5M acid solution and erosion, proved to be the most aggressive environment leading to the fastest and most intense degradation of the concrete specimens. The developed aged concrete surfaces will support the evaluation of potential coatings in a further stage of the investigation.

FIU is also investigating the development of a platform to deploy the potential coatings. A wall crawler system is being developed to climb the walls of the canyon tunnel and will house a mechanism to apply the protective coating. Different adhesion mechanisms have been evaluated and a ducted fan has been selected to provide the adhesion force necessary to adhere to the jagged walls of the tunnel. A prototype has been developed and has proven to be capable of navigating up the walls as well as on the ceiling. A spray mechanism is also being developed that could potentially be used to apply the coatings that are being considered.

Subtask 18.2: Development of Inspection Tools for DST Primary Tanks

Subtask 18.2: Introduction

In August of 2012, traces of waste were found in the annulus of the AY-102 double-shell tank storing radioactive waste at the Hanford Site, prompting the need for developing inspection tools that can help assess the structural integrity of the DST primary liner. In addition, evaluations of the DST secondary liners within the tank annulus have also shown thinning of the secondary liner. This has prompted the development of an inspection tool for the secondary liner as well.

Figure 12 shows three possible entry points for inspection in a typical DST (AY-102):

1. refractory air slots through the annulus,
2. leak detection piping, and

3. Ventilation header piping.
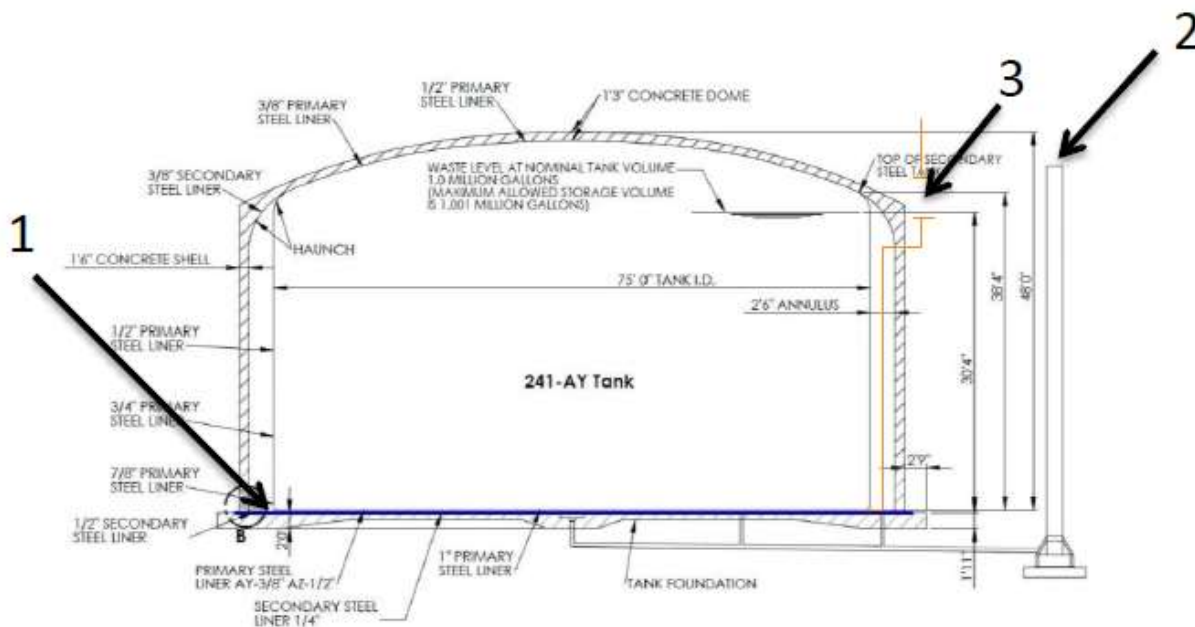
Figure 12. Inspection entry points of the AY-102 double-shell tank.

The inspection tools that are currently being developed and tested at FIU include:

- A *magnetic miniature rover* that will travel through the refractory air slots,
- A *UT sensor rover* that will travel through the refractory air slots and inspect the tank floor,
- A *90-degee rover* that will travel through the refractory slots of AY-101 and
- A new *marsupial crawler* that will inspect the secondary liner by traversing through the drain line to the concrete foundation.

Subtask 18.2: Objectives

The objective of this task is to develop inspection tools that can provide information regarding the DST bottoms from within the insulation refractory pads and concrete foundation leading to the tank liners. FIU engineers will continue to work directly with site engineers to develop and test systems that can assist in the health assessment of the tanks. After the technologies have successfully demonstrated specified capabilities, FIU will work with site engineers to meet requirements for deployment at the sites. Specific subtasks include:

- Improvement of the design concepts that will allow for the navigation of a remotely controlled device through the refractory channels of DST at Hanford and provide visual feedback. The inspection tool has been successfully tested in a full-scale sectional mock-up test bed. A test plan has been developed for identifying any unforeseen issues and to ensure a successful deployment of the system at Hanford.

- Continuing the development and testing of a rover that can house and deploy a UT sensor for thickness measurements of DST primary liners through the refractory air slots.

- Development and improvement of the design of a rover that can navigate through the straight sections and 90° turns in the refractory slots of AY-101.

- Test and improve the design of a marsupial robotic inspection tool that includes a 6-inch pipe crawler that can navigate through drain lines to the concrete foundation of the DSTs. The crawler will house a rover that can navigate through the tank drain slots and provide information on the integrity of the secondary liner.

Subtask 18.2.1: Methodology - Preparation for the Deployment of Mini-Inspection Tool at Hanford

One of the primary challenges in the development of the mini rover was its ability to traverse over surfaces with weld seams. Some of the initial design concepts for the rover led to systems that had difficulty traversing the seams. After numerous tests, design changes and modifications, the current version of the rover was developed. The concept with the final design was to give the unit clearance in its middle, which provided the means for one end of the system to go over the seam while the other end was firmly attached to the plate. With this concept in place, a bevel gear design was incorporated to allow for the use of right-angle motors. This position change made it possible to utilize micro motors with higher stall torques (140 oz.in).

Figure 13. Current miniature rover design.

This rover uses 1/2" x 1/4" x 1/10" magnets to keep it attached to the metal plate. The number of the required magnets and size of the wheels were calculated based on the torque of the motors, required pull force (5 lb.) and the distance of the rover from the surface. The relations between the number of the required magnets, size of the wheels and the distance of the rover from the surface are shown in Figure 14 and was used to finalize the design.
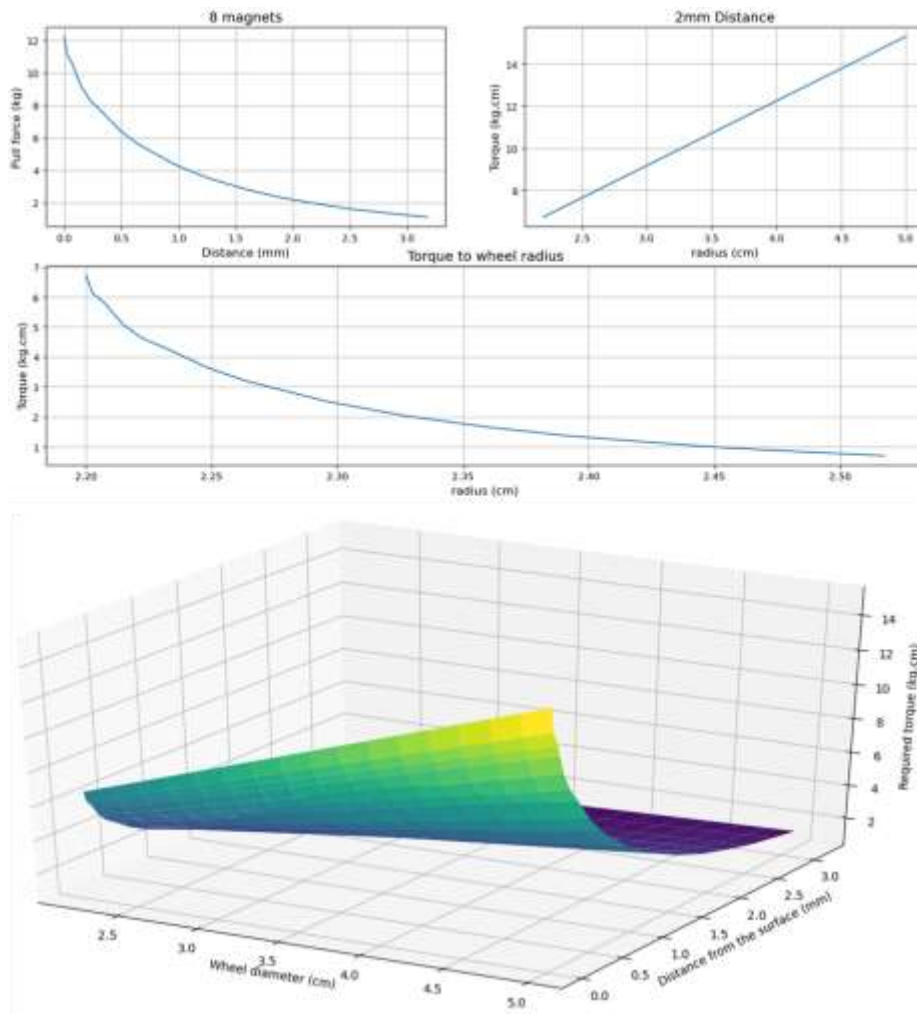
Figure 14. Torque needed based on wheel diameter and distance from the surface.

Testing of the rover also demonstrated that the unit with the bevel gear design, was not only able to traverse forward and backward over welds seams up to 1 inch in height, but it also improved its turning capability with the aid of high stall torque motors. Two sets of camera boards were also installed on the back and front of the rover.

With the long tether requirement, power was lost due to the voltage drop and video quality was also reduced for similar reasons. In order to address this issue, the current control box for the mini rover was designed to utilize stronger DC motors and a longer tether. The new control box includes a RoboClaw 2X7A as a digital controller and is controlled through serial communication using a python library. The computer receives the commands from the Xbox controller and sends the commands to the motor controller through the serial communication. The RoboClaw also receives its power from the power supply, which can go up to 34V and generate a 34V PWM signal to control the DC motors.
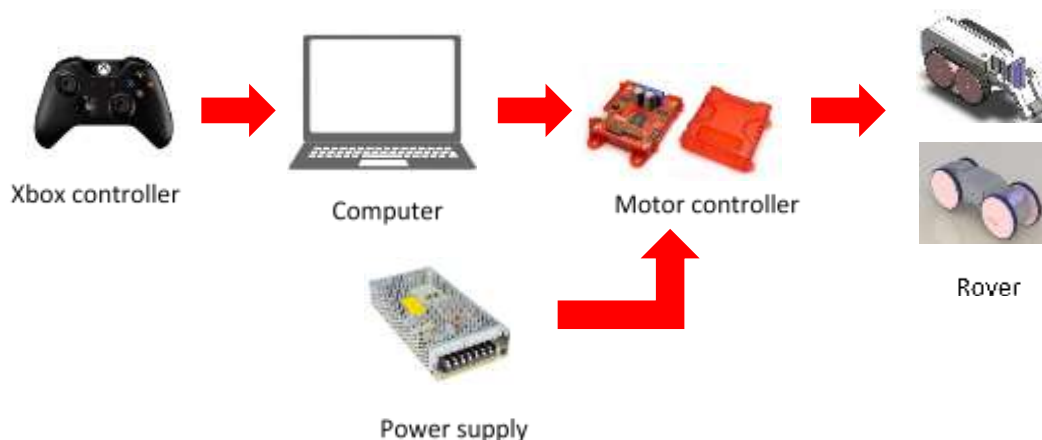
Figure 15. Control process.

To be able to deploy the miniature rover system at DOE facilities, an electrical safety inspection is required for the control box. After the control box design was finalized and fabricated, it was subjected to an electrical safety check and received the required certification to be considered for use at Hanford. The inspection validated the capabilities of the control box and ensured safe operating conditions.

Figure 16. Final control box design.

FIU has also worked with engineers from Washington River Protection Solutions (WRPS) to develop a test plan that will ensure that the mini rover is safe and can complete the necessary tasks when deployed. A test plan has been developed in conjunction with WRPS that includes four areas for testing and validation: durability, emergency retrieval, weld seam traversal and corrosion surface testing. The following sections highlight the procedure for each of the tests.

Durability Testing

The durability test will assess the durability of the mini rover while subjected to a thermal load. For this test, the rover will be driven inside one of the mockup's channels from the annulus until it reaches the central plenum and then return to the channel entrance. Multiple trips will be conducted to ensure the components on the rover can withstand long-term operation. During the testing, the channels will be heated to emulate the conditions with the slots of typical tanks.

The process of heating will include blowing hot air into the channel using two heating fans placed at the central plenum and annulus (Channel 0 & 3 in Figure 17). The blower's temperature and flow rate will be adjusted to attempt to maintain roughly 130°F in the channel. Side channels (branches) will be blocked using a thermal insulation foam and filler material. The gaps between the primary liner plates and the space between the plates and the concrete sections along the air slot channel, will be sealed using insulation foam. Thermocouple probes will be inserted into the channel via the side channel gaps and insulation at four points (C0, C1, C2 and C3 in Figure 17). These four points will be used to obtain real-time temperature measurements. K-type thermocouples with 4 feet bendable metal probes connected to a USB-UTC 8-channel data acquisition system will be used for temperature monitoring.
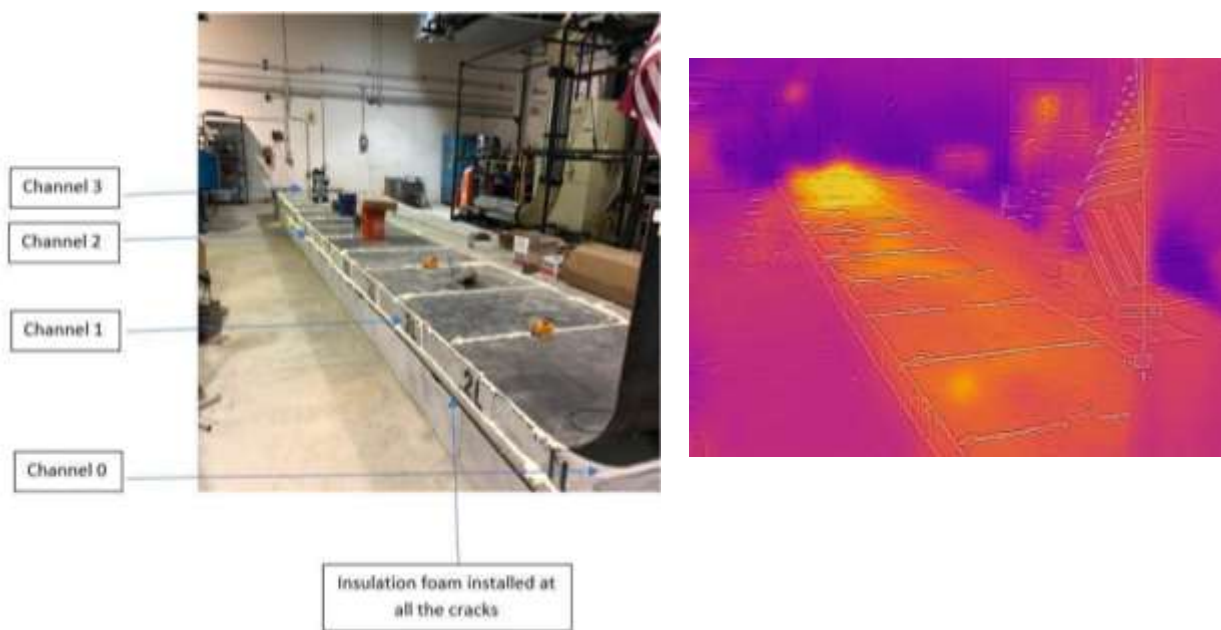
Figure 17. Durability test mockup.

To evaluate the process, the channel was heated with the two heating fans installed at the two ends. Table 1 shows the temperature measured at four locations for two hours.

Table 1. Heating the Channel for Two Hours

Time	C0	C1	C2	C3
10:45	73.88	76.2	76.13	76.30
11:00	128.24	89.48	105.72	156.12
11:15	131.80	94.28	112.46	158.21
11:30	133.52	97.53	116.52	158.44
11:45	134.57	99.71	120.7	159.56
12:00	134.92	101.05	121.76	159.62
12:15	136.57	103.35	123.64	161.08
12:30	137.32	104.82	125.01	161.32
12:45	137.23	105.97	126.07	160.38

The heating fan was then removed at the entrance and the temperature drop was monitored for 15 minutes (the time that rover needs to go all the way to the end of the channel and come back). After 15 minutes, the heating fan was reinstalled and it took 8 minutes to get back to the temperature before removing the fan.

Table 2. Temperature Drop after Removing One Fan

Time	C0	C1	C2	C3
12:45	137.23	105.97	126.07	160.38
12:47	123.48	101.72	126.32	161.12
12:49	122.29	101.53	125.98	161.57
12:51	120.31	101.86	126.60	161.25
12:53	118.84	102.03	126.42	160.86
12:55	117.61	102.38	127.27	161.55
12:57	116.52	102.50	127.15	161.41
12:59	115.48	102.42	127.33	162.08

Emergency Retrieval Testing

The emergency retrieval test will assess if the rover is capable of being withdrawn from within the channel in the event of a unit failure, or if the unit falls from the tank. To assist with emergency retrieval, the rover is equipped with a tether that is secured with a locking cap. The tether consists of the main cable, a stainless steel wire cable for strength support and expandable braided sleeve (Figure 18). The stainless-steel wire cable has up to 368 lbs of load before failing. The tether may be pulled manually from grade through the riser, annulus, and refractory to retrieve the unit. The test will evaluate whether the tether and locking cap can withstand the loads applied to the crawler during the retrieval process.
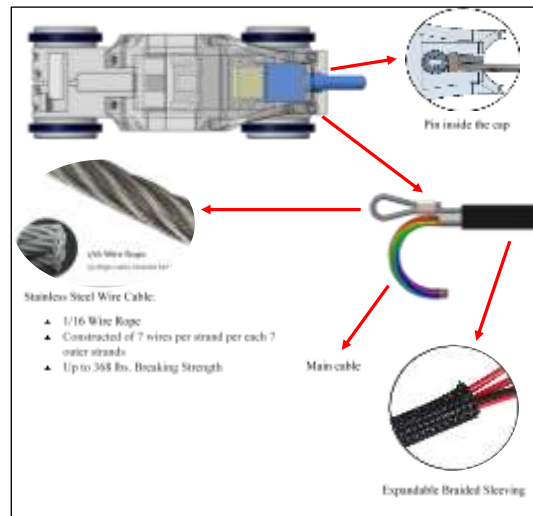
Figure 18. Tether details.

Weld Seam Testing

The weld seam test will assess the mini rover's ability to traverse weld seams on the primary liner of the tank. Two mockups of weld seam variations will be utilized. Figure 19 shows a steel plate with 5 weld seams ranging from 1/8th to 1 inch in height that will be used to represent semi-circular weld seams. The weld seam plates will be placed near the central plenum. The rover will be required to traverse the weld seams while pulling the tether, extending the entire length of the mockup.

Figure 19. Half-round weld seams with different heights.

Corroded Surface Testing

The corroded surface test will assess the rover's ability to traverse corroded surfaces (Figure 20) without change in the unit's performance. A critical issue will be the observation of corroded material accumulation on the magnets and its effect on performance.

Figure 20. Corroded surface setup.

Subtask 18.2.1: Conclusions

The miniature rover was developed to be deployed through small risers and gain access to refractory slots in the Hanford DSTs. The rover traverses through the slots on the primary liner, inverted via magnets to avoid debris in the slots. The current version of the miniature rover uses bevel gears in order to utilize right angle motors. Right angle motors are needed to create side-by-

side motorized wheels so that enough clearance in its middle can be generated for traversing weld seams on the primary liner. Using bevel gears to make right angle motors make it possible to utilize micro-motors with higher stall torques (140 oz-in).

In addition, the design of the control box for the rover was finalized and assembled. The new control system makes it possible to utilize stronger DC motors and allows the use of a longer tether cable while avoiding significant voltage drop.

Prior to deploying the mini rover at Hanford, a test plan was developed in conjunction with engineers at WRPS that tests the rover in harsh and strenuous environments using FIU's DST mockup. After execution of the test plan, the miniature rover will be available for deployment in Hanford DSTs.

Subtask 18.2.2: Methodology - UT Sensor Rover

The design of the UT sensor mini rover was significantly influenced by the final design of the miniature rover (discussed in the previous section). One of the major challenges was to incorporate the UT sensor, a brush for surface preparation and a means to deploy a couplant into the unit. Including a second module was considered, but it was decided to try to generate one module that included the all the necessary operations. The design of the UT rover was modified after initial testing to ensure the dimension constraints to move within the channel were met. The modified design, which included smaller wheels, is shown in Figure 21.
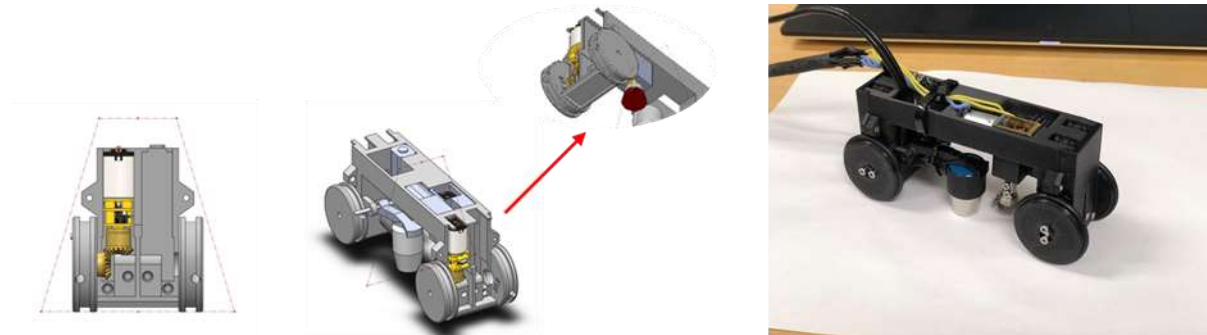
Figure 21. UT sensor rover.

In order to evaluate the new systems ability to traverse weld seams, the unit was tested on weld seams ranging from 1/8th to 1 inch in height. As shown in Figure 22, the system was capable of traversing seams up to 0.5 inches in height, which is above the maximum height expectation based on conversations with engineers at WRPS.
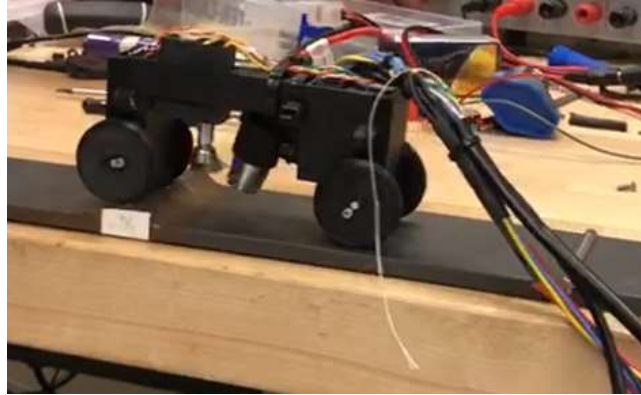
Figure 22. Weld seam testing.

As noted previously, the surfaces on the tank may require some level of cleaning prior to thickness measurements. A wire brush has been incorporated into the rover and was evaluated for its functionality. The figure below shows a surface with debris and scaling both before and after the prepping process.

Figure 23. Surface preparation demonstration.

In order to evaluate the UT sensor, a means for applying a couplant is required. Rather than incorporating a reservoir pump into the unit, taking up valuable space, it was decided to include a tube in the tether and utilize a water pump external to the unit. The pump supplies the couplant, in this case water, through the tube that is attached to the rover and places a small amount of water on the surface to be examined as shown in Figure 24. For this testing, a tube of 150 ft in length was used.

Figure 24. Water pumped as a couplant.

The UT system was then tested and evaluated for functionality and accuracy of the UT measurements. The figure below provides a sample of the data measured. The UT rover measurements were compared with measurements from a handheld UT sensor gauge and demonstrated a high level of accuracy.
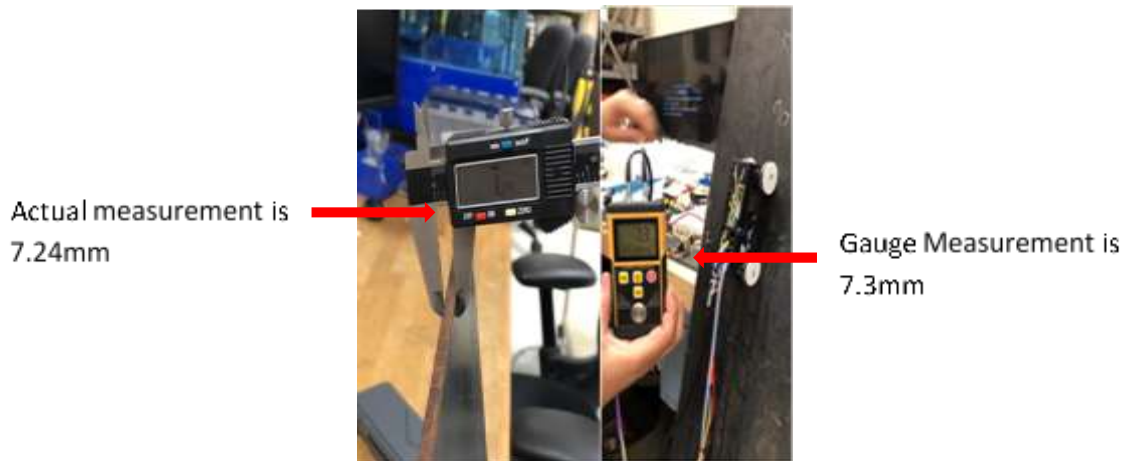
Figure 25. UT sensor unit during the thickness measurement test.

To demonstrate the maneuverability of the UT rover and its ability to pull a tether, the system was evaluated in FIU's DST mockup. The figure below shows the 8 ft wide sectional mock-up. The metal plates represent the primary liner and cover the refectory air slots.
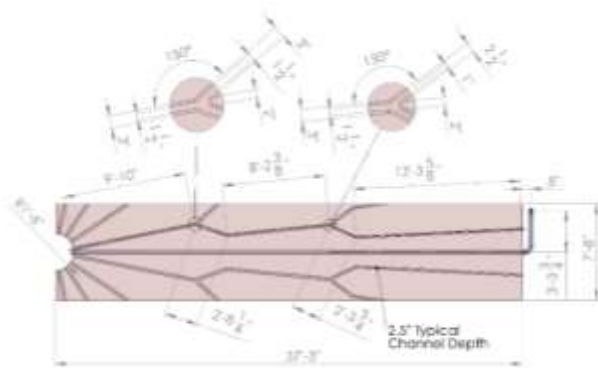
Figure 26. The full-scale mockup.

In order to navigate the UT sensor unit within the channels, the UT rover was configured with the same controller that was utilized for the original mini rover. The controller includes a RoboClaw 2X7A, power supply, voltage adapters, analog to digital video converters and a computer. The UT sensor rover was placed on the side wall above the tank knuckle and driven into a refractory slot from the annulus. The system was easily able to navigate from the annulus to the central plenum. Figure 27 shows the entrance location and a picture taken from the video feed from the rover near the central plenum.

Figure 27. UT rover entering and exiting mockup.

Subtask 18.2.2: Conclusions

A UT sensor mini rover has been developed to assess the thickness of the secondary liners of high-level waste tanks at Hanford. The design is based on the original mini rover and includes a motorized brush for surface preparation and a deployment mechanism that places a UT sensor on the cleaned surface. The additional mechanisms have been incorporated into a single rover, simplifying its operation. The rover was evaluated with several tests including maneuverability over various weld seam heights, thickness measurement of a steel surfaces and navigation through a full-scale mockup of the DSTs. The rover was able to meet all requirements and successfully navigated from the annulus to the central plenum in the full-scale mockup.

Looking forward, FIU will focus on the development of the data acquisition device for the UT transducer, which must be capable of measuring the thickness of the plate from grade (~150 ft from the rover). FIU will also investigate the improvement of the tether and its connection to the UT sensor rover. This tether will be more complicated than the tether of the first miniature rover due to the addition of the cleaning mechanism, UT sensor arm, hose for the couplant and data acquisition line. Lastly, FIU will explore options for configuring the control box for the desired UT sensor system based on our current mini rover control box.

Subtask 18.2.3: Methodology - 90° Rover for AY-101

Since there is only one functioning tank with a concentric circle refractory configuration (AY-101), most inspection tools are being developed for the 25 DSTs with the friendlier tree structure configuration within the refractory slots. Site engineers, however, remain interested in inspecting the AY-101 primary liner. The 90° rover is being specifically developed for AY-101 tank floor.

During the past period of performance, the 90° rover design incorporated a few design changes that optimized space and improved the performance of the rover. The changes were made to ensure the system could traverse weld seams and navigate through 90° turns. A schematic of the system is shown in the figure below.
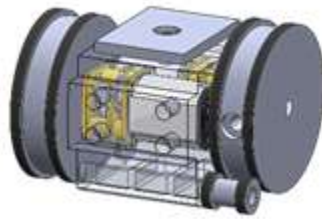
Figure 28. Schematic of the 90° rover.

After the modifications were completed, a prototype of the rover was printed and assembled and is shown in Figure 29.

Figure 29. 3D printed 90° rover.

The new prototype of the rover was successfully tested for its ability to navigate around 90° turns and over weld seams. The maximum pull force of the unit was also measured and found to be 3.7lbs. Additional tests will be conducted to ensure functionality of the rover and optimize its pull force. Testing of the rover over weld seams and through turns are shown in Figure 30.
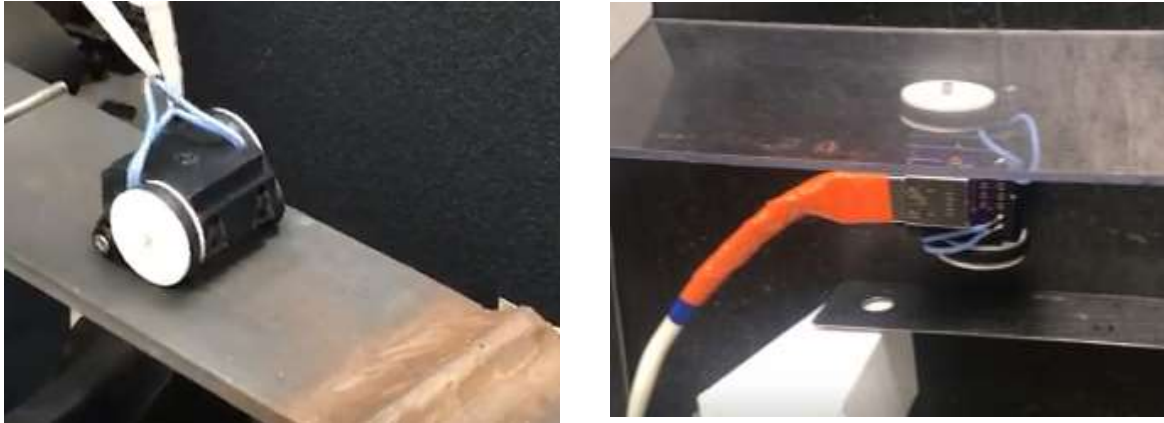
Figure 30. Testing of the 90° rover over weld seams and through sharp turns.

Subtask 18.2.3: Conclusions

The current design of the 90° rover is a single rigid body that is 1/3rd the size of our current miniature rover, which allows the inspection tool to be capable of traversing around 90° turns. Although the rover is smaller than the miniature rover, it needs to retain the same pull force in order to be able to navigate through multiple (four) 90° turns. The rover system has been tested and is capable of navigating over weld seems and around multiple 90° turns.

FIU will continue to test the unit, improve its design and incorporate a camera for visual inspection. To test the unit in a larger scale mockup, FIU plans to modify the current DST mockup to incorporate 90° turns and emulate the configuration of the slots in tank AY-101.

Subtask 18.2.4: Methodology - 6-Inch Crawler Testing and Design Modifications

Marsupial Crawler for Secondary Liner Inspections

FIU has been developing a robotic marsupial system that uses a mother pipe crawler to navigate through the ND 150 (6") drain pipeline and deploys a miniature child-rover into the drain slots. Figure 31 shows a rendering of the conceptual design and approach that will be utilized to access the drain slots and gain access to the secondary liner.
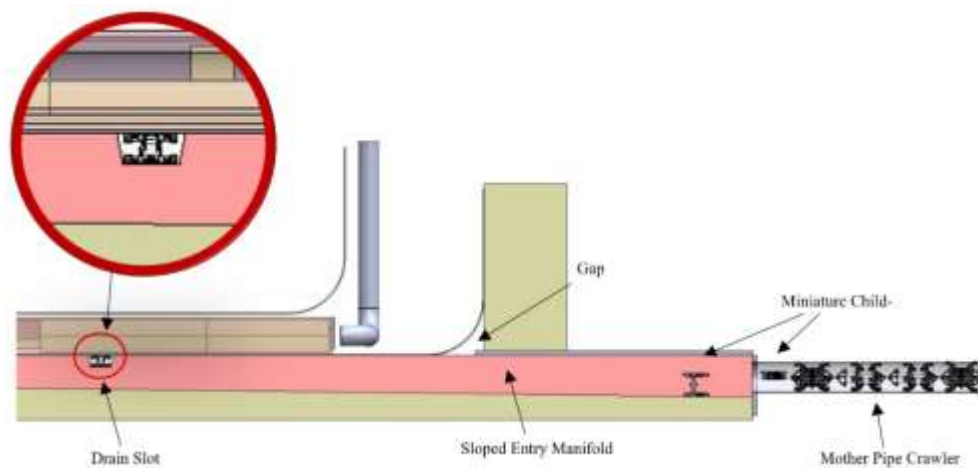
Figure 31. Secondary liner inspection approach.

The mother pipe crawler has multiple functions including:
1) traversing the entry drain pipeline,
2) deploying the miniature child-rover,
3) managing the tethers of both units, and
4) rescuing the miniature tool in case of failure.

The crawler operates using pneumatic actuators on the same peristaltic principles of other inspection tools previously developed at FIU. The crawler, which was developed in the Year 9 period of performance, is shown in the figure below.

Figure 32. Mother pipe crawler prototype.

Testing on the crawler was conducted to evaluate the pull force of the grippers before slipping occurs between the gripper pads and the pipe wall. The test was conducted using 80 psi of air pressure to the pistons and in a PVC pipe. The crawler held 41 lbs of force with one gripper actuated and 46 lbs with two grippers. Note that these results are conservative since the coefficient of friction should increase with steel pipes. The pressure could be increased to 100 psi if additional force is needed.

Child Miniature Rover

The miniature inspection rover's current prototype resembles a broader version of the magnetic unit developed in ~~subtask~~ Subtask 18.2.1. As illustrated in Figure 31, the bottom of the secondary liner's proposed inspection presents additional challenges. The tool needs to overcome a gap between the foundation's sloped manifold and the secondary liner to access the lateral slots that branch from this manifold. In most DSTs at Hanford, the foundation manifold slopes from 9" at the ingress to 2.5" at the central plenum. Consequently, FIU's current prototypes have a retractable scissor mechanism that can lift the unit and reach the secondary liner.

This lifting concept was exhaustively explored during the past performance period, and a functional prototype was successfully tested. Figure 33 shows this original version of the rover that successfully extended the mechanism, magnetically attached to an overhead metal surface, retracted, lifted the unit, and drove on the surface.
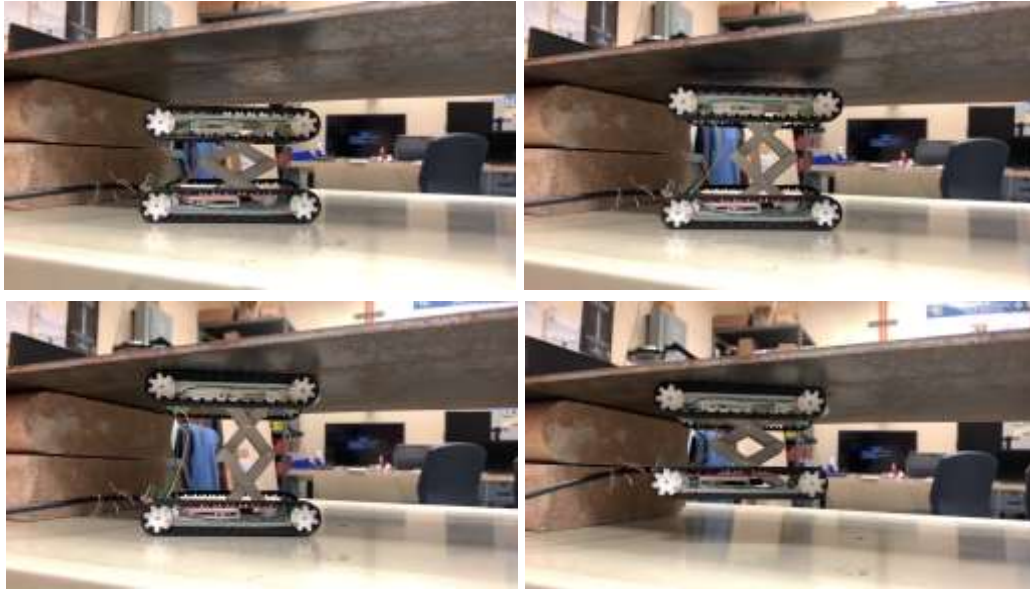
Figure 33. Original miniature inspection tool.

The rover can navigate either on the concrete floor or maneuver upside down magnetically attached to the tank during inspections within the lateral slots using the mechanism. The rover's ability to transition between the floor to the liner might also be crucial to overcoming unforeseen conditions present in the concrete foundation and the secondary liner.

This original version of the miniature inspection tool also uses additional lateral scissor mechanisms to control the gap between the magnets and the secondary liner, allowing the unit's eventual disengagement during retrieval, as illustrated in Figure 34.
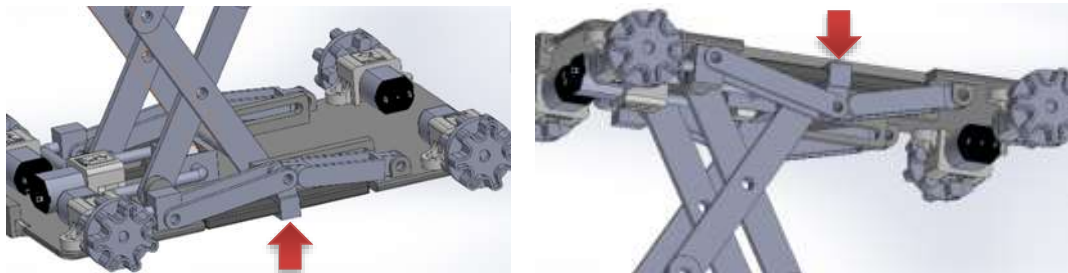
Figure 34. Magnet displacement mechanism engaged (left) and disengaged (right).

Figure 35 shows images from previous inspections of the DST's primary tank liner, presenting challenging conditions to navigate magnetically attached. Conditions could potentially be worse in the secondary tank liner, with a lack of humidty control in the ventaliation system.

Figure 35. Primary liner weld seams (left and center) and flakey corrosion spot (right).

Based on the surface challenges that the rover may have to overcome, a series of more capable designs were developed to traverse over the weld seams, corrosion, and buildups potentially on the secondary liner. The lessons learned from each design were incorporated into newer, more capable designs, as presented below.

Figure 36 shows a design that uses large wheels, approximately 2" in diameter, replacing the original bottom and top tracks. Larger wheels have the ability to overcome unexpected obstacles than the current small tank treads.
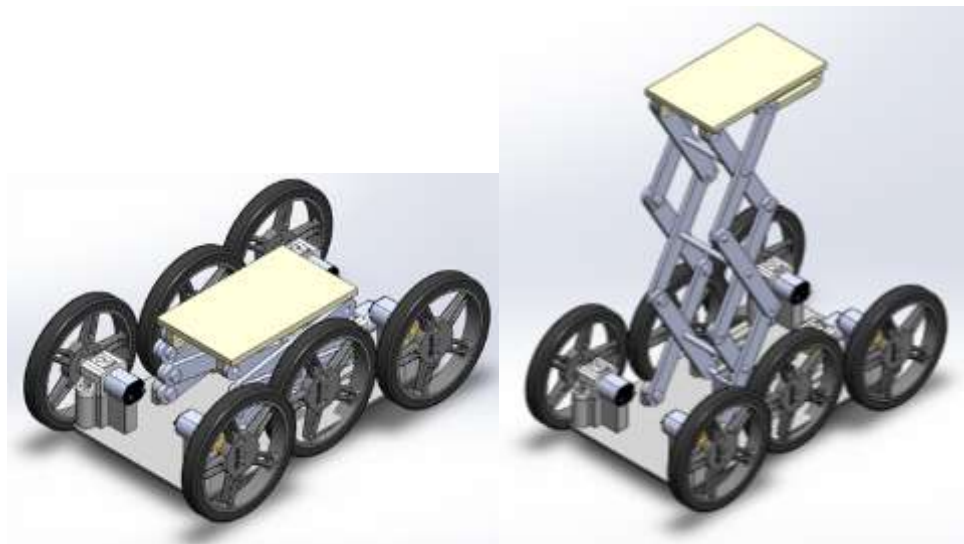
Figure 36. Alternate design using large wheels.

The alternative design reduces the total number of motors from ten in the original using bottom and top tracks to five. It also eliminates the additional mechanism to control the magnet gap. As illustrated in Figure 37, the proposed magnetic attachment is directly controlled by the scissor-lift assembly, pushing itself against the large wheels.
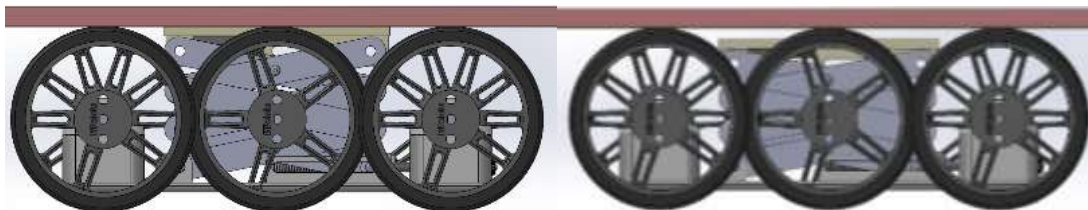
Figure 37. Engaged magnets (left) and gap control (right).

Figure 38 shows a subsequent version of the miniature inspection tool with a more compact footprint than the previous version. The overall dimensions fit in a standard module size of 4" by 6", which is convenient for deployment.
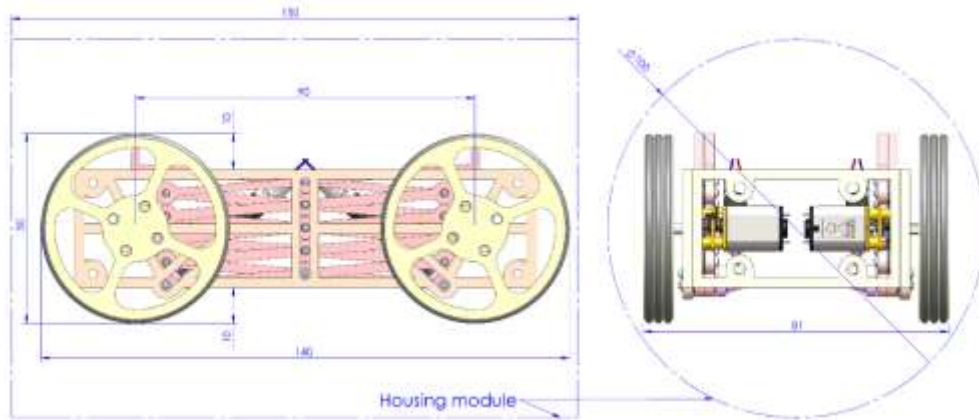
Figure 38. Improved miniature inspection tool.

This version also has a larger clearance between the chassis and the floor that allows for traversing weld seems up to 3/8" in height. As shown in

Figure 39, the rover uses micro gear motors that diagonally open the scissor lift mechanism allowing the extended floor clearance. The current reach of the arrangement is approximately 9".
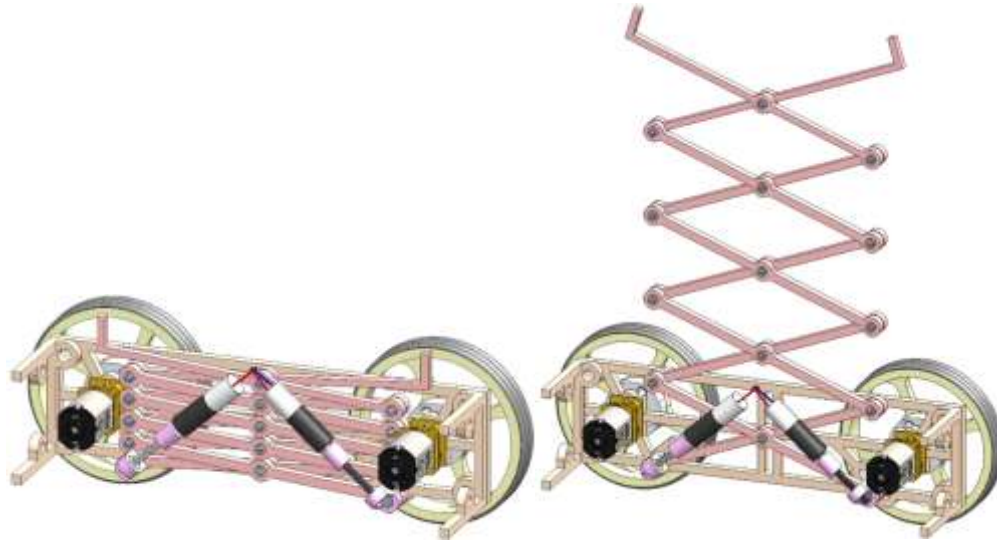
Figure 39. Rover's scissor lift mechanism.

Based on permanent magnet lifters, a switching magnetic attachment was also designed to control the inspection tool magnetic engagement to the secondary liner, illustrated in Figure 40. In the magnetic attachment system located at the scissor lift ends, the relative movement between the permanent magnets inside the lifter adds and cancels the magnetic field strength on the working surface, switching between loading and unloading conditions. However, finding small, powerful motors capable of dealing with neodymium magnets' strong repulsion was challenging to implement in such a small device.
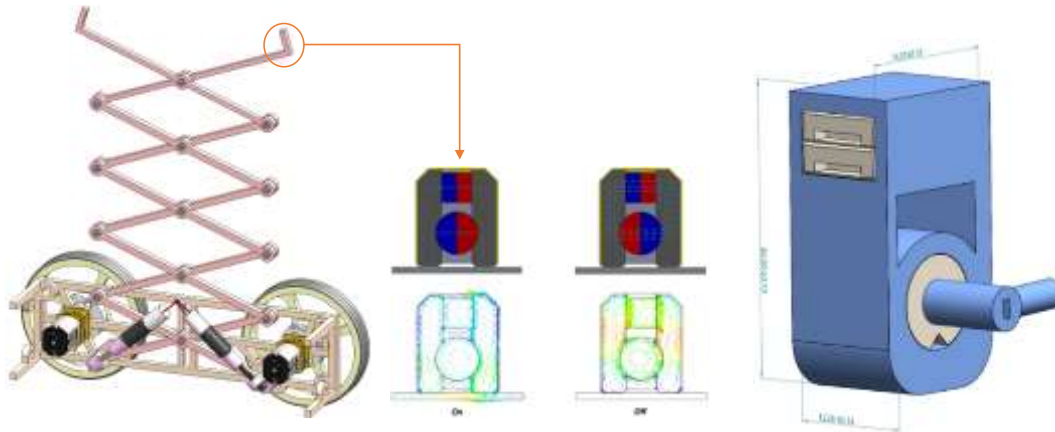
Figure 40. Rover's scissor lift mechanism (left) and magnetic attachment (right).

In the previous versions of the lift mechanism, the links' flexibility prevents the scissors' full extension. Figure 41 shows a finite element structural analysis that compare redesigned links to the original ones, demonstrating stress reduction at critical points ~~and~~ which leads to a more robust and stable mechanism.
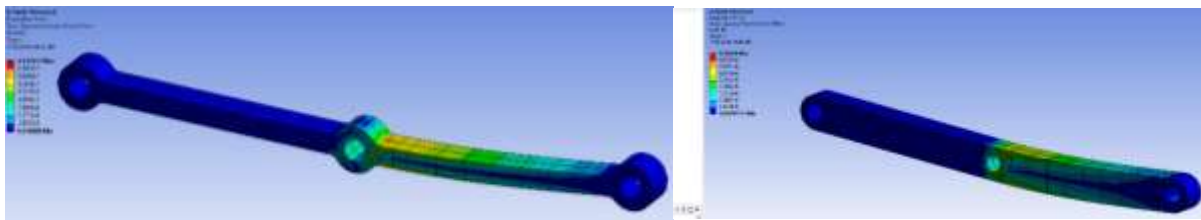
Figure 41. Scissor lift mechanism prototype.

Figure 42 shows the significant design evolution of the lift mechanism's actuators. The current design uses two lateral motors on each side. The actuators were shifted to the outside of the rover frame between the wheels, freeing interior space for embarked electronics but keeping the same overall design's footprint.
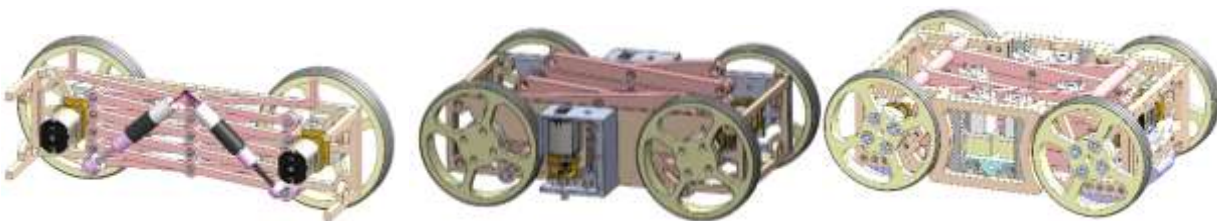
Figure 42. Scissor lift design evolution, original (left), previous (center), and current (right).

The Current Prototype

Figure 43 shows a prototype of the current scissor lift mechanism.
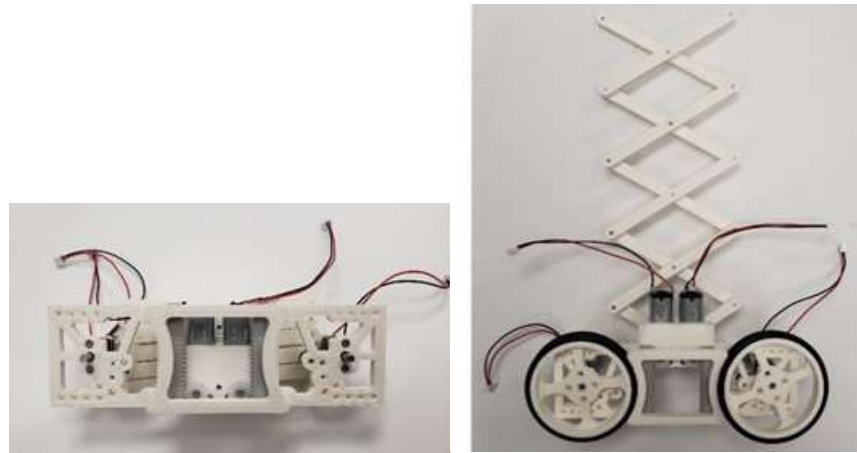
Figure 43. Scissor lift mechanism current prototype.

The current design uses permanent magnets at the top to engage the secondary liner. As illustrated in Figure 44, the rover uses lateral release mechanisms for retrieving the unit. The release mechanisms are motorized arms that push the magnets away from the secondary liner, disengaging in synchrony with the scissor lift mechanism's opening.
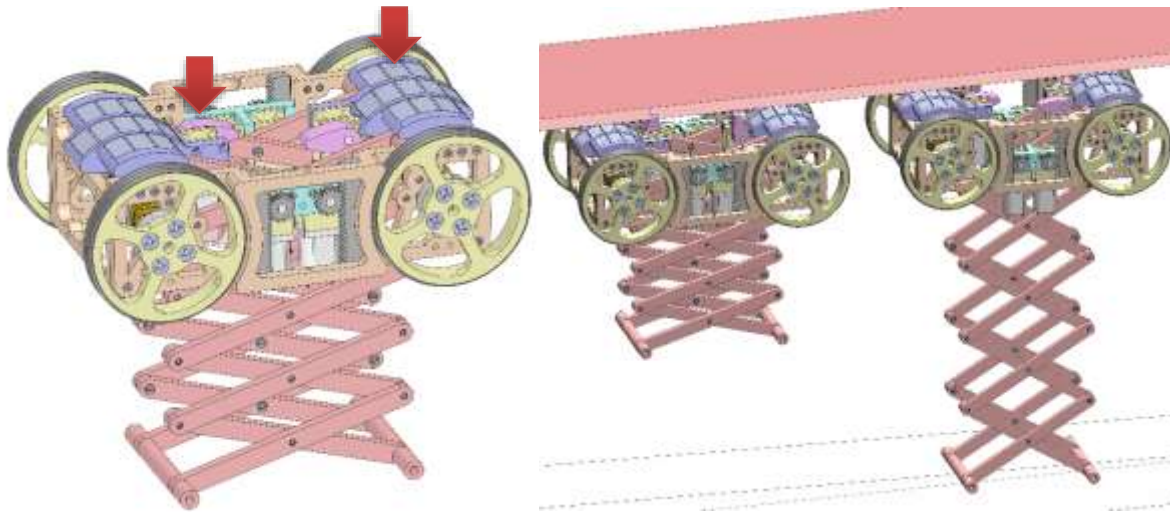
Figure 44. Current inspection rover design (left) and release mechanism (right).

Figure 45 shows a schematic of the child miniature rover using its lift mechanism and magnets to inspect the lateral channels, transitioning at the entrance manifold from the floor and the secondary liner's bottom plates.
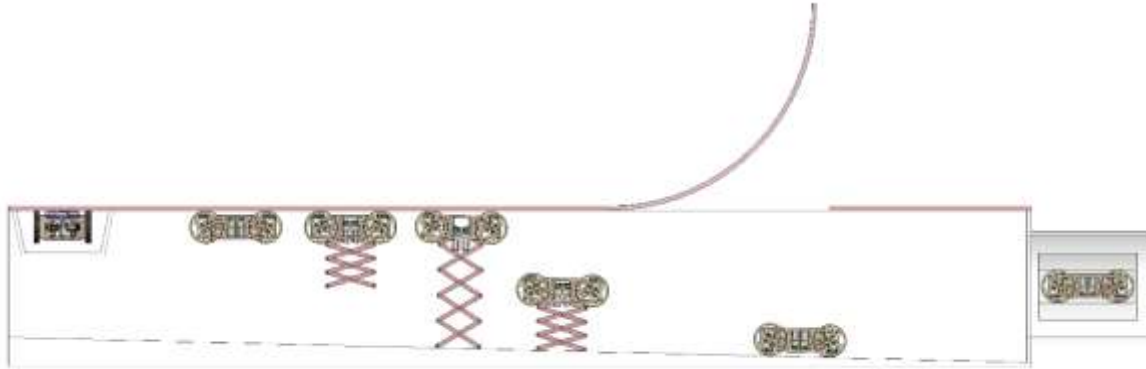
Figure 45. Proposed inspection of the secondary liner.

Embedded Electronics and Controls

The embarked electronics that control the miniature rover includes:

a. motor controllers for the wheels, scissor lift, and attaching/detaching mechanism
b. camera modules at the front, rear, top, bottom, and sides of the frame
c. analog video multiplexer
d. voltage regulators
e. Controller Area Network (CAN bus) module for communication
f. main microcontroller

Figure 46 shows a functional prototype tethered to a remote-control box composed of an embedded computer, a display screen, a gaming controller, a power supply, and a video capture device.
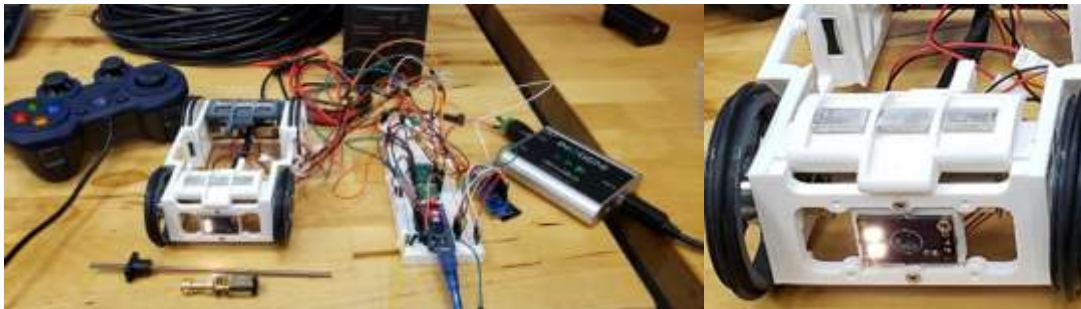
Figure 46. Miniature rover assembly (left) and camera module (right).

The prototype's analog video multiplexer was tested switching between the camera modules, successfully delivering quality colored feeds at the controller's command. The rover's maneuverability was also tested to navigate under a carbon steel plate using the magnets to attach to it. Figure 47 shows the rover magnetically attached to a top metal plate, moving, turning, and stopping as needed, without any issues.
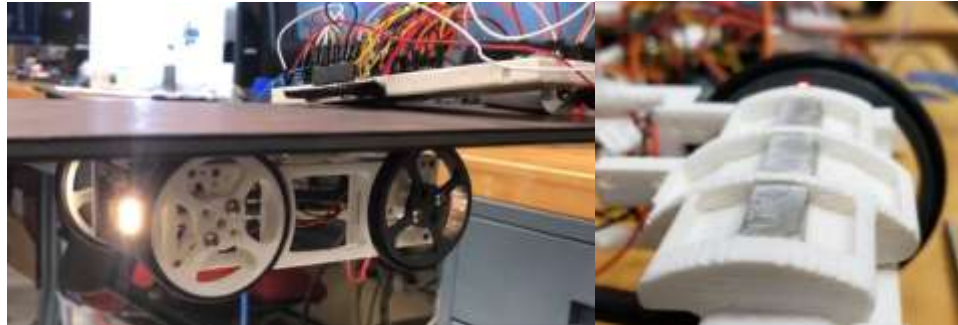
Figure 47. Miniature rover maneuver tests (left), and magnetic module (right).

An overall system diagram, including the miniature rover's main components, is shown in

Figure 48. In the chart, a tether distributes power (12 volts) and ground and includes two communication lines for the CAN bus module and one line dedicated to analog video signals.
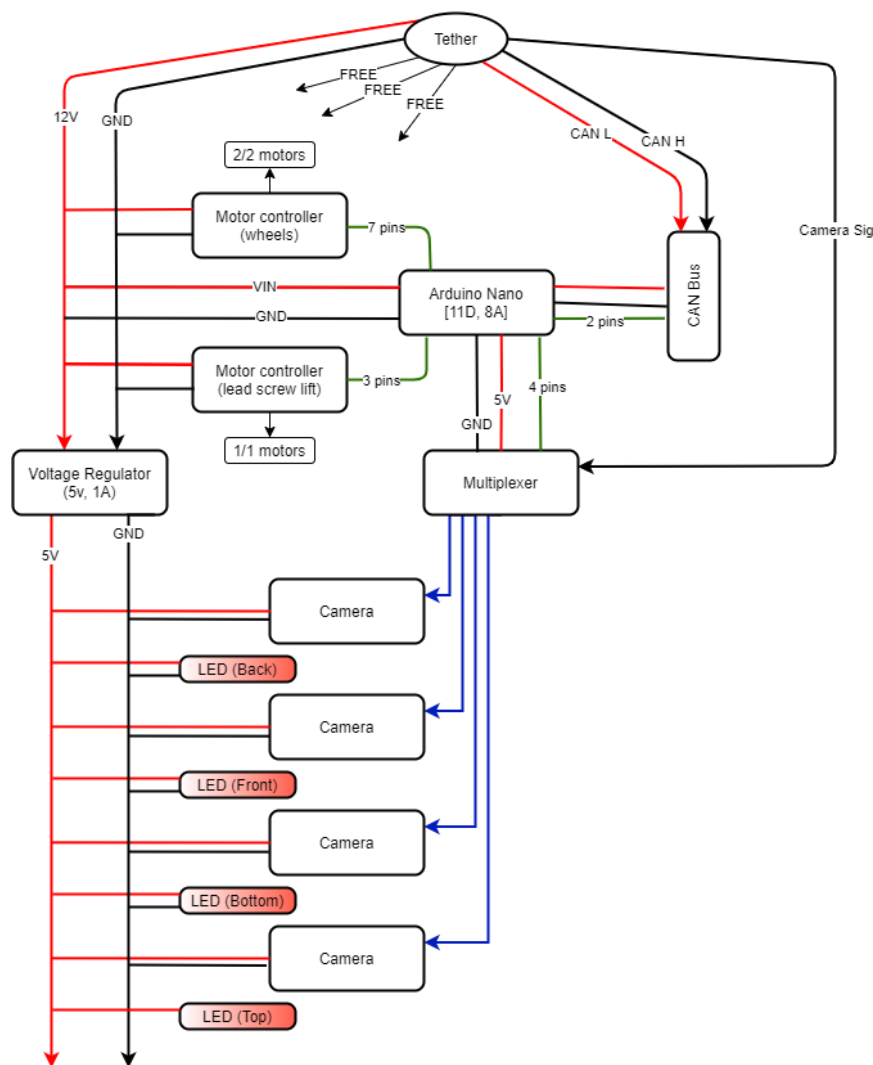
Figure 48. Miniature rover overall schematic.

The current tether is a standard Category 6 Ethernet cable, providing four twisted-pair lines. The current rover design uses five cable lines in total, leaving three unused lines for future expansion.

Housing Module and Deployment Mechanism

During this performance period, an additional pipe crawler housing module was conceptualized to deploy the child miniature inspection tool. The module will carry the rover during the traversal of the mother crawler through the entry drain pipeline. The apparatus will also be responsible for managing its tethers, and rescuing the device in case of failure.

As shown in Figure 49, the distance between the rover and the floor is about 3.5", which requires a deployment apparatus to deliver the inspection rover from the housing module to the floor of the leak detection manifold.
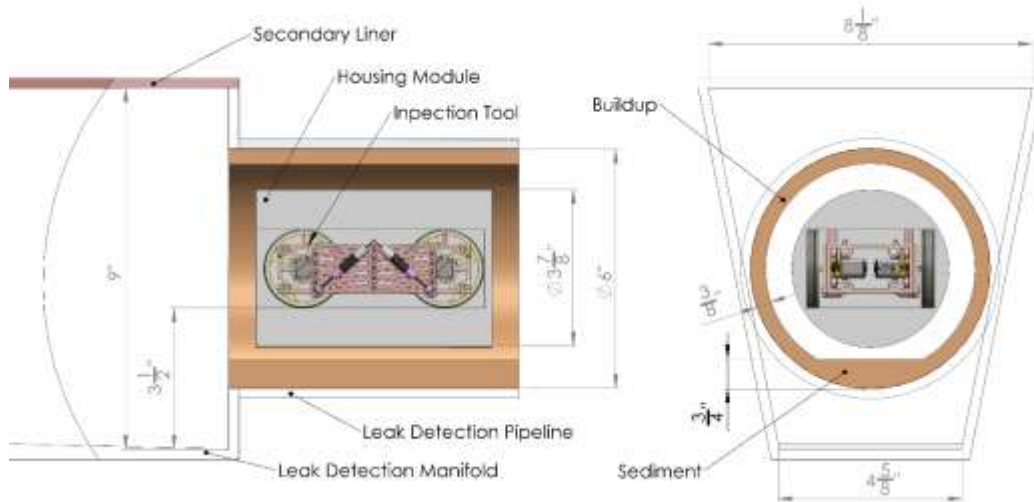
Figure 49. Housing module.

The pipe crawler modules are approximately 4" in diameter and centered by guides to avoid existing sediment and build up in the leak detection pipeline. Figure 50 shows the drain lines' current conditions from previous inspections at Hanford.
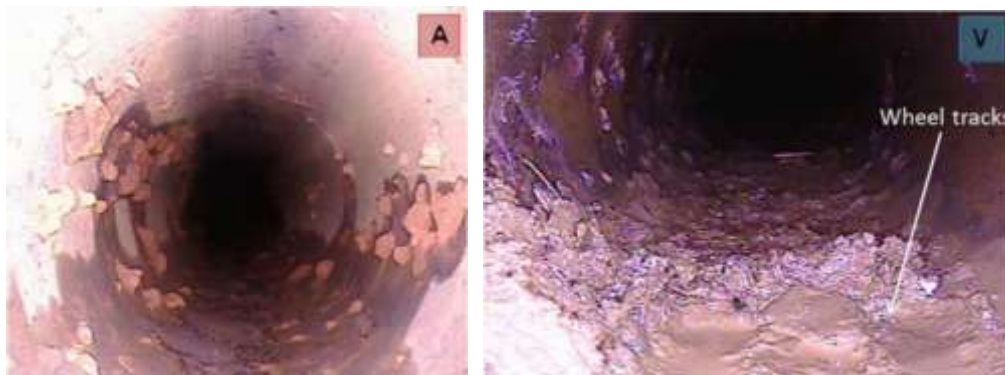
Figure 50. Existing sediments and buildup in the leak detection pipeline.

One of the deployment options considered was to use an overhead ramp. Figure 51 shows the scissor lift magnet attaching to the ramp that deploys and retrieves the unit using the scissor lift mechanism.
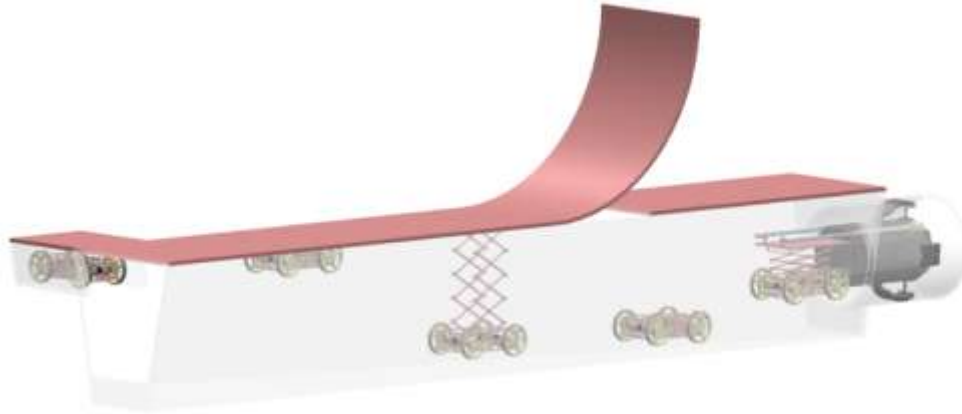
Figure 51. Overhead deployment ramp.

Figure 52 demonstrates a more reliable option using a retractable ramp that allows the rover to drive in and out of the module.
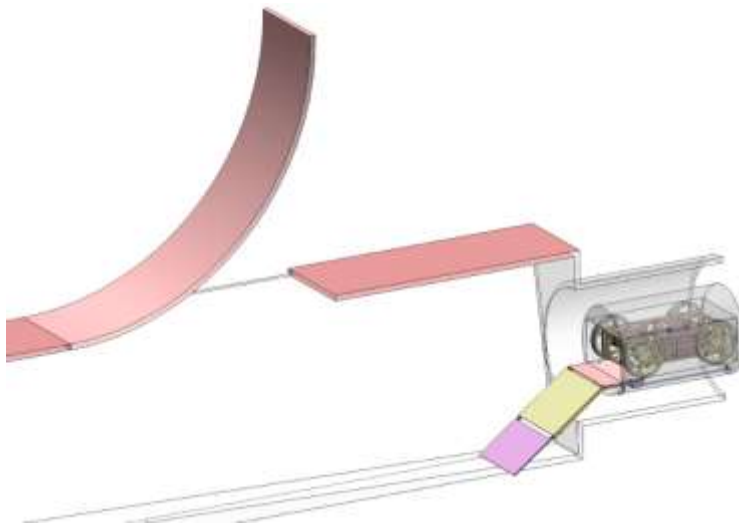
Figure 52. Retractable deployment ramp.

Figure 53 shows the ramp stages in a multibody dynamics simulation. The ramp uses a sequence of three foldable panels, the first one operated by actuators, the second by guides and gravity, and the third one by springs and followers.
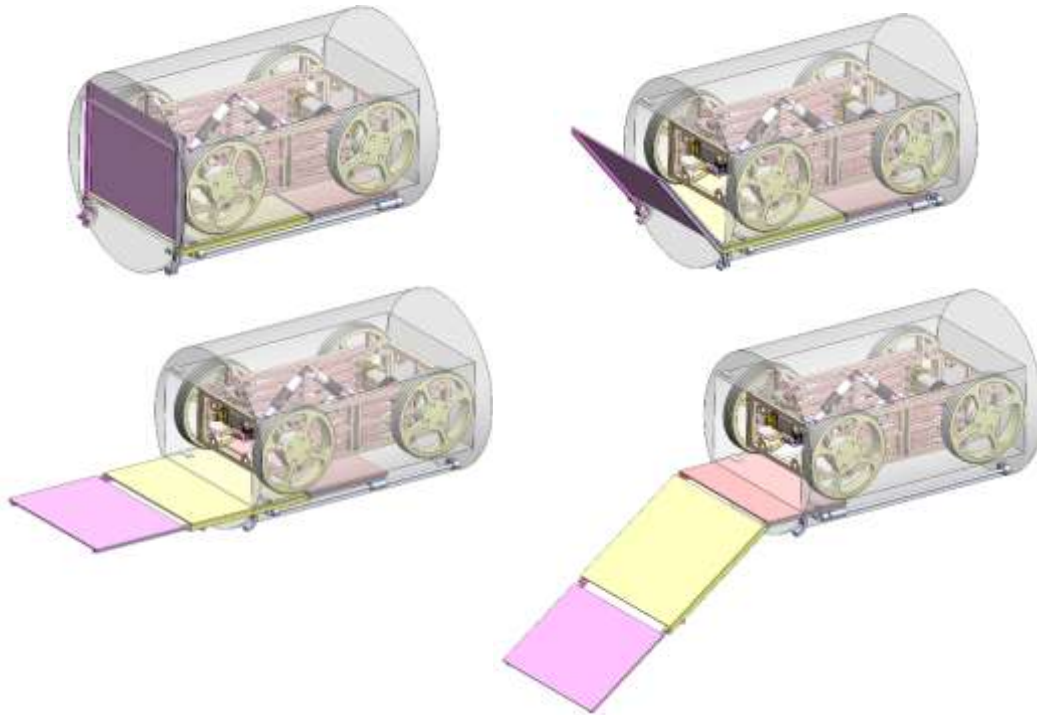
Figure 53. Retractable deployment ramp multibody dynamics simulation.

Mockups and Testing

Finally, exhaustive full-scale tests were designed to verify and validate the complete crawler system. FIU will utilize the DST mockup constructed at our facilities for engineering scale testing and validation of the robotics and sensor technologies. The testbed emulates the concrete foundation with drain slots, 6" drain line, concrete shell, secondary tank liner, refractory pad with cooling channels, 4" air supply line, primary tank, and central plenum.

Figure 54 shows the drain slots' layout in the concrete foundation, under the mockup's secondary tank liner. The leak detection system is a maze of sloped drains carved in the foundation. In the mockup, the drains are precisely sloped and angled accordingly to the DST's shop drawings. They will be suitable to address corrosion issues in inspecting the bottom of the secondary tank liner.
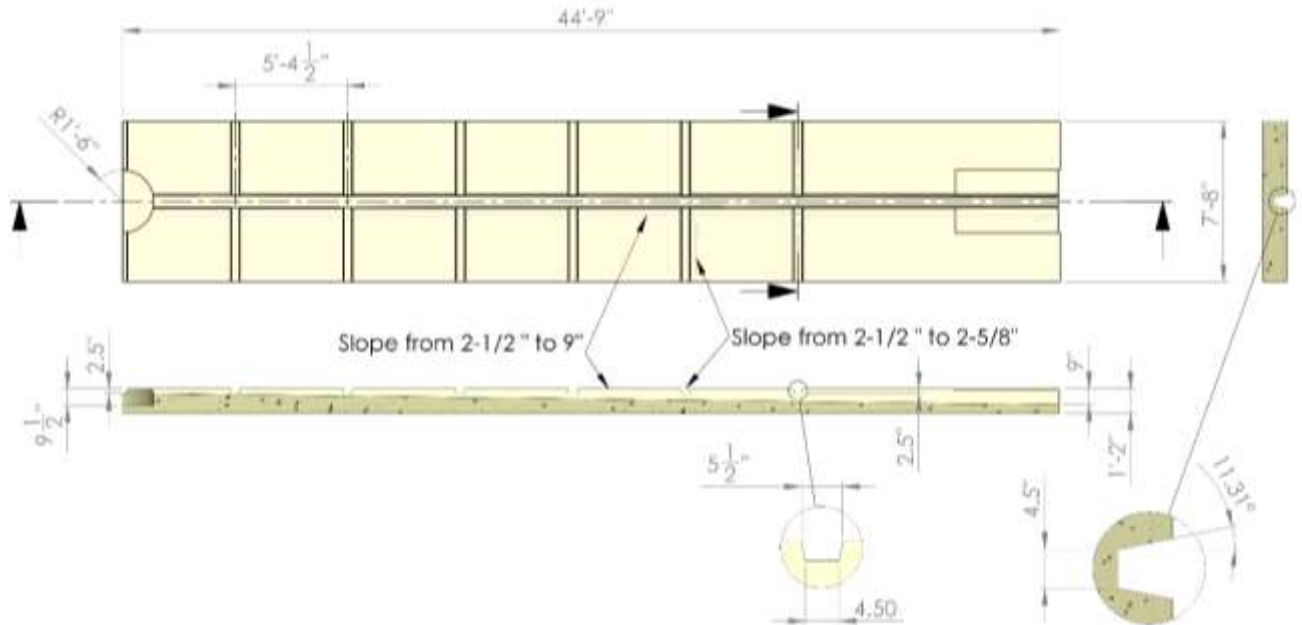
Figure 54. Concrete foundation with drain slots.

In addition, a transparent bench-scale mockup (Figure 55) was also designed and manufactured for debugging early stages in the deployment of the miniature inspection.
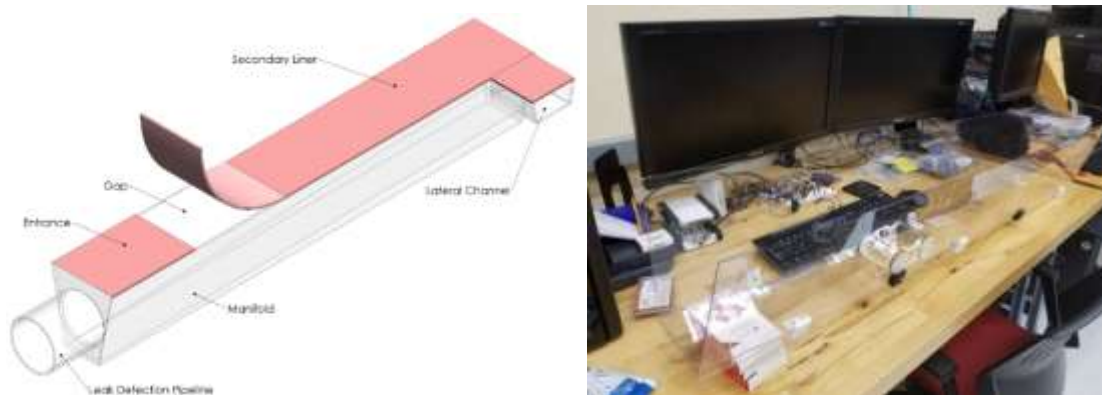
Figure 55. Bench-scale mockup.

Subtask 18.2.4: Conclusions

During this period of performance, the design efforts streamlined the marsupial robotic system, incorporating improvements in the mother delivery crawler, the child miniature inspection, and the control box, based on exhaustive bench-scales.

FIU will continue improving the overall functionality and robustness of the inspection tool. A prototype of the housing module will be finalized and seamlessly integrated. The improvements will include better cable management, power, communication, and controls. There are also plans to integrate additional sensors, such as an ultrasound probe for thickness measurements, a LiDAR module for channel mapping, a temperature, and a humidity sensor for environment

characterization. The system will be demonstrated during a potential visit from WRPS engineers in FIU's DST mockup. Modifications will be made based on the engineering-scale test results and incorporating Hanford deployment requirements.

Subtask 18.3: Evaluation of Coatings for the H-Canyon Exhaust Tunnel (NEW)

Subtask 18.3: Introduction

The H-canyon is the only remaining chemical processing facility in America capable of reprocessing plutonium, highly-enriched uranium and other radioactive materials [1]. The exhaust air flow from the H-canyon chemical processing areas and HB-line are transported through the H-Canyon Exhaust (HCAEX) tunnel, where radioactive contamination is removed. Robotic inspections of the tunnel have revealed significant ongoing degradation of the reinforced concrete structure that was associated with acid attack. The degradation observed could compromise the mechanical strength of the structure. Hence, the search for solutions to mitigate and prevent further degradation is necessary [2-3]. The application of a protective coating on the degraded tunnel walls could mitigate and prevent further degradation, which constitutes the main goal of this investigation. This research effort has been divided into two phases: 1) Development and evaluation of aged concrete under accelerated aging conditions (which is the focus of this paper) and 2) Evaluation of potential coatings applied on aged and non-aged concrete under simulated aggressive conditions.

In the preliminary stage of the investigation, a comprehensive literature review was performed and major findings included: 1) the characterization of the tunnel degradation conditions, 2) the identification of the chemical attack and erosion as the primary degradation mechanisms affecting the tunnel concrete walls, 3) the identification of the acid-type immersion tests as a well-known method for evaluating the materials' resistance to acid attack and, 4) the preliminary selection of potential coatings for aggressive environments similar to the tunnel [3].

Lessons learned and research findings of the initial testing of concrete in acid solutions supported the development and ongoing execution of a comprehensive test plan that will be presented in this report. The test plan execution is an ongoing task allowing the development and evaluation of aged concrete surfaces, with 1) protruded aggregates, 2) exposed steel rebar, and 3) chemically damaged, similar to the tunnel walls after more than 60 years of operation. The degraded (aged) concrete surfaces were developed through various accelerated aging conditions including the effect of some variables such as acid concentration, erosion, mode of action of the aggressive agent, and the presence of steel rebar [3]. Finally, the developed aged concrete surfaces will be used as the substrate for the evaluation of potential coatings in a further stage of the investigation. Because this is an ongoing investigation, preliminary results of the accelerated aging of concrete specimens will be presented in this report.

Due to the hostile environment of the HCAEX tunnel, the ability to enter the tunnel and perform any type of investigative, or in this case damage mitigation to the concrete walls, have been restricted to the use of robotic platforms equipped with the tools necessary to accomplish said goals. The robotic platform would need to work in tandem with another larger ground platform capable of traversing the difficult terrain of the tunnel. The ground platform would need to deploy the secondary platform onto the concrete walls to apply a down selected coating.

The secondary robotic platform will need to be capable of traversing the HCAEX tunnel concrete walls in a manner that does not further damage the surface of the walls and allows accurate positioning of the platform to apply the coating. A literature review regarding the different methods available that would allow a mobile platform to maintain contact with the walls, regardless of the platform's orientation, will be highlighted in this report.

After determining the appropriate adhesion mechanism for the mobile platform, the results obtained from constructing two prototypes will be detailed in this report with the goal of showing the viability of the platform as an option to a unit capable of traversing a concrete surface without introducing further damage to the wall's surface and at the same time, maneuver across the surface to reach a desired location when tele-operated.

Subtask 18.3: Objectives

The identification and evaluation of potential coatings to mitigate and prevent further degradation of the concrete walls of the HCAEX tunnel is one of the main objectives of this subtask. FIU has been working and continues to work very closely with the Savannah River Site's engineers in order to meet the objective. The first stage of the investigation is to develop and evaluate aged concrete specimens under accelerated aging conditions (preliminary results included in this report) that will be later used as the substrate for evaluating potential coatings.

Two objectives have been proposed related to this effort, 1) to define important aspects regarding the concrete specimens such as concrete mix design, configuration, dimensions, exposure mode to the aggressive environment, and 2) to develop and execute a test plan, including the research scope, the experimental design, data collection approaches (measurements), etc.

In addition to the objectives for the concrete aging, above, objectives for the development of the robotic platform include: 1) the completion of a literature review detailing the different adhesion mechanisms available for a mobile platform, and 2) evaluation of a prototype utilizing the selected adhesion mechanism appropriate for the conditions inside the HCAEX tunnel and the concrete walls. These additional objectives to the subtask will support the investigation into developing a robotic platform capable of entering the HCAEX tunnel and applying a protective damage coating to the walls of the tunnel.

Subtask 18.3: Methodology

1. **Concrete Aging: Initial Testing and Development and Execution of Test Plan**

Experimental Design

Based on the literature review and the knowledge of the aggressive conditions inside the HCAEX tunnel, a factorial design 2^4 (2 levels and 4 variables) leading to 16 experiments was proposed, discussed and finally approved by Savannah River Site engineers. Table 3 shows the test plan resulting from the experimental design with a selection of the most representative interactions (12 experiments selected) among the variables.

Table 3. Test plan for Accelerating Aging of Concrete

Test number	Acid concentration	Mode*	Erosion	Steel Rebar
1	Low	Std. aging	Erosion	No rebar
2	Low	Std. aging	No erosion	No rebar
3	Low	Enhanced aging	Erosion	No rebar
4	Low	Enhanced aging	No erosion	No rebar
5	High	Std. aging	Erosion	No rebar
6	High	Std. aging	No erosion	No rebar
7	High	Enhanced aging	Erosion	No rebar
8	High	Enhanced aging	No erosion	No rebar
9	High	Std. aging	Erosion	Rebar
10	High	Std. aging	No erosion	Rebar
11	High	Enhanced aging	Erosion	Rebar
12	High	Enhanced aging	No erosion	Rebar

*: Mode of action of the aggressive agent, Std.: Standard.

The 4 variables under study are 1) acid concentration, 2) mode of action of the aggressive agent, 3) erosion and 4) presence of steel rebar. The individual and synergistic effect of these variables on the concrete degradation process is evaluated. The two levels of the variables are explained below:

- Acid concentration: High (0.5M nitric acid solution) and low (0.025M nitric acid solution)
- Mode of action of the aggressive agent: Enhanced (continuous immersion) and standard aging (cyclic experiment)
- Erosion: Erosion and no erosion
- Rebar: Rebar and no rebar embedded in the concrete

Various aging conditions were considered depending on the variable's interaction (Table 3). These aging conditions are not intended to simulate the tunnel conditions but will consider the primary variables affecting the concrete degradation process. Similar aging conditions will be used in a further stage of the research for evaluating the protective performance of potential coatings.

Concrete Specimens

Concrete specimens with the mix design 25-32, believed to be used in the H-Canyon construction, were prepared for the aging tests. Table 4 summarizes the quantities and proportions of raw materials to prepare a small batch of concrete cylinders with the mix design 25-32.

Table 4. Concrete Mix Design 25-32

Mix components	Weight (lb) or Volume (gals)
Portland Cement	4.94
Slag	1.47
Quartzs fine aggregate (sand) # 4 to #100	19.03
Schist coarse aggregate ¾ " to # 4	11.54
Schist coarse aggregate 1¼" to ¾ "	11.54
Water	0.38
Total	**48.90**

Based on the test plan, concrete specimens with and without embedded rebar were developed for this study. Concrete cylinders without rebar and dimensions of 4 inches in diameter and 8 inches in height were prepared following ASTM C192/C192M-18 [4]. These specimens were used for compression testing and the generation of smaller specimens, used for accelerated aging tests. After mixing the raw materials, the mix was poured in plastic molds in three separate layers. A tapping and rodding process was done after each layer was poured to remove possible air voids inside the mix. Then, the molds were closed with a lid and stored in an isolated location without vibration for 24 +/- 8 hours. After this time, the concrete specimens were removed from the mold and immersed in limewater for curing purposes for 28 days.

Concrete specimens for the aging tests were smaller cylinders with dimensions of 4 inches in diameter and 2 inches in height. The small cylinders were obtained by cutting the 4 x 8 inch cylinders into 4 pieces. At least 6 replicates were utilized for each aging condition, facilitating the development of different measurements over time.

The concrete mix for the specimens with rebar was prepared following the same procedure described above. These specimens' dimensions are 4 inches diameter and 2 inches in height. A first layer of fresh concrete was poured inside the cylindrical plastic mold up to a height of 1.5 inches, followed by the tapping and rodding procedure. Then, a clean steel rod (3.8 inch in length and 0.25 inch diameter) was placed parallel to the surface. A second and final layer of concrete that is 0.5 inches in height was poured on top, also followed by tapping and rodding. The molds were covered with a plastic lid to prevent water evaporation for the next 24 hours. After, specimens were removed from the molds and placed in limewater for 28 days for curing. The end of the concrete cylinder closest to the steel rebar (~ 0.5 inch) was exposed to the aging conditions.

Accelerated Aging Procedures: Enhanced and Standard

Based on literature review and initial test findings, immersion-type tests in nitric acid solutions was proposed as an accelerated aging method for the concrete specimens. The immersion test is not intended to simulate the tunnel's aggressive conditions, but it will allow the development of exemplar aged concrete surfaces, similar to the degraded tunnel walls. Previous immersion-type

experiments performed in our laboratories support this approach [3]. Figure 56 shows the schematic of the experimental test setup developed, where only one end of the concrete cylinder is exposed to the acid solution. This agrees to the HCAEX tunnel situation where only one side of the wall is exposed to the adverse environment. The test setup was placed inside a fume hood to reduce the risk of operator exposure to nitric acid fumes.
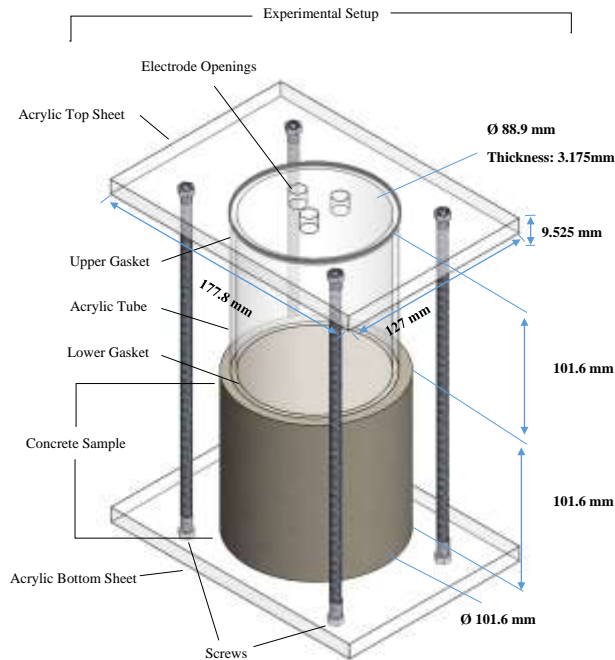
Figure 56. Schematic of new test setup for immersion-type test in acid solutions.

Two modes of the aggressive agents were utilized, enhanced and standard aging. Enhanced aging included continuous immersion of the specimen's top surface in the acid solution and was considered the worst-case scenario at the highest acid concentration. Standard aging, an additional mode of action of the aggressive agent, was centered on cyclic aging.

Cyclic aging included three consecutive steps: 1) immersion in acid solution, 2) exposure in humidity/temperature chamber and 3) exposure to an erosive environment. The times initially proposed for the steps of the cyclic aging were 1) 24 hours immersion, 2) 5 days in the chamber and 3) erode the surface until the removable particles are eliminated from the surface. The proposed times may vary pending on the test results and further discussion with the Savannah River engineers. Figure 57 shows the schematic of the cyclic aging test with all the steps included. The cycle was repeated as many times as needed in order to reach the desired level of degradation. The initial times proposed for each stage of the cyclic experiments are the following: 1) Immersion in the acid solution: 24 hours, 2) Exposure in an environmental chamber: 5 days and 3) Exposure to erosion: approximately a minute, until all removable particles are eliminated.
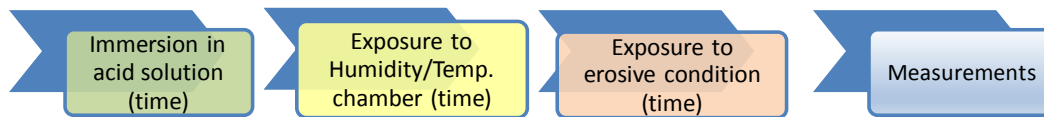
Figure 57. Schematic of a cycle as a standard concrete aging.

The enhanced and standard aging modes were combined with and without the effect of the erosion, as well as with and without the presence of the steel rebar inside the specimen. More details regarding the aging procedures used are described in the summary document with the Test Plan developed [5].

Several durability and mechanical strength measurements such as visual inspection, mass loss, pH changes, porosity, density, compressive strength and others were used for evaluating aged concrete specimens over time, including before and after the aging. More details of the procedures followed for each measurement is detailed in the Test Plan Summary Document [5].

2. Review of Potential Robotic Systems for Deployment

<u>Mobile Platforms</u>

Mobile robotic platforms are designed to interact with environments that are difficult for human beings, under normal or harsh conditions, to enter and traverse under their own power where there is some level of danger posed to them. These platforms can be designed to interact with the environment in many ways, ranging from a multi-legged, a wheeled, or tracked based platform [11]. One of the main attributes the robotics platform requires is the ability to traverse surfaces that lead to a change in orientation, namely moving from a horizontal surface to a vertical surface. Regardless of the method chosen to move along a surface, one must be able to take advantage of some other characteristic that the platform was designed with, in order to maintain its position in a vertical or upside-down orientation.

A multitude of parameters will need to be taken into consideration when developing a platform capable of traversing terrain with varying levels of complexity [12]. The type of surface and surface conditions will play a role in determining which mechanism of transfer is best suited for getting from point A to point B on a planned course. From that point, the mechanism used to create the necessary forces to maintain contact with a surface, specifically the adhesion mechanism, can then be determined. The different types of adhesion mechanisms available range from magnetic, suction, thrust to electrostatic and vacuum [11].

The different adhesion mechanisms will be discussed in the next section where the advantages and disadvantages associated with the use and design of said mechanism will be detailed. The intention here is to simplify the selection process of a surface adhesion mechanism for the development of a multi-use platform capable of performing its task with a high enough confidence level.

<u>Surface Adhesion Mechanisms</u>

The different adhesion mechanisms that are used on robotic mobile platforms whose task is to traverse over a vertical wall, where these units tend to be called wall crawlers, will be described below along with their associated advantage and disadvantage depending on the surface type, surface condition and other associated parameters which may be platform and task dependent.

Vacuum and Suction Cup Systems

The operation of a vacuum ejector, Figure 58, also known as a Venturi vacuum pump, is used to generate a vacuum through an ejector where compressed air is directed towards a nozzle, section A, which results in a jet flow that enters an internal chamber, section B. The air in this chamber with its interaction with ambient air already inside a secondary chamber, creates a pressure difference known as the Venturi effect which causes the air mixture to exit via section C [13]. The vacuum effect is utilized through the use of a port, section D, which is connected to another device called a vacuum cup pictured in Figure 58 below.
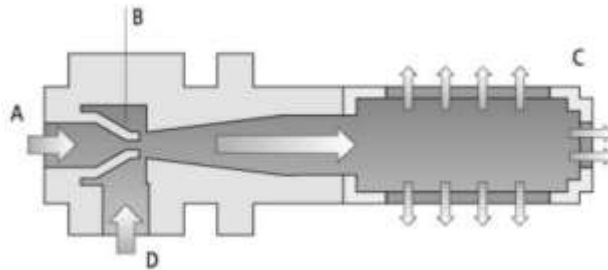
Figure 58. Vacuum ejector [14].

Different types of vacuum cups may be selected based on the geometry of the surface to which the system needs to adhere. Several types of designs are available depending on the condition and surface variations the unit will be dealing with. There are vacuum cups designed to work with smooth and even surfaces, surfaces with small and large variations. In regards to the large surface variation, the EPDM foal seal suction cups would be selected due to the amount of suction force needed to compensate for the large area and low flow rate. Regardless of the cup chosen, the method by which the vacuum is created will remain the same as described above.

Figure 59. Vacuum cups with different geometries [15].

Several wall-climbing robots have applied the vacuum and cup principle, ranging from a sliding suction cup method for locomotion to a robot featuring six legs to aid in locomotion [16], [17].

Ejectors need less maintenance than most other adhesion systems due to the lack of moving parts or complex electronic controls. As long as the ports on the ejector are cleaned periodically, the system can be used continuously. An additional benefit to using the ejector system is the ability to create a compact size ejector unit capable of creating vacuum pressures in a small footprint.

Although there are not moving parts, particle buildup over time can cause clogging within the vacuum at exit ports, which can lead to operation failure of the vacuum system. Vacuum cups are

also highly reliant on seals to create the localized vacuum and are not suitable for surfaces that contain large gaps or have highly imperfect surface conditions.

Non-Contact Pads

Non-contact pads or grippers are normally circular in shape and discharge air towards the target surface, which generates a vacuum zone in the central region near the discharge port. The gripper maintains an equidistance gap between itself and the surface because of the air being discharged in a radial fashion. This method of adhesion relies on having a reliable source of high-flow rate and high-pressure compressed air [18]. Normally, non-contact grippers are used for handling fragile, porous, or sensitive materials, which could include solar cells, food products, and computer chips. Figure 60 below depicts the basic setup of a non-contact gripper and how it interacts with the surface which the adhesion reacts with.
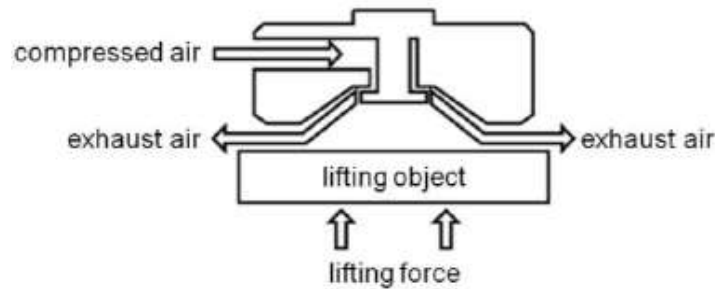
Figure 60. Non-contact adhesion apparatus [18].

Non-contact grippers can be categorized into one of two types: the Bernoulli-type or the cyclone-type grippers for example the grippers produced by SMC Corporation [19]. Bernoulli-type grippers allow for a higher level of stability when dealing with work pieces. This stability stems from the gripper being designed to minimize the amplitude of vibration between the work piece and the gripper.

Cyclone-type grippers are designed to generate a vortex by creating a whirlwind flow originating from the outside of the gripper radius. The flow exits through a gap between the gripper and the target surface. The cyclone effect creates a vacuum zone in the center of the gripper and can create a higher lifting force when compared to that created via the Bernoulli-type gripper. As stated before, the benefit of utilizing the Bernoulli-type gripper is the stability in the air flow gap between the gripper and the surface target.

Although these types of grippers are widely used to handle sensitive products within various industries, wall-climbing robots that use non-contact adhesion are very limited. An example of wall-climbing robot utilizing these types of non-contact grippers is the NCAP robot unit pictured in Figure 61, or the wall-climber that is able to traverse varying surfaces including brick walls and a gap between a wall and door [20].

Figure 61. NCAP robot equipped with non-contact grippers [21].

The main benefit of using this method is the fact that the non-contact grippers require little to no maintenance, since any dust or small debris that enters the system is blown out due to the natural operation of the gripper.

The non-contact gripper does not contact the target surface, for example a wall surface, so one of its disadvantages is that there are no lateral forces produced between the gripper and the target surface. This means the gripper is free to move along the surface with little to no resistance. This can be remedied by having some other method of creating friction forces to restrict movement, for example rubber wheels. Another drawback is the need to have a pressure line to the unit for continuous air supply to create the adhesion force. Another disadvantage to this system is the distance that needs to be maintained between the underside of the gripper and the surface. If there is a large enough surface variation, this causes the force of adhesion to be reduced which could lead to failure.

Fan-Based or Thrust Based Units

The thrust-based or fan-based method of adhesion discussed here is the most widely applied method to wall climbing since it utilizes fans to provide a reliable and efficient means of high-force surface adhesion. Fan blades attached to high-power electric motors are used in a variety of ways, providing thrust normal to the target surface, inducing suction underneath a robot body, propelling the system forward itself. Some of the different types of fans available are electric ducted fans (EDF) which is used for high volume air output and the impeller-based fan which creates a large pressure difference that in turns creates a low pressure suction zone.

A very popular example of a fan-based wall-climbing system is the Vertigo robot pictured in Figure 62, which was co-developed by Disney and ETH Zurich. Some of the design factors that were considered when developing this unit were high mobility, horizontal to vertical surface transition capabilities and maximized thrust output to weight ratio. In order to minimize the weight of the unit, the Vertigo unit does not have motorized wheels, but is able to move along a surface by utilizing the fans to produce forward movement and a tandem servo setup to turn the wheels. The platform also takes advantage of low weight and high strength carbon fiber for the chassis construction.

Figure 62. ETH Zurich and Disney collaboration robot: Vertigo [22].

For most fan designs, air flow is induced through constant contact with the blades. Fan-based systems contain high-RPM motors along with a variety of blade designs such as propellers and impellers. This allows one to choose the type of adhesion mechanism created. The use of impellers can be used to create negative pressure zone within a chamber, which in turns creates a suction force of attraction between the unit and the target surface. If a propeller is used, a large thrust vortex can be created, which if directed correctly, can be utilized to create a contact force between the mobile unit and the surface. With the correct design configuration, EDFs can be used to created either one of the suction forces or thrust force if enough power is delivered to the unit in a constant manner [23], [24].

One of the drawbacks to using these fan-based systems is the need for a large power source to power the fans. Another disadvantage to the use of the system are the integrity of the blades. If any of the blades are damaged, this could create an imbalance in the system, which will be exaggerated because of the associated RPMs of the fan. This can lead to catastrophic failure of the fan as a ,whole which in turns means that if the unit was transitioned to an orientation different from horizontal, then the platform will no longer be experiencing the forces needed for it to maintain contact with the target surface.

Dry Adhesive Pads

The driving force behind the development of the dry adhesive pads is to have a self-cleaning, reliable, and low release force adhesion to both smooth and rough surfaces. The pads are similar to a gecko's foot, seen in Figure 63 and Figure 64, which it uses to traverse vertical and overhanging surfaces. A gecko's foot consists of layered structures, which allows the gecko to apply directional adhesive forces onto a surface and a low detached force. Directional adhesive pads allow for the adhesion forces that are proportional to the tangential load parallel to the direction of movement, while exhibiting a low detachment force that allows for a more efficient movement [27].
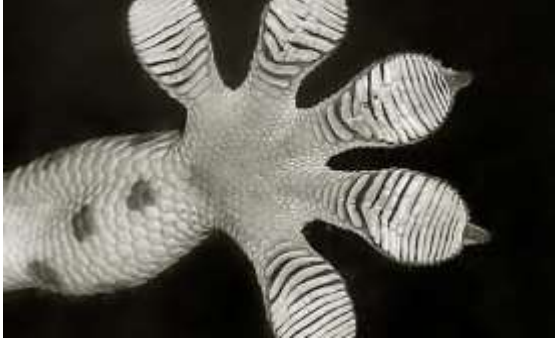
Figure 63. Gecko foot and pad structure [25].
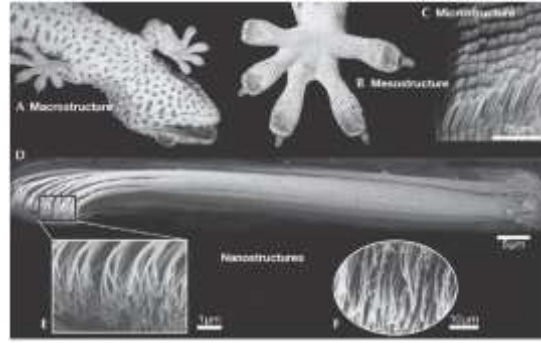
Figure 64. Microstructure of a gecko's foot [26].

Considerable efforts have been directed towards mimicking gecko pads and characterizing the behavior of their movement along a surface. Advances have been made in moving along a vertical surface and their overhang movement capabilities [28]. Additionally, high payload capability of directional dry adhesive pads has been documented, with a miniature single-actuation robot supporting a payload more than 100 times its own weight [29]. This leads to other research that focuses primarily on simplified locomotion mechanisms that can benefit from the low lift-off force required by dry adhesives [30].

Advantages of these adhesive pads are low maintenance and long-term use. Since a small amount of force is needed to detach the pad from the surface, this can lead to a more natural movement of the platform along the surface and less energy usage on detachment. Another advantage of the pads is their ability to stick to a wide variety of surfaces and still allow for movement along horizontal, vertical, and overhanging surfaces.

The primary drawback for dry adhesion also happens to be related to one of its many strengths: directionality. Although the pads would allow for efficient movement in a single direction, it may prove difficult to move back in the opposite direction depending on the orientation of the system. For example, if a robot using dry adhesives at the ends of its legs climbs up a wall, the only feasible way for it to come back down would be to move backwards due to its directional nature. If the robot were to make a 180-degree turn and try to move forward to descend the wall, the dry adhesive would not be able to provide sufficient holding force.

Adaptive Claw and Spine Mechanisms

This adhesion mechanism is inspired from how insects and other clawed animals climb up trees and walls and hold their position. Robots that use this method rely on claws or hooks as well as spines to grasp surface aberrations that are present on the climbing surface. Depending on the surface quality, a specifically sized and designed holding mechanism like hooks can be used to match the surface conditions which allow for grasping or securing of the platform via its interaction with its surroundings. Most applications of the adaptive claw and spine mechanism make use of it by featuring multiple hooks that can move independently from one another so that the chances of hooking the surface are increased.
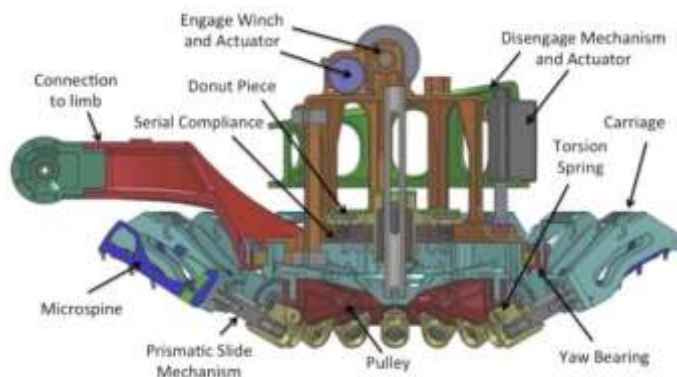
Figure 65. Mechanism for NASA's LEMUR gripper [31].

An example of a claw mechanism is the LEMUR robot developed by NASA's Jet Propulsion Laboratory, which features four circular claw arrays such as the one displayed in Figure 65. The overall operation of the claw mechanism involves the actuation of the carriage in which hundreds of micro-spines reside, resulting in a dragging motion across the target surface in all principle directions within reach of the gripper. Each micro-spine set within the carriages can move independently from each other and can stop moving when either the micro-spines catch onto surface asperities or reaches the end of the actuation travel. It should be noted that the entire dragging movement can be achieved using only a single actuator located at the top of the gripper. As a commonly used climbing method, quite a few applications exist ranging from claws and grippers that grab onto wall protrusions to robots with many claws that attempt to grip onto a variety of surfaces [32]. For our purpose, crawlers that feature micro-spines are of particular interest, especially due to the success of a prototype rock-climbing robot developed alongside NASA JPL [33].

Advantages of using the adaptive claw mechanism is its ability to adapt to irregular surfaces and the array of claws and spines, in a single gripper, to allow for a high chance of catching onto surface imperfections. Examples of these irregular surface are brick walls, concrete walls or rocky surfaces. Adaptive claw mechanism-based platforms can also maintain their position on the appropriate surface for a long period of time with minimal risk of falling off when loss of power is experienced.

The major disadvantage to using the claw-based system is that the system payload is dependent on the surface of interest and the design of the claws and spines for the grippers. Another is the smoothness of the target surface, if it is something like glass, the spines or claws will not be able to secure itself for proper adhesion force generation. Claw-based systems are also limited to speed since adequate time needs to be set aside for proper surface adhesion.

Electrostatic Adhesion

Electrostatic adhesion, or electro-adhesion, uses an electrostatic force between the target surface and a pad, generated from the potential difference between two sets of electrodes. Generally, these electrodes are high in voltage but require very low current to create the adhesion force, or clamping force, on the surface. The potential difference between the electrodes create an electric field that results in an opposite charge being set up on the target surface. The pad should exhibit high workability and compliance to allow for use on multiple surfaces, but rigid variants can also be used depending on the surface in question. The flexibility of the material used enables the pad to conform to rougher surface types by maintaining proximity to the surface as the pad deforms.
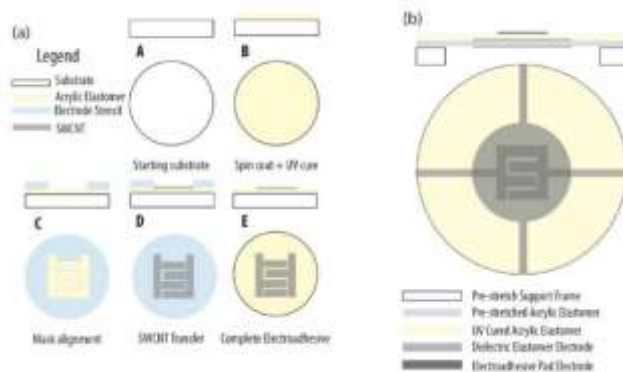
Figure 66. Breakdown of an electrostatic adhesion pad [34].

Figure 66 depicts an electrostatic adhesion pad along with the components necessary for its construction. Adhesion pads are used for handling fragile materials in an automated production system [35]. An electrode or electrodes are sandwiched together between an acrylic support creating a disk that can be placed on a mechanism that makes it touch the target surface. Also, electro-static adhesion based units can be a replacement for dry adhesion for applications that seek to mimic the gecko locomotion pattern [36].

Advantages of this adhesion mechanism is its ability to adhere to multiple types of surfaces even when dust or moisture is present. The design of the electro-static adhesive pads requires a small amount of power to generate the forces for surface adhesion. The adhesive pads can also be retrofitted over wheels, treads, or feet of legged platforms. Maintenance is simplified via cleaning the contact pads when power is turned off.

Magnetic Adhesion

Magnetic adhesion relies on the attraction of onboard system magnets to a magnetic surface. Either permanent magnets, electromagnets, or a combination of both can be used as the primary means of creating the forces for adhesion to the surface. Magnets can be designed to replace locomotion components composed of a different material, such as a wheel manufactured from a permanent magnet. This also means that the magnetic adhesion force can be developed separately from the locomotion mechanism. This type of adhesion is an example of an entirely surface-dependent operation. This means that the platform can be designed freely without much constraint as long the magnetic forces that are created can handle the weight of the unit along with its payload.

Applications that utilize this adhesion mechanism are centered on the inspection of metallic surfaces such as those found on tanks and ships. Examples of robotic platforms utilizing this adhesion method are the ReconRobotics Recon Scout ship climber, Figure 67, which is used for ship hull inspections and the mini rover being developed at the ARC robotics lab, Figure 68. The mini rover uses magnets to cling to metallic tank floors for inspection in nuclear waste tanks [37].

Figure 67. ReconRobotics Recon Scout magnetic ship climber [38].

Figure 68. FIU Applied Research Center's Mini Rover.

A major advantage to the magnetically-based platform is the simplicity of the design that can be achieved along with the use of currently available magnets that are now manufactured in small scale with magnetic properties that rival their larger counterparts. Adhesion force to unit weight ratio is substantial enough to allow for significant payload sizes. The ability to find permanent magnets in small factor form allows one to design wheels that can be embedded with these magnets and used as part of the motion inducing mechanism.

The one major disadvantage to the magnetically-based adhesion system is the limitation on the type of surfaces one can target for surface movement. Another factor is that as the distance between the magnet and the surface increases, the magnetic force of attraction between the magnet and the metallic surfaces drops significantly.

Subtask 18.3: Results and Discussion

1. Concrete Aging: Initial Testing and Development and Execution of Test Plan

In this section, the preliminary results and discussion of the ongoing accelerated aging of concrete specimens through various aging conditions are presented. Durability and mechanical measurements including visual inspection, weight loss, pH changes (test solution), water absorption, porosity and compressive strength results are discussed. The results of the initial testing performed and preliminary data of the execution of the test plan are reported here.

Compressive Strength

Figure 69 shows the surface of the concrete cylinders before and after the test. Crack formations were observed on the concrete surface indicating the end of the compression test.

A   B   Zoom
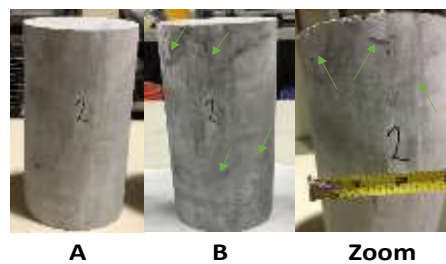
Figure 69. Images of the concrete cylinders (replicate 2) before (A) and after (B) the compression test. Arrows represent the cracks after compression test.

The compressive strength, f, was calculated using the following equation ($f = \frac{Pmax}{A}$), where P_{max} is the maximum load that the concrete specimen could hold and A is the circular area exposed to the load [6]. For each specimen, the P_{max} was obtained during the test and the area was calculated. The average compressive strength of the concrete was approximately 3625 psi, slightly higher than the value reported by the Savannah River engineers (2500 psi) for a similar concrete mix. This value is acceptable, considering the composition of the raw materials (e.g. schist coarse aggregates) utilized for the specimen's preparation is likely different from the material used for preparing the concrete at the H-Canyon 60 years ago.

<u>Density, Water Absorption and Voids</u>

The calculated density, water absorption and voids (porosity) of the concrete specimens in the as-received conditions (before testing) are presented in Table 5. The ASTM C642-13 standard was followed for the experimental procedure and the necessary calculations performed [7].

A recent study investigated the positive effect of the addition of nanomaterials on the material's properties such as porosity, water absorption, weight loss, compressive strength. In general, the concrete specimens with nanomaterials showed a decrease of porosity and water absorption, with values less than 7% and 3%, respectively, compared to concrete without nanomaterials [8]. The porosity and water absorption values of the H-Canyon concrete are greater (~ 13% and ~6%, respectively) than the former values reported in the literature. These results will lead to a faster degradation of the material after being exposed to aggressive conditions.

Table 5. Average, Maximum and Minimum Values of Water Absorption, Density and Voids (porosity) of Hardened Concrete Specimens before Testing

Parameters	Water absorption [%]	Density (mg/m^3)	Voids (%)
Average	5.58	2.31	13.36
Maximum	6.50	2.35	15.21
Minimum	4.83	2.26	11.82

It is well established that the increase of concrete porosity has a negative effect on the strength and durability. A more porous material will favor an increased entry of water and aggressive agents (oxygen, acids, etc.) and consequently, will negatively impact its durability. It is expected that the acid attack will lead to a more porous and less dense concrete, which will favor water absorption. Tracking porosity, water absorption and density over time can provide insight of the material degradation and its durability. These properties can be correlated with other durability measures (e.g. weight loss) and mechanical properties (e.g. compressive strength).

Enhanced Aging: Test 7 and Test 8

<u>Visual Inspection</u>

Based on findings of the initial testing developed in our laboratories, where concrete specimens immersed in the 0.5M solution depicted a fastest degradation, the enhanced aging condition of Test 7, with the highest concentration of the acid solution and erosion, was considered the worst-case scenario of the test plan. Figure 70 shows images of a selected concrete specimen of Test 7, identified as HEE1, exposed to 0.5M nitric acid solution and erosion over time. It is evident from the figure the progress of the degradation with time, characterized by the loss of material from the

matrix and protrusion of the coarse aggregate. The action of the steel wire brush on the aged surface exposed to the acid solution accelerates the aging process by eroding the surface and eliminating all removable particles. Three different views of the images (angle, side and top) were taken to facilitate the observation of degradation.
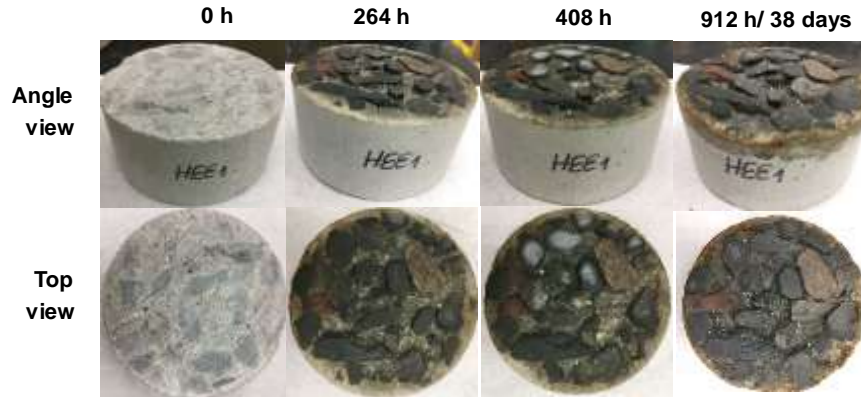
Figure 70. Images of a concrete specimen before and after enhanced aging conditions of Test 7. HEE1 was selected as representative of the 6 replicates tested. (Surface was wet at the time the pictures were taken, except for the initial images).

Figure 71 shows images of a concrete specimen from Test 8, identified as HE1, exposed to 0.5M nitric acid solution. There is a slight degradation of the concrete surface exposed to the acid solution, but it is not as evident as in specimen HEE1 of Test 7. Also, no protrusion of the coarse aggregate was observed, although a slight loss of material from the matrix was observed.
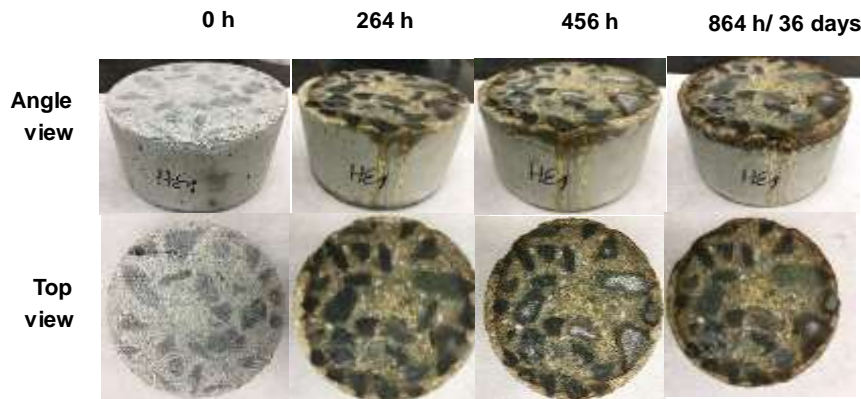
Figure 71. Images of a concrete specimen before and after enhanced aging conditions of Test 8, immersion in 0.5M nitric acid solution, over time. Surface was wet at the time the picture was taken, except for the images at initial time. HE1 was selected as representative of the 6 replicates tested.

Figure 72 shows a comparison of images of the concrete specimens exposed to the Test 7 and Test 8 enhanced aging conditions at the end of the experiment. There is a greater degradation of concrete specimens of Test 7, exposed to acid immersion and erosion, compared to specimens of Test 8, only exposed to acid immersion.

912 h/ 38 days   **864 h/ 36 days**
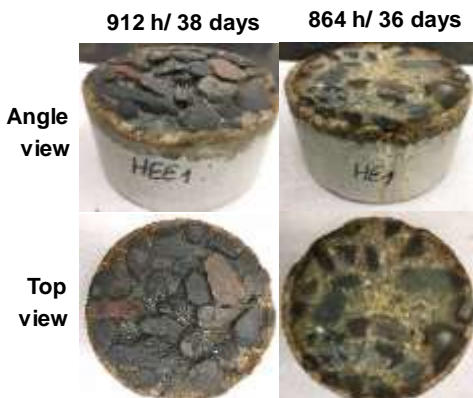
Figure 72. Comparison of Images of a selected concrete specimen HE1 exposed to immersion in 0.5M nitric acid solution without erosion.

Weight Loss

Weight loss is a quantitative parameter that measures the degradation of the material and it is related to its durability. Figure 73 shows the average weight loss of the concrete specimens exposed to the aging conditions of Test 7, 0.5M acid solution and erosion, and Test 8, 0.5M acid solution. As a general trend, the weight loss increases with time for concrete specimens exposed to the aging conditions of Test 7 and Test 8. The fastest and greatest weight loss was confirmed for those samples exposed to the Test 7 aging condition that lost an average of ~ 9% (~78 g) of their weight in 38 days. However, specimens submitted to the aging conditions of Test 8 experienced a slower weight loss, up to ~ 3% (~ 23 g) of their average weight in 36 days. This is because concrete specimens of Test 7 were submitted to the combined effect of the acid solution and erosion, compared to specimens of Test 8 exposed to the single effect of the acid solution. These results agree with the visual inspection findings.
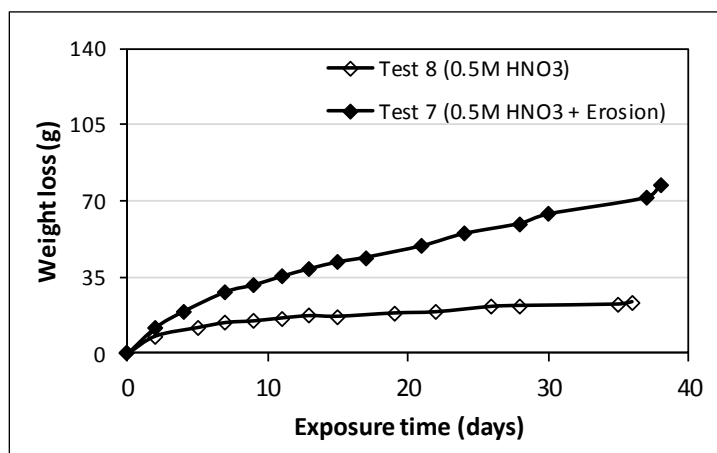
Figure 73. Average weight loss with time of concrete specimens exposed to Test 7, 0.5M HNO3 solution and erosion, and Test 8, 0.5M HNO3 solution, enhanced aging conditions.

pH Changes

The pH change of the nitric acid solution was also monitored with time, as shown in Figure 74. The pH change is an indicator of the occurrence of acid attack on the concrete surfaces due to an acid-base reaction between the concrete and the acid [3] that will lead to a pH increase of the

solution. Consequently, the pH and alkalinity of the concrete samples will be affected leading to the material deterioration. The figure shows variation of the solution pH, which was faster at the initial stages than later in the aging. The pH variations are represented by peaks from the expected pH value for the 0.5M solution (pH=0.3), indicating acid consumption. The concentration of the acid solution was adjusted to the corresponding pH value by adding concentrated acid.
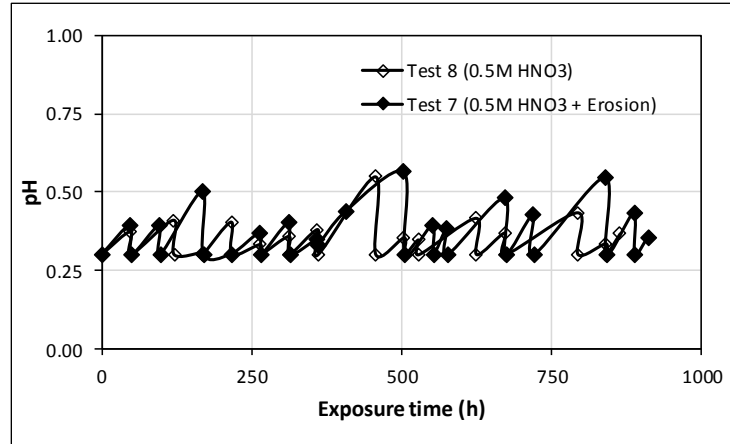
Figure 74. pH changes of the 0.5m nitric acid solutions used for Test 7 and Test 8.

The strong nature of the nitric acid combined with the high concentration of the acid (pH<1) influenced in the degradation observed. This is in agreement with previous studies [3], [9-10] related to concrete acid attack that demonstrated the key role of the type of acid, the concentration, the type of concrete, etc. on the intensity of the degradation. In addition, preliminary research findings confirmed a good correlation among the monitored parameters (visual inspection, weight loss, pH of the solution) [3].

Distance of Protruded Aggregates

The distance of the protruded aggregates is also a quantitative parameter that directly relates to the degradation and durability of the material. The distance of protruded aggregates for concrete specimens of Test 7 increased with time, with an average value of 0.73 cm (0.3 in), after 38 days of aging conditions. This data supports previous findings. However, specimens with Test 8 aging conditions that were not exposed to erosion did not show protruded aggregates with time.

2.   Review of Potential Robotic Systems for Deployment

Mobile Platform Construction Utilizing Surface Adhesion Mechanism

The platform design chosen to test the selected adhesion mechanism is a wheel-based platform. The adhesion mechanism selected is a thrust approach, which was chosen based on the environmental conditions inside of the HCAEX tunnel along with the type of payload necessary to accomplish the task of coating the concrete walls without further damaging the walls. The fan unit used to create the thrust to provide contact with the target surface is the Dr. Mad Thrust 90mm EDF unit, Figure 75. This fan is capable of generating 3.8kg of thrust.

Figure 75. Dr. Mad Thrust 90mm EDF unit (blade and side view).

The design for the wheeled based platform was generated in Solidworks, Figure 76, and 3D printed using PLA, Figure 77. The platform utilizes four motors that work independently to create the movement necessary to reach a desired location. The prototype is designed to operate on power supplied through either an on board LiPo battery or connected to a dedicated power line via a tether. The platform is also equipped with an inertial measurement unit (IMU) which is used to detect the orientation of the system and a camera for visual based navigation via teleoperation.

Figure 76. CAD design of thrust based prototype.
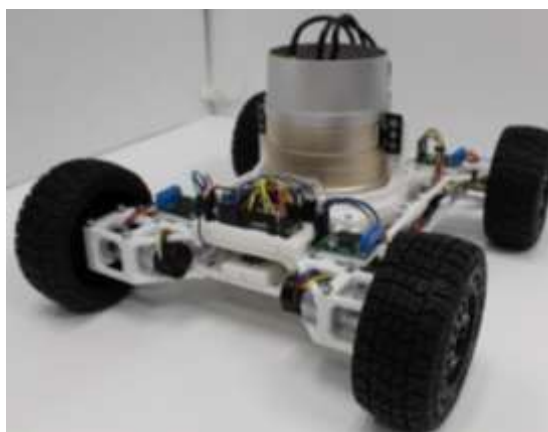
Figure 77. Current thrust based prototype with EDF unit as its center.

The robotic mobile platform is controlled remotely using a gamepad via a Robot Operating System (ROS) serving as the middleware between the end user, the operator, and the platform itself. The platform also makes use of large rubber tires whose main purpose is to create as much traction with the wall surface as possible increasing the friction force needed for movement and transitioning to walls or ceilings.

Small Scale Concrete Wall Mockup

A small-scale concrete wall mockup was constructed to test the ability of the prototype crawler to traverse a surface of varying conditions, Figure 78. The mixture for the concrete mix is composed of large aggregate pieces that is intended to represent the exposed aggregate on the tunnel wall. The mockup also includes smooth surfaces as well as an exposed mesh section.

Figure 78. Varying surface condition of small-scale concrete wall.

The objective of constructing the mockup is to test a wall crawler's ability to transition from the ground to the wall while maintaining contact with the concrete surface, regardless of the surface conditions.

Testing of Robotic Concrete Wall Crawler

Figure 79 depicts the initial prototype transitioning from the floor to the wall and traversing the wall vertically along the various surface conditions. Since this platform adheres by thrust, it is important that the forces generated by the fan and motors are enough to overcome the effects of the surface anomalies and gravity.
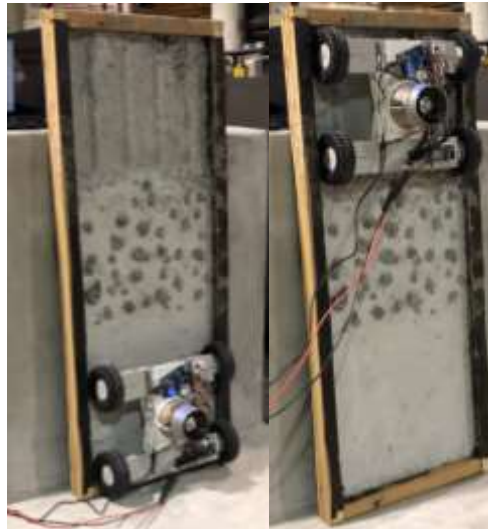
Figure 79. Prototype completing horizontal to vertical transition (left) and completing test over varying surface conditions along a vertical wall (right).

Even though the crawler was capable of transitioning from the floor to the wall and traversing along the scaled wall in the vertical direction, the system was redesigned to reduce the weight of

the unit by 25% while maintaining the strength and stiffness in the chassis design. Figure 77, above, depicts the current design of the single EDF based platform.

A small-scale wind generator was also constructed to test the capabilities of the platform to remain in contact with the surface when exposed to 25 mph wind speeds. As depicted in Figure 80, the unit was able to withstand the wind and traverse the vertical surface while generating the necessary adhesion forces required.
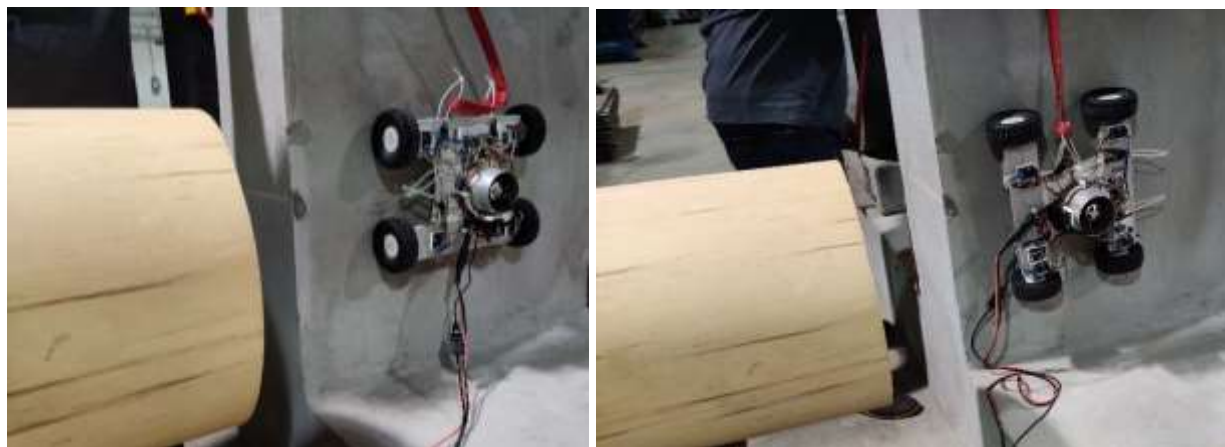
Figure 80. Prototype 1 under 25mph wind speed test.

Subtask 18.3.2: Conclusions

Based on lessons learned and preliminary research findings of concrete aging (previous testing phase), a comprehensive test plan for the development of aged concrete surfaces similar to the tunnel degraded walls was developed and approved by our Savannah River collaborators. Various accelerated aging conditions including the synergistic and single effects of potential variables (acid concentration, erosion, action mode of the aggressive agent, etc.) affecting the concrete degradation process were included. From the preliminary results of concrete specimens exposed to the enhanced aging conditions of Test 7 and Test 8 with and without erosion, and using the highest concentration of the nitric acid solution (0.5M), multiple conclusions were obtained. These include:

- The enhanced aging tests proved to be an adequate and feasible method to perform accelerated aging of concrete, providing valuable insights regarding the aging process.
- The enhanced aging Test 7, combining the action of the 0.5M acid solution and erosion, proved to be the most aggressive environment leading to the fastest and most intense degradation of the concrete specimens. The fastest and greater deterioration of the concrete matrix contributed to the protrusion of the coarse aggregates.
- Concrete specimens submitted to erosion degraded faster than specimens that were not eroded.
- A good correlation among the tested parameters (visual inspection, weight loss, pH and distance of the protrusion) was observed for the aging conditions investigated (Test 7 and Test 8).

In addition, a detailed literature review was conducted for different adhesion mechanisms for the development of a platform designed to navigate on a vertical surface, in this case a degraded

concrete wall. FIU then developed a proof-of-concept mobile platform that could navigate in the hostile environment of the HCAEX tunnel, which includes 30 mph winds and low lighting conditions. A thrust based adhesion system was selected as the initial approach to generate the adhesion forces required by a platform to transverse a vertical wall. A 4-wheeled platform was designed and its primary components were 3D printed. Electronic components were also integrated onto the platform for wired and wireless communication and visual and data sensor feedback. A scaled mockup was constructed to test the ability of the mobile platform to transition from the floor to the wall and maintain its orientation in the vertical direction as it traverses up the concrete wall. The prototype was tested under normal environmental conditions on a concrete surface and then exposed to 25 mph wind speeds generated by a small-scale wind generator. The unit was successful in traversing the surface while subjected to the wind and continued to generate the thrust necessary to maintain contact with the surface.

Subtask 18.3.2: References

1. Gilliam, Bob J., Ray, J., and Giddings, B. "Inspection and assessment of the H-Canyon ventilation system at The Savannah River Site". Phoenix, Arizona. s.n., 2015. Waste Management Conference.

2. Staff Report, Defense nuclear facilities safety board. "H-Canyon exhaust tunnel fragility analysis input and assumptions". 2018.

3. Echeverria, M., Nunez Abreu, A., Lagos, L., McDaniel, D. "Aging of concrete for the evaluation of repair materials to protect the HCAEX tunnel at Savannah River". Waste Management 2020 Conference, Phoenix, AZ, March 2020. (Best Poster of Track). Paper # 20301

4. ASTM C192/C192M-18. Standard Practice for Making and Curing Concrete Test Specimens in the Laboratory. 2018.

5. Echeverria, M, McDaniel, D, Nunez, A, Lagos, L, et al. 2020. "Test plan developed for the H-Canyon study. Accelerated aging of concrete". (FIU-ARC- 2018-800006470-02c-269). Work supported by U.S. Department of Energy Office of Environmental Management under Cooperative Agreement # DE-EM0000598.

6. ASTM C39/C39M-18. Standard Test Method for Compressive Strength of Cylindrical Concrete Specimens.

7. ASTM C642-13. Standard Test Method for Density, Absorption, and Voids in Hardened Concrete.

8. Diab, A., et al. "Effect of nanomaterials additives on performance of concrete resistance against magnesium sulfate and acids". Construction and Building Materials 210 (2019), pp. 210-231.

9. Pavlík, V. "Corrosion of hardened cement paste by acetic and nitric acids. Part I: Calculation of corrosion depth". Cement and Concrete Res., 24 (1994), pp. 551-562.

10. Alexander, M., Bentur, A. and Mindess, S. "Durability of concrete. Design and construction". CRC Press Taylor and Francis Group, 2017.

11. D. Schmidt and K. Berns, "Climbing robots for maintenance and inspections of vertical structures-A survey of design aspects and technologies", *Rob. Auton. Syst*, vol. 61, no. 12, pp. 1288-1305, 2013.

12. C. Balaguer, A. Gimenez and A. Jardon, "Climbing Robots' Mobility for Inspection and Maintenance of 3D Complex Environments", *Auton. Robots*, vol. 18, no. 2, pp. 157-169, Mar. 2005.

13. F. D. Berkeley, "*Ejectors have a wide range of uses*", Petroleum Refiner, 1958.

14. Vacuum ejector information. [Online] Available: https://www.schmalz.com/en/vacuum-knowledge/the-vacuum-system-and-its-components/vacuum-generators/vacuum-ejectors/.

15. Vacuum cups information. [Online] Available: https://www.destaco.com/vacuum-cups.html.

16. Z.-y. Qian, Y.-z. Zhao, and Z. Fu, "Development of wall-climbing robots with sliding suction cups", *IEEE International Conference on Intelligent Robots and Systems*, pp. 3417–3422, 2006. doi: https://doi.org/10. 1109/IROS.2006.282579.

17. Y. Li, M.-t. Li, and L.-n. Sun, "Design and passable ability of transitions analysis of a six-legged wall-climbing robot", *IEEE International Conference on Mechatronics and Automation*, pp. 800–804, 2007. DOI: https: //doi.org/10.1109/ICMA.2007.4303647

18. K. Stuhm, A. Tornow, J. Schmitt, L. Grunau, F. Dietrich, and K. Droder, "A novel gripper for battery electrodes based on the bernoulli-principle with integrated exhaust air compensation", Procedia CIRP, vol. 23, no. C, pp. 161–164, 2014. DOI: https://doi.org/10.1016/j.procir.2014.10.065.

19. S. World. Non-contact gripper information, [Online]. Available: http://www.smcworld.com/newproducts/en/pdf/xt661.pdf

20. M. Wagner, X. CHen, M. Nayyerloo, W. Wang, and J. G. Chase, "A novel wall climbing robot based on bernoulli eff ect", IEEE/ASME Inter-national Conference on Mechatronics and Embedded Systems and Applications, pp. 210–215, 2008. DOI:https://doi.org/10.1109/MESA.2008. 4735656.

21. NCAP Robot Platform information: [Online] Available: https://spectrum.ieee.org/automaton/robotics/industrial-robots/robot-uses-supersonic-jets-of-air-to-stick-to-almost-anything.

22. ETH Zurich and Disney mobile platform information. [Online] Available: https://spectrum.ieee.org/automaton/robotics/drones/disney-vertigo-combines-car-helicopter-to-drive-up-walls.

23. J. Li, X. Gao, N. Fan, W. Zhu, J. Yin, and Y. Jia, "Wall climbing robot based on negative pressure-thrust suction method", Proceedings of 2008 IEEE International Conference on Mechatronics and Automation, ICMA 2008, pp. 604–609, 2008. DOI: https://doi.org/10.1109/ICMA.2008. 4798825.

24. P. Sekhar and R. S. Bhooshan, "Duct fan-based wall climbing robot for concrete surface crack inspection", 11th IEEE India Conference: Emerging Trends and Innovation in Technology, INDICON 2014, 2015. DOI: https: //doi.org/10.1109/INDICON.2014.7030589.

25. Gecko feet and pad structure information. [Online] Available: https://www.greenbiz.com/blog/2014/07/01/gecko-dry-adhesive-slow-disruptive-innovation.

26. Microstructures of gecko feet information. [Online] Available: https://www.scpr.org/news/2016/03/21/58699/jpl-sending-spider-man-like-adhesives-to-space/.

27. D. Santos, M. Spenko, A. Parness, S. Kim, and M. Cutkosky, "Directional adhesion for climbing: Theoretical and practical considerations", Journal of Adhesion Science and Technology, vol. 21, no. 12-13, pp. 1317–1341, 2007. DOI: https://doi.org/10.1163/156856107782328399.

28. D. Santos, B. Heyneman, S. Kim, N. Esparza, and M. R. Cutkosky, "Gecko-inspired climbing behaviors on vertical and overhanging surfaces", Proceedings - IEEE International Conference on Robotics and Automation, pp. 1125–1131, 2008. DOI: https://doi.org.10.1109/ROBOT.2008.4543355.

29. E. W. Hawkes, D. L. Christensen, and M. R. Cutkosky, "Vertical dry adhesive climbing with a 100x bodyweight payload", Proceedings - IEEE International Conference on Robotics and Automation, vol. 2015-June, pp. 3762–3769, 2015. DOI: https: / / doi.org/10.1109/ICRA.2015. 7139722.

30. Y. Liu and T. Seo, "Anyclimb-ii: Dry-adhesive linkage-type climbing robot for uneven vertical surfaces", Mechanism and Machine Theory, vol. 124, pp. 197–210, 2018. doi: https://doi.org/10.1016/j.mechmachtheory. 2018.02.010.

31. NASA LEMUR gripper information. [Online] Available: https://www.engineering.com/Education/EducationArticles/ArticleID/6598/Weve-Just-Seen-NASAs-Rock-Climbing-Robot-and-it-is-Awesome.aspx.

32. S. Kim, A. Asbeck, M. Cutkosky, and W. Provancher, "Spinybotii: Climbing hard walls with compliant micro-spines", 2005 International Conference on Advanced Robotics, ICAR '05, Proceedings, pp. 601–606, 2005. DOI: https://doi.org/10.1109/ICAR.2005.1507470.

33. A. Parness, N. Abcouwer, C. Fuller, N. Wiltsie, J. Nash, and B. Kennedy, "Lemur 3: A limbed climbing robot for extreme terrain mobility in space", Proceedings - IEEE International Conference on Robotics and Automation, pp. 5467–5473, 2017. DOI: https://doi.org/10.1109/ICRA.2017. 7989643.

34. Mihai Duduta, Robert J. Wood, and David R. Clarke "Flexible, stretchable electroadhesives based on acrylic elastomers", Proc. SPIE 9798, Electroactive Polymer Actuators and Devices (EAPAD) 2016, 97981D (15 April 2016); https://doi.org/10.1117/12.2218911.

35. G. Monkman, "Electro-adhesive microgrippers", Industrial Robot, 2003. DOI: https://doi.org/10.1108/01439910310479595.

36. R. Chen, "A gecko-inspired electro-adhesive wall-climbing robot", IEEE Potentials, vol. 34, no. 2, pp. 15–19, 2015. DOI: https://doi.org/10. 1109/MPOT.2014.2360020.

37. M. DiBono, A. Abrahao, D. McDaniel, and Y. T. Tan, "Development and testing of robotic inspection tools for the hanford high-level waste double shell tanks", *30th Florida Conference on Recent Advances in Robotics*, FAU, 2017. DOI: http://public.eng.fau.edu/design/fcrar2017/papers/DevelopmentTestingofRoboticInspection.pdf.

38. ReconRobotics Recon Scout throwable robot information. [Online] Available: https://spectrum.ieee.org/automaton/robotics/military-robots/new-recon-scout-throwbot-can-climb-ship-hulls-spy-on-pirates.

TASK 19: PIPELINE INTEGRITY AND ANALYSIS

Task 19: Executive Summary

Structural health of waste transfer and storage infrastructure is of utmost importance to DOE and communities surrounding the active sites. A Fitness-for-Service (FFS) program for the Waste Transfer System has been implemented by the US Department of Energy (DOE) through the contractor - Washington River Protection Solutions (WRPS), for the purposes of evaluating and quantifying the structural integrity of critical components such as the pipelines, tanks and tank farm waste transfer system. The purpose of the program was to inspect primary piping, encasements, and jumpers for corrosion/erosion, which has been accomplished in the previous years. Various sensor systems have been investigated, down selected and tested. The Ultrasonic sensor system from Permasense has been evaluated for the measurement accuracy and performance under high temperature and humidity conditions. This past year, focus has been on studying the feasibility of radiation effects on the Permasense ultrasonics sensors. An additional sensor system was also investigated for the leak and fault detection in pipe loops using the fiber optic electro acoustic principles. This system is called the Fiberstrike Sensor System from Cleveland Electric Limited (CEL). This task had stemmed due to the collaborative talks between DOE, industry (sensor vendor (CEL)), WRPS and FIU. The sensor vendor leased the system to FIU in order to investigate the faults and leak detection in carbon steel pipe loops and validate their technology on an engineering scale, for potential deployment at the DOE sites. FIU conducted the experiments and results indicated that the system was successfully able to detect pipeline faults, leaks, pump malfunctions and valve blockage issues related to the waste transfer system and is capable of the cold test demonstrations at the sites. Further, SRNL has tasked FIU with lab, bench and engineering scale testing of their patented mass loss coupon technology for small scale wear detection in pipes and transfer lines. The coupons are used to measure slight changes in mass loss due to erosion and to quantify the thinning in the pipe diameter on a precise level using the UT pencil sensor probes. The coupons were able to provide the visual erosion when inspected under the microscope/SEM. This past year, the task concentrated on completing the carbon steel coupon testing on the engineering scale loop and initiated the evaluation of the stainless-steel coupons and decisions regarding the caustic simulant testing have been finalized.

Structural integrity of non-metallic materials is also being investigated under the current research work. Nonmetallic materials used in the Hanford Site Tank Farm waste transfer system include the inner primary hoses in the hose-in-hose transfer lines (HIHTLs), Garlock® gaskets, ethylene propylene diene monomer (EPDM) O-rings, and similar other nonmetallic materials. These materials are exposed to radiation, caustic solutions and elevated temperature and pressure stressors. While the individual effect of these stressors has been well established, their combined effect is of significance to the Hanford site. FIU has been supporting this task by developing a test loop and testing the non-metallic materials under simultaneous stressor exposures. Previous testing included aged HIHTL and material coupons for 6 months and 1 year using elevated temperatures and exposure to caustic material as well as exposure to water only at 170°F for 1 year. The mechanical and material properties of the samples were characterized and compared with those of the unexposed samples (baseline). Evaluations included burst pressure tests of the EPDM hose-in-hose transfer lines and material tensile strength tests of EPDM dog-bone coupons. It was observed

that both the tensile strength of the EPDM material dog bones and the burst pressure of the HIHTLs significantly decreased with the increasing temperature and increasing exposure time. This phase of testing includes aging of HIHTL and EPDM dog bone specimens at various concentrations of NaOH as well as water only at the elevated temperatures. Four test loops were developed at FIU allowing for the aging of HIHTL as well as dog bone specimens utilizing 6.25%, 12.5% and 25% NaOH and only water respectively at 170°F.

This task will provide information that will assist engineers with understanding the wear rates in metal pipes and transfer lines along with the effect of various stressors on nonmetallic components. The research will aid in determining the remaining useful life of both metallic and non-metallic components by establishing more detailed/accurate guidelines and avoiding unexpected failures in transfer lines.

Subtask 19.1: Pipeline Corrosion and Erosion Evaluation

Subtask 19.1: Introduction

The Hanford Site Tank Farm has implemented a Fitness-for-Service (FFS) program for the Waste Transfer System. The FFS program, based on API-579-1/ASME FFS-1, examines structural parameters of the waste transfer systems in order to develop erosion/corrosion rates for relevant system components. The FFS information is acquired from opportunistic evaluations of pipelines that have been removed from service. FIU-ARC engineers work closely with key Hanford high level waste (HLW) personnel and the contractor, Washington River Protection Solutions, LLC (WRPS), to support the FFS program, deliver solutions for sensor evaluations, conduct bench-scale testing followed by data acquisition and analysis for corrosion and erosion assessment. Previous efforts at Hanford included the installation of sensors on a number of the POR 104 components, to provide real time pipe wall thickness measurements. Due to various limitations, alternative approaches for remote permanently mounted pipe wall ultrasonic thickness measurement systems are being investigated.

FIU efforts to support this scope have included investigating key options available in the market for remote permanently-mounted ultrasonic transducer (UT) and other sensor systems for HLW pipe wall thickness measurements and wear. Specific applications include straight sections, elbows and other fittings used in jumper pits, evaporators, and valve boxes. FIU assessed the use of various ultrasonic systems that are either commercially available or used previously at Hanford and selected the most promising systems for further evaluation. One of the two down selected systems (Permasense UT sensor system) was acquired, and initial bench-scale validation testing was conducted. Following the initial bench scale tests, engineering scale testing was implemented on an in-house designed and installed test loop. The design loop has been established using 2- and 3-inch diameter straight and bends pipe sections to mount the sensors. The loop was eroded using sand-water slurry and the Permasense sensors were used for thickness measurements [2,3,4]. The sensors were also tested for their performance in extreme environmental conditions under high humidity and temperatures. Finally, the feasibility of conducting radiation testing on the sensors was considered and a test plan was developed for implementation. In addition to the Permasense UT sensors, two other systems were evaluated for erosion, corrosion and anomaly detection in the pipe loop at FIU. These included the SRNL coupons with the Pencil UT sensor and the Fiber optic sensors from CEL [1,2,17].

Currently, FIU is in the process of testing the SRNL stainless steel coupons on the engineering scale test bed at FIU and constructing a bench scale mock-up loop for the caustic simulants. Additionally, the test results from CEL's Fiber optic sensor system for leak detection in carbon steel pipe sections are being analyzed for automating the leak detection process. The benefits of this research include providing validation for new methods and technologies that will assist engineers in understanding the fault potential of HLW nuclear waste transfer components due to corrosion and erosion. By providing insights into determining if and when lines need to be removed/replaced, the unneeded excavation of transfer lines can be avoided saving valuable time and resources. Also, more detailed and accurate guidelines can be developed governing the life expectancy of the transfer system and its components. By being able to have accurate predictions of points of failure from erosion, and by being able to monitor an entire pipeline's status in real-time, resources can be targeted to tackle preventative measures instead of reactive.

Subtask 19.1: Objectives

The motivation for this task is to assist DOE and WRPS in providing realistic estimates of the remaining useful life of the components and to incorporate those estimates into future design plans. This task includes the investigation of various sensor systems to detect thinning in pipes and tanks along with real-time evolution of the wear using SRNL's mass loss/erosion coupons. Hence, there are three objectives for this task for structural health monitoring using various types of sensors. Including:

- Development of a radiation test method for Permasence UT sensors.
- Erosion and wear detection in pipes using SRNL coupons.
- Pipe leak and fault detection using CEL's fiber optic sensors.

Subtask 19.1: Methodology

Development of radiation test method for testing of Permasence UT sensors

Previous year's research included evaluation of the Permasense UT sensors for bench and engineering scale testing on FIU's pipe loop including the elevated environmental conditions. The conditions are humidity and temperatures that the sensors would be exposed to at the sites. This year's work incorporated investigating the various methods to irradiate the UT sensors for low-level radiation including alpha and beta radiations. A milestone was completed by investigating the radiation evaluation options for commercial microelectronics and sensors by shielding with materials currently available in the market.

Radiation test plan:

Ionizing radiation refers to energy released by atoms in the form of electromagnetic waves or particles [6]. The spontaneous disintegration of the atomic nuclei (radioactivity) results in the emission of electromagnetic waves (gamma or x-rays) or particles (neutrons, beta, or alpha) [6]. Electronics are particularly susceptible to the effects of ionizing radiation due to their dependence on the flow of electrons. A charged particle can influence a current in circuits and materials, leading to noise and spikes. This often results in inaccurate readings, poor transmission quality, and/or permanently damaged circuits. Most ionizing radiation sources that are sufficiently enough to cause noticeable damage or interference are in space. The Earth's atmosphere and magnetic field protect most operating environments from the harsh radiation of space. However, nuclear

reactors produce large amounts of gamma rays and neutron radiation, along with the nuclear waste they produce.

Damage Mechanisms for Electronics:

There are two fundamental mechanisms of damage that take place in electronics when exposed to ionizing radiation [7]. One is **lattice displacement**, in which charged particles bombard a material, occasionally colliding directly with the nuclei of the atoms in the material. Over time, this can cause atoms in the material to be knocked loose, resulting in permanent damage. The other mechanism of damage is called **ionization effects**, the result of charged particles that do not have enough energy to cause lattice effects. These effects can cause glitches in logic circuits and distort analog measurements. Soft errors do not directly damage the device but can still lead to permanent damage due to corrupting data or memory and causing secondary effects that lead to permanent damage.

The resultant effects of these types of damage can be categorized into two general groups that will be briefly described below [8], they are:

Total ionizing dose (TID) – Due to prolonged exposure to radiation, threshold voltages of some types of transistors change due to trapped charges in the silicon dioxide gate insulator [3]. This leads to leakage currents and increased power consumption during normal operation, which in itself may lead to secondary damages related to heat and excessive currents through circuits. Damage by TID may lead to lattice displacement as well as the deterioration of some materials.

Single event effects (SEE) – Highly ionized particles can create a charge significant enough in the silicon to disrupt the operation of electronic circuits. These effects can further be sub-divided. With a **single event upset (SEU)**, a transient charge in the silicon is sufficient to flip a bit in a digital signal. This type of damage is most prevalent in memory circuits such as RAM, Latch, or flip-flop [8]. **Single event latchup (SEL)** primarily affects CMOS technologies in which a transient charge can trigger bipolar transistors to short circuit between power and ground. The large currents generated by this short circuit can cause irreparable damage to components if they are not protected against short circuits and power dissipation [8]. **Single event burnout (SEB)** simply refers to the destructive failures of MOSFET transistors in power applications.

Radiation hardening refers to the process of making electronics and subcomponents resistant to the types of damage and interference that can be caused by ionizing radiation. *Physical hardening techniques* refer to using different physical materials in the make-up of the electronic device to better withstand the effects of radiation. Chips are often manufactured on substrates that are insulators instead of semiconductor wafers, while other strategies are to choose particular component technologies that are naturally more resistant to radiation such as BJTs versus CMOS [9]. Another approach is shielding, usually used in conjunction with other hardening methods. The shield seeks to block radiation by surrounding the electronics with materials that will absorb or reflect the ionized particles such as lead or tungsten. *Logical hardening* techniques refers to modifying the lower level system logic of a device and components to catch issues caused by ionizing radiation such as corrupted data and flipped bits [10]. A purely programmatic approach would aim to increase the redundancy of operations to ensure consistent results, such as multiple microprocessor units computing the same calculation and comparing answers.

Radiation Hardness Tests:

For electronic devices intended to operate in environments with even the slightest bit of ionizing radiation, radiation qualification tests are highly desired, if not mandatory. However, radiation hardness testing is made complicated by limited access to radiation sources, and the fact that many commercial electronics and components do not always share the same attributes of radiation hardness, despite having the same part number. Many times, at a chip or component level, different runs of the same design by different manufacturers will result in highly varied results when tested. Typically, a full radiation hardness qualification would require three tests [11]:

1. Total dose using a Cobalt 60 gamma source and/ or X-ray source exposed to unpackaged chips.

2. Displacement damage with a nuclear reactor source producing neutrons.

3. Single event testing using proton or ion beams (60 Mev and above).

This outlines general criteria for radiation qualification of electronics. However, for different types of electronics testing, criteria become more intricate and complex. In some cases, bipolar transistor technologies suffer increased radiation damage when using low dose rates [11]. The Low Dose Rate effect is sometimes required to be tested by some radiation standards, using "low dose rates" compared to the intended environment.

In order to create a comprehensive test plan for sensors and electronics intended for use at DOE sites and facilities where ionizing radiation may be present, it is important to design tests and criteria congruent with preexisting radiation hardness test standards. Therefore, the test plan will follow recommendations from the CERN "ATLAS Standard Radiation Test Methods" [12], Sandia National Laboratory "Radiation Hardness Assurance Testing of Microelectronic Devices and Integrated Circuits: Radiation Environments, Physical Mechanisms, and Foundations for Hardness Assurance" [13], American Society for Testing and Materials "Standard Guide for Ionizing Radiation (Total Dose) Effects Testing of Semiconductor Devices" [14], and US Military Standard "Environmental Test Methods for Semiconductor Devices".

Irradiation of UT sensors:

Permasense UT sensors and wireless gateway have previously been identified as an effective means for remotely and reliably monitoring pipe wall thickness changes in harsh environments. For their implementation to be feasible for DOE use and in areas of radiation, the appropriate electronic testing is required. Based on industry standards for radiation exposure testing, it was decided to outline the necessary steps to conduct Enhanced Low Dose Rate Sensitivity (ELDRS) testing on the Permasense UT sensors. Further, research revealed that in order to prove radiation hardness of the sensors it is best to test the standard MIL-STD-883E TM1019 - IONIZING RADIATION (TOTAL DOSE). This standard refers to the total ionizing dose that an electronic device may encounter over a long period of exposure (months to years). The suggested test would consist of a total of 50krad (Si) radiation exposure of the sensor at 10mrad (Si)/s rate with increments of 10krad (Si) for electrical testing. With this type of testing, the sensor should uphold to the radiation-filled environments that might be encountered across the DOE complex. The McClellan Nuclear Research Facility at UC Davis, CA was contacted for recommendations on proceeding with testing as well as timelines and feasibilities. It was confirmed by scientists at the facility that the testing could be done to the standard specified with only a small deviation. A quote (@ $9000) was received from McClellan to conduct the radiation testing and a tentative timeline was proposed of 2-4 months to complete testing.

Radiation test plan details:

The literature study along with discussions with McClellan Nuclear Research Center at UC Davis and talks with the collaborators resulted in a suggested test plan for the Permasense sensor radiation testing. Details of the final test plan are as suggested below:

- Timeline – 2-4 months
- TID – 50 krad(Si)
- Ionization rate – 10mrad (Si)/s
- Increments (intermediate levels) – 10 krad (Si)
- In between the intervals, the sensor will be shipped to FIU for testing (electrical/functional)
- Quote received - @$9000
- Type of Testing – MIL-STD-883E TM1019 - IONIZING RADIATION (TOTAL DOSE).

In addition to the TID testing, Single Event Testing is also recommended for sensors/electronics which are exposed to the radiation environments for a short duration of events such as the inspection tools. Based on the availability of the budget, the work will progress in the upcoming year.

Radiation shielding materials:

Initial research on radiation hardness testing resulted in compiling a list of different radiation hardness tests and a generic test plan for evaluating off the shelf commercial electronics for low-level radiation environments. The methods for shielding commercial grade electronics were investigated with a focus on ease of implementation and not requiring any disassembly of the original device. Several solutions were found that could significantly increase the durability of off-the-shelf electronics to low levels of ionizing radiation without adding significant weight or costs. Lead as an element has proven to be one of the most effective means of absorbing radiation and shielding both electronics and organic matter from the harmful effects of ionizing radiation. Unfortunately, it is toxic and risks leaching into the environment if deployed in its raw state. Newer technologies have emerged, though, that solve this issue by combining lead with other materials to make it easier to apply and reduces the risk of it contaminating the environment. Lead vinyl sheeting is available from a company called RayBar, it is available in thickness from 1/32" to ⅛" and is extremely flexible [16]. Other solutions for shielding include lead paint, and conformal coatings that use heavy element particles. Some of the options of the lead-based materials that can be used for radiation shielding are shown in Figure 81 and Figure 82. Evident from the figures are the sheeting, foil tape, gamma and neutron absorbent foams. Depending on the application, any of these could be easily applied as a shield against radiation for the sensors and electronic devices.

Figure 81. Lead Vinyl Sheeting (left), lead foil tape (center), lead lined foam (right) [16].
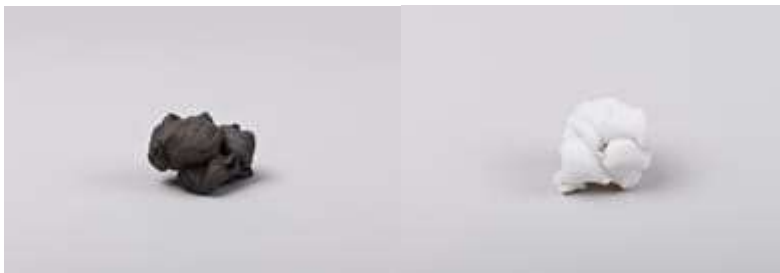
Figure 82. Gamma absorbent putty (left), Neutron absorbent putty (center) [16].

The test plan was submitted to WRPS and DOE as a deliverable with only minor comments, after which confirmation was received from WRPS to proceed with the radiation testing. The scientists also assessed FIU's test plan with similar testing conducted by SWRI. The difference in both test plans was compared. As shown in Figure 83, SWRI used a test set up with electronic components attached to a plywood board and the entire set up was placed in a hot-cell facility for radiation exposure using cobalt-60 sources. FIU proposed a similar process except for the sensors to be tested at the McClellan Nuclear Research Center at UC Davis using their radiation chambers.

Figure 83. Cameras and sensor system electronic component set up board for radiation chamber testing SWRI [20].

For both test methods – shipping the sensors to the radiation-testing laboratory at UC Davis and the application of a shield material for radiation will be evaluated. This task will progress in the upcoming years subject to the availability of resources, budget and the site needs.

Erosion and wear detection in pipes using SRNL coupons

Collaboration with SRNL scientists during the previous year led to the initial testing of SRNL coupons for erosion in pipe sections. The process included use of small coupons of steel (Figure 84

Figure 84) made of the same material as used in pipelines across DOE nuclear waste sites. The intention was to measure the changes in thickness using UT sensors and to measure the mass loss on a minute level to detect and quantify pipeline wear. By measuring the minute erosion of the coupon, the life expectancy of sections of pipelines in the field may be calculated. The coupon is inserted into a coupling welded to the pipe surface and the head of the coupon is made flush with the inside of the pipe. By being subjected to the same abrasive forces as the pipe walls, the coupon represents a fully observable model of the pipe section. The advantage of the coupon is that it is easily removable. Mass measurements of the coupon before and after testing were taken to provide insights into the degradation of that particular pipeline, or a pipeline made of similar material.

Figure 84. a) SRNL coupon b) coupon weight (without sleeve) and c) with sleeve.

To quantify the erosion taking place in the pipe, the coupons were weighed and measured using a balance (Figure 84) and caliper before being inserted. The surface of the coupon head was also viewed under a microscope and photographed for later comparison after erosion had occurred. During the test, measurements were taken in situ using an Olympus V260-SM UT pencil sensor [18] that was modified to fit specifically in the provided channel within the coupon. Thickness measurements were collected every 30 minutes from both a handheld UT pencil sensor and the permanently mounted UT sensors on the loop. After testing, the coupons were removed from the pipe loop and measurements were taken again in order to quantify mass and height loss, and validate the measurements taken by the pencil sensor.

The coupons were tested on the pipe loop with varying sand and water slurry mixtures and grit sizes. Upon completion of the carbon steel coupon testing, this year the next phase of testing has been initiated with stainless steel coupons to evaluate the erosion effects on the stainless-steel material. The pipe loop was thoroughly cleaned by circulating water and the SRNL coupons were inserted. The new coupons were tested using sand and water mixtures. The pipe loop at FIU has been updated with changes to the pump and installation of the coupons. During the process, the coupons were unable to flush with the inner surface of the pipe loop. Hence, the coupons were machined to have a tight fit in the pipe sections for appropriate testing. The borescope images of the coupons in the pipe are shown in Figure 85.

Figure 85. Borescope images of the coupons in the pipe loop.

During the process of experimental testing, there have been issues related to the pump. The pump has been running for a couple of years now and hence needed upgrading. FIU spent a major portion of the efforts on this subtask in troubleshooting the pump. The disassembled pump, replacement of the shaft seal, impeller reassembly is shown in Figure 86. The leakage after the reassembly is also shown in the same figure. Currently, we are evaluating the pump and a decision will be made on procurement of a new pump and upgrade of the loop. Experimental results from the initial testing of the stainless steel coupons are presented in the results section.

Figure 86. a) Pump assembly stages (left and center) and b) assembled pump - leakage after testing (right).

Pipe leak and anomaly detection using CEL's fiber optic sensors

In addition to the UT sensors and the SRNL coupons, a new sensor system was also evaluated for structural health monitoring of tanks and transfer lines. The Fiberstrike sensor system developed by an Ohio based engineering firm, Cleveland Electric (CEL) [6], for the purposes of pipeline monitoring, was tested and validated on a bench scale pipe loop. Current monitoring systems on the market rely on measurements such as flow rate, pressure, temperature, etc. These sensors transmit wired or wirelessly and usually must be powered by an electrical source. This can lead to increased operational costs and accidental downtime. In comparison, the Fiberstrike sensors are acoustic transducers based on the principle of optical interferometry, using light to detect the

slightest of vibrations. One large advantage is that they require no power source. Only a fiber optic cable linking the sensor to the gateway is required. The sensors emit no form of radiation and therefore cannot interfere with any other nearby equipment. They are also not susceptible to any forms of external interference, making them ideal for harsh, radioactive environments. By measuring the acoustic energy of an object, the power spectral density (PSD) can be observed. A pipeline exhibits an acoustic or vibrational signature, when conditions in and around the pipeline are stable, the signature remains stable as well. This signature is known as the pipelines power spectral density (PSD), the distribution of power into frequency components. By placing acoustic transducers at intervals along a pipeline, continuous, real time monitoring of the pipeline's PSD can be realized. Under ideal operating conditions, the baseline signature is captured and comparisons are made against it to detect anomalies along the pipeline. Any parameter that translates into even the slightest physical movement can be quantified by monitoring the PSD.
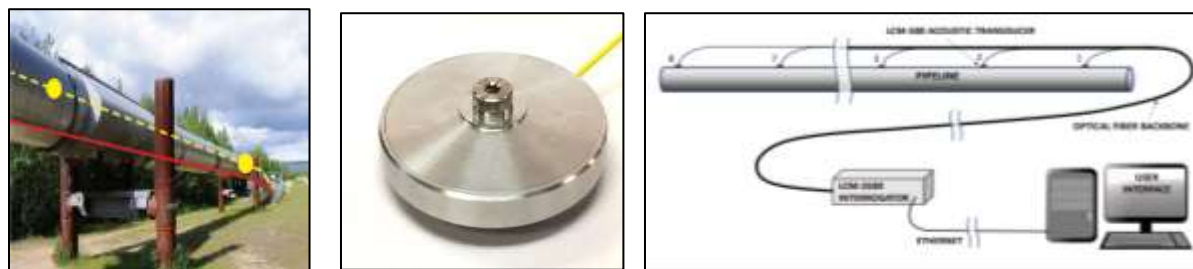
Figure 87. Fiberstrike a) sensor system b) sensor c) monitoring system layout [19].

Events such as impacts to a section of pipe, drilling, or leakage, can all be translated into unique signatures represented by the change in the pipeline's PSD. The location of the event can then be determined by comparing the magnitude of signatures on neighboring sensors. The higher the magnitude ratio of sensor A to sensor B, the closer the event has taken place to sensor A. By relying on fiber optics, near instantaneous, measurements can be made with a maximum reported latency of 3 seconds and a nominal latency of 1.5. All sensors on the pipeline have no electrical components and are connected via non-conductive optical fiber. This allows for the sensors to be located more than 20 km from the monitoring equipment.

The sensors resemble a small metal disk approximately 6 inches in diameter with a center hole. When installed they have a thin plastic shell the same shape. The sensors are mounted on a threaded stud that may be welded to the surface of the pipeline or a tank wall. The sensors may also be attached using a metal clamp with a threaded stud. Direct physical contact is required for optimal signal integrity, and the sensors need to be fastened tightly to avoid any movement or shifting from continuous vibrations. The interval at which the sensors are installed on a pipeline varies depending on configuration; for long straight sections it has been shown that spacing can be more than 500 meters apart, but for geometries such as elbows or complex configurations with valves and pumping stations, more frequent placements of sensors is necessary. Use of the LCM-500 transducers requires a fiber optic "backbone" to be installed on the pipeline containing single-mode SMF-28 fibers. The cabling is then connected to an LCM-2500, which serves the purpose of an optical interrogator. Finally, the interrogator(s) can be connected either directly to a local station via Ethernet, or to a router for remote access. A layout of the monitoring system along with the transducer locations is as shown in Figure 87.

The FIU loop previously described was used to install the fiber optic sensors as shown in Figure 88. In this set up, both straight and 90º elbow sections were used and joined by a reducer. The pipe sections were welded and the sensors were installed per the manufacturer's instructions. A threaded boss is attached to the exterior of the pipe. Typically, it is physically attached to the pipe by clamping it with an industrial rated strap or clamp. The transducer shown in Figure 88b is attached to the threaded boss using a supplied nut and washer.

Figure 88. a) Fiber optic sensors on the loop; b) single transducer (LCM-500); c) LCM-2500 Interrogator and user control station.

Figure 88b shows the installation of one of the three LCM-500 acoustic transducers mounted on a 2 in. section of pipe. Once installed, each sensor must have their pigtail fiber cables fusion-spliced into the fiber optic backbone cable that travels the length of the pipeline to the interrogator. Figure 88c shows the monitoring station placed several feet away from the scale pipeline with a laptop sitting on top of the LCM-2500 interrogator.

In the past year, the testing of the fiberoptic sensors was conducted on the FIU loop depicting the following pipeline fault scenarios:

- Leaks
- Blockages
- Valve Position
- Pump Operation Modes
- Physical Impacts to the Pipeline – strikes

To simulate a leak in the pipeline two holes of different sizes were drilled on the vertical 2-inch section of the loop between the two FiberStrike sensors as shown in Figure 89. To collect variable datasets data one leak was opened at a time to see if there would be a difference in the signature between the two. To simulate a blockage in the pipeline a control valve on the main path was closed partial way and then reopened while recording data from all four sensors. In another test, a bypass valve was opened all the way that allows for flow to be redirected into the reservoir tank through a shorter path while keeping the main overhead path fully open. To simulate physical impacts the pipeline was struck in different locations using hammers, wrenches, and other blunt objects. Finally, data recordings were made while there was no activity on the loop and then while the pump turned on and established a stabilized flow through the loop. The fiber optic acoustic signals obtained in each case is discussed in the results section in detail.
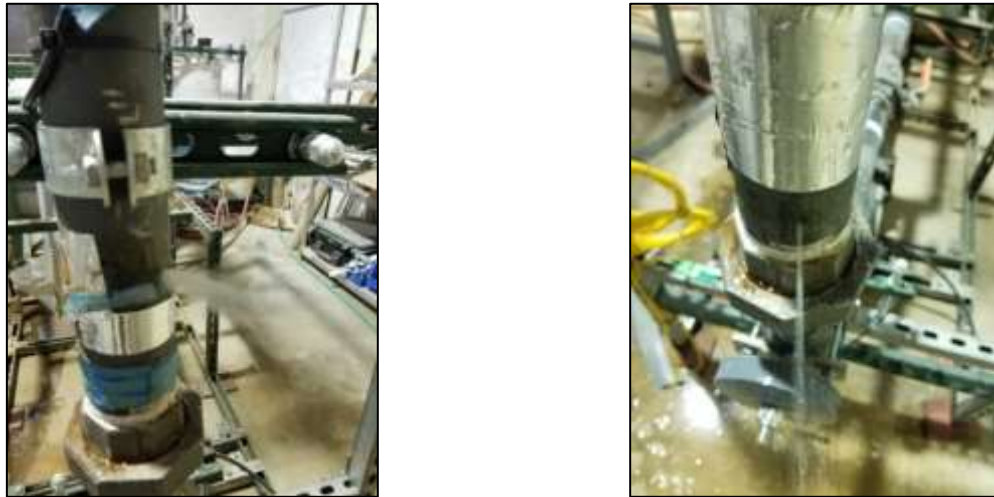
Figure 89. Leaks in the pipe loop   a) ¼ inch hole   b) 1/8 inch hole

In additional to the detection of the fault in the pipe sections, the actual location of the event happening is also to be determined for immediate repairs saving lives. This feature was not covered by the sensor system. Hence, FIU developed a mathematical cross-correlation based method to locate the exact location of the events. The process is described next.

Cross-Correlation method for pipeline fault location detection:

The relative location of a leak can be found using the cross-correlation method by first finding the time lag τ_{max} between signals from two acoustic sensors spread apart on a pipeline. The cross-correlation function is used to measure the similarity of two sets of data and returns a coefficient between -1 and 1; 1 meaning a perfect correlation, 0 meaning no correlation, and -1 meaning a negative relationship between the two signals [21]. When a signal is recorded at two locations varying distances from the origin, the cross-correlation function will result in a low correlation coefficient because initially the signals are out of sync as represented in Figure 90.
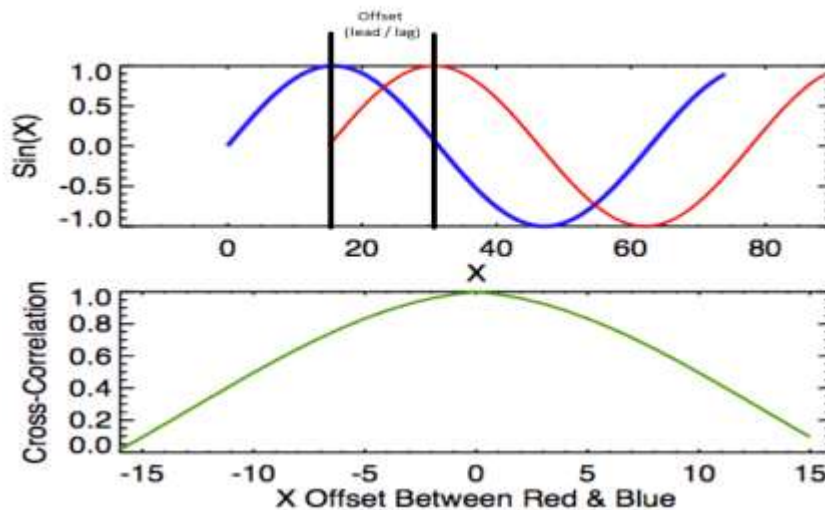
Figure 90. Calculating time lag with cross correlation function [21].

By increasing the phase shift of one signal versus the other and calculating correlation coefficient at each interval, the resulting continuous function will have an absolute maximum, which represents the time lag between the two signals as shown in Figure 91.
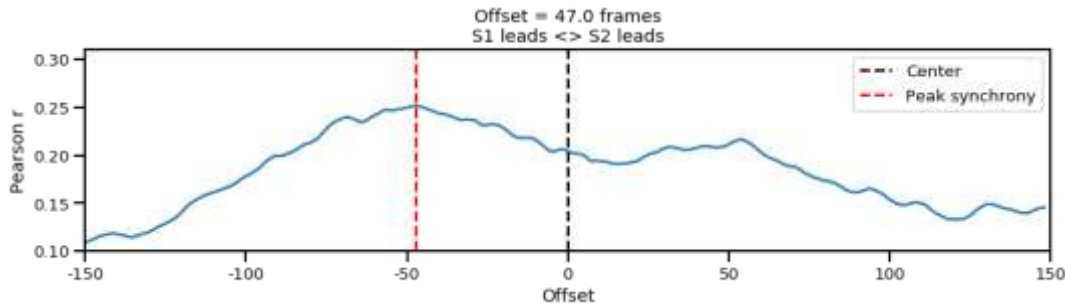
Figure 91. Correlation coefficient as a function of signal offset.

The offset is the number of samples or data points that the shifted signal is moved until peak synchrony is achieved. The time lead or lag of the signal is then simply calculated by multiplying the offset by the time interval between each measurement.
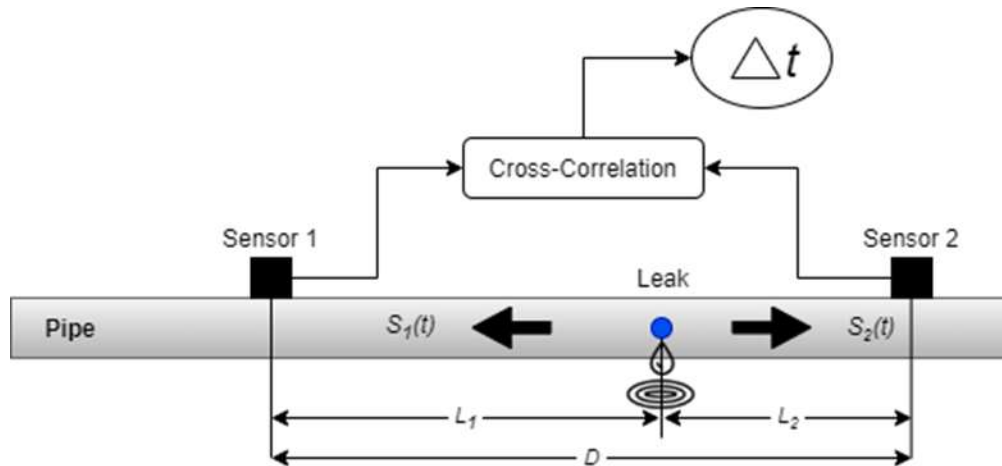
Figure 92. Pipe leak location detection using cross correlation.

Figure 92 provides a visual representation of how the distance to the leak is then determined after finding the time delay Δt between the two signals. Then using the equations below to find the distance to the leak [22].

$$L_1 = \frac{D + c\Delta t}{2}, \qquad L_2 = D - L_1$$

The distances to the leak relative to sensor 1 and sensor 2 are denoted as **L₁** and **L₂**; **c** represents the velocity of sound propagating through the pipe; **D** is measured as the length of pipe between sensor 1 and sensor 2. The term '**Δt**' represents the time difference between the peaks of the two sensor signals captured during the leak. Knowing **D**, **c** and **Δt** in any leak process, the location of the leak from sensors (**L₁** and **L₂**) can be calculated. Localization of leaks is highly useful in the case of nuclear waste transfer for immediate repairs and to prevent disasters.

Subtask 19.1: Results and Discussion

Results of SRNL coupon experiments:

Erosion testing was conducted by circulating a sand and water mixture with a 5-8% volume fraction. The SRNL coupons were placed at the 3-inch elbow and 3-inch straight section (one at the bottom and the other at the top). Another 2 coupon holes were blocked using pipe plugs. During the process, a Pencil UT sensor (Omega V260 SM Sonopen) is used to detect the change in thickness. Calibration of the UT sensor and measurement during the testing are as shown in Figure 93 .
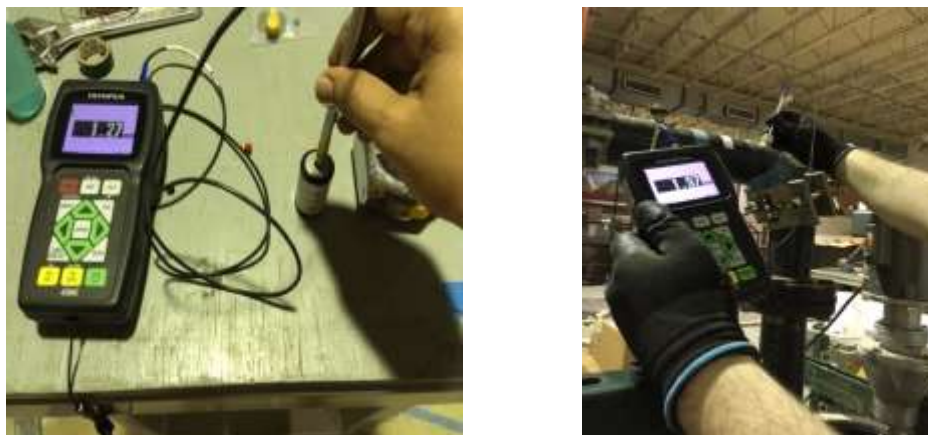
Figure 93. a) UT sensor (V260 SM) calibration and b) real-time coupon thickness measurement.

The next steps included weighing the coupons using a Mettler Toledo scale with an accuracy of 5 decimal places in grams. The weighing process has been described previously and the weights of the three coupons before and after testing are provided in Table 6. It is evident from the table that the coupon at the bottom had the maximum mass loss as expected due to the mass erosion caused by the coarse sand and water at high velocities.

Table 6. Erosion Test Results for SRNL Coupons

Coupon Number	Initial Weight (gm) (with sleeve)	Initial Weight (gm) (without sleeve)	Weight (After erosion) (gm) (without sleeve)	Weight loss (gm)
1 (elbow)	8.12616	7.35128	7.34924	0.002
2 (top)	8.30051	7.35125	7.34921	0.002
3 (bottom)	8.26943	7.36321	7.35998	0.003

Erosion of the coupon surfaces and sides for the elbow and the bottom coupons are as shown in Figure 94. The surface erosion was observed to be maximum at the elbow face followed by the bottom face. From the tests, it is concluded that the stainless-steel coupons are not eroded as much as the previous mild steel coupons. Further testing will be continued in the upcoming year.

Figure 94. Eroded Coupon surfaces removed from the elbow and bottom sections of the pipe.

Caustic Testing Initiation

SRNL scientists have provided FIU with their requirements for potential chemical and glass beads testing using the currently existing larger loop and a small-scale bench loop. A new bench scale test loop will be designed and constructed this upcoming year. Three phases of testing will be conducted with the following simulant options replicating the nuclear waste. The recommendations are:

1) A glass frit simulant that can primarily act as an eroding agent representative of the waste in the recycle system. Evaluations must be conducted on the abrasivity of the frit.

2) Second simulant designed to evaluate the corrosion component of the waste will be a 0.6 M neutral chloride solution (representing the chloride concentration in seawater). It will be circulated to detect flow-assisted corrosion on stainless steel coupons. This testing will be conducted in the new bench scale loop being constructed.

3) The final simulant will be a sludge/supernate simulant (typically a 2M sodium solution). This simulant is designed to look at the erosion/corrosion components together and is expected to closely represent a sludge slurry at SRS. The simulant will also be tested in the small flow loop in the hood as it will be caustic.

Currently, FIU is in the process of finalizing the caustic simulants with the SRNL team to develop a bench scale loop that can test the coupons. The SRNL team will develop a recipe to simulate the waste streams as being transferred in the waste transfer plant system at SRNL.

<u>Results from Fiber-optic Sensors:</u>

Experimental testing was conducted on the FIU's pipe loop by circulating sand-water mixtures. A fault or anomaly in the pipe was detected as a change from the baseline flow signals. To make any conclusions about the deviation of performance of a pipe system from normal operation, the baseline acoustic signal must first be captured. The raw acoustic signals of all channels are shown in Figure 95. Due to the proximity of the pump, there is a lot of noise that exhibits harmonic tendencies. It can easily be seen that the signal from channel 1 (red) has a noticeably lower amplitude compared to the other signals. This can be explained by its proximity to a brace supporting the pipe loop, dampening the vibrations. The other sensors are mounted higher and are subject to more movement. Regardless of amplitude, it can be seen that each channel maintains relatively consistent behavior.
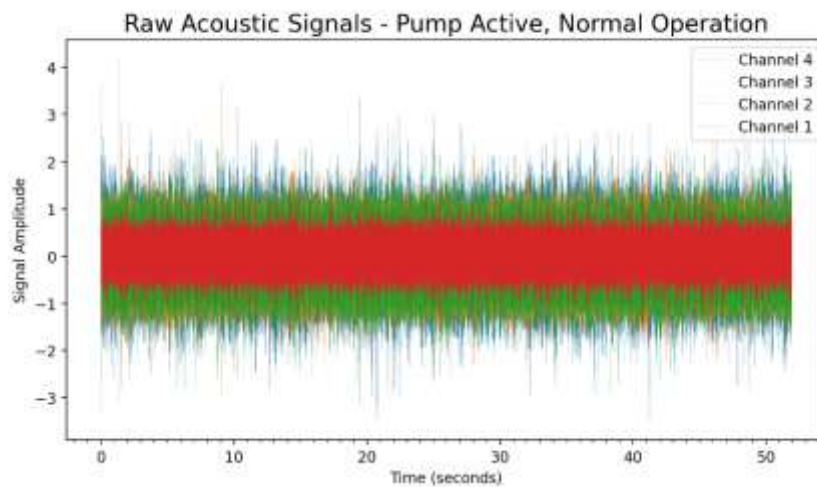
Figure 95. Raw signal for baseline data (pump is active – normal operation).

The raw signal is hard to extrapolate finer details from as the noise can obscure signal behavior in the frequency domain. The next step is to analyze the frequency spectrum and how energy levels in individual frequencies change over time.
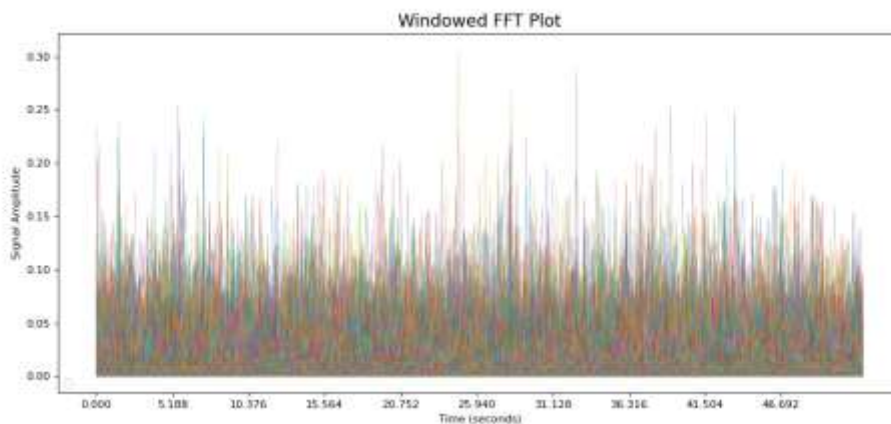
Figure 96. Windowed FFT for normal pipeline operation.

The raw signal is segmented into sets of 5000 data points (approximately 100 ms); FFT is applied to each set resulting in 2500 values representing vibrational energy present in different frequency components between 1-25KHz. Each set of 2500 points is then plotted, each frequency represented by a time series as seen in Figure 96. Due to the high density of series, extrapolation of information again becomes difficult.
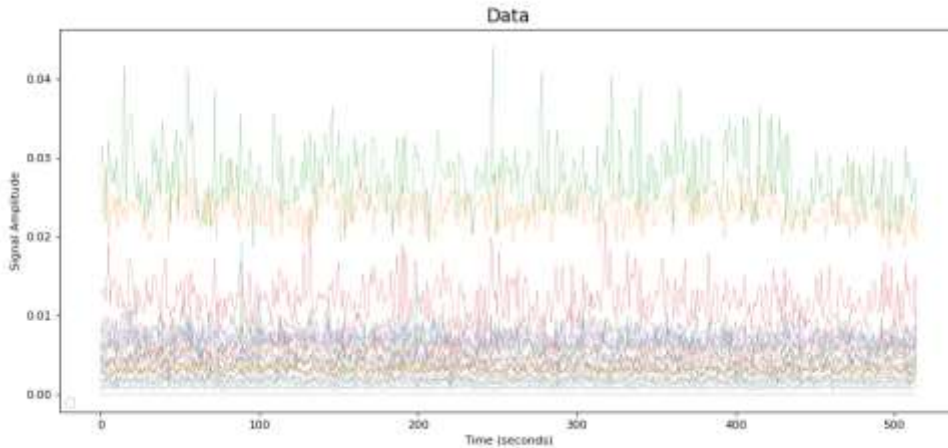
Figure 97. Windowed FFT (averaged frequencies) plot of normal pipeline operation.

By again segmenting the 2500 data points per FFT set and taking the average of 25 equal and contiguous sets, a more effective plot of the change in frequencies can be achieved as shown in Figure 97. Once the baseline was achieved in different representations, data collected during faults could be compared.
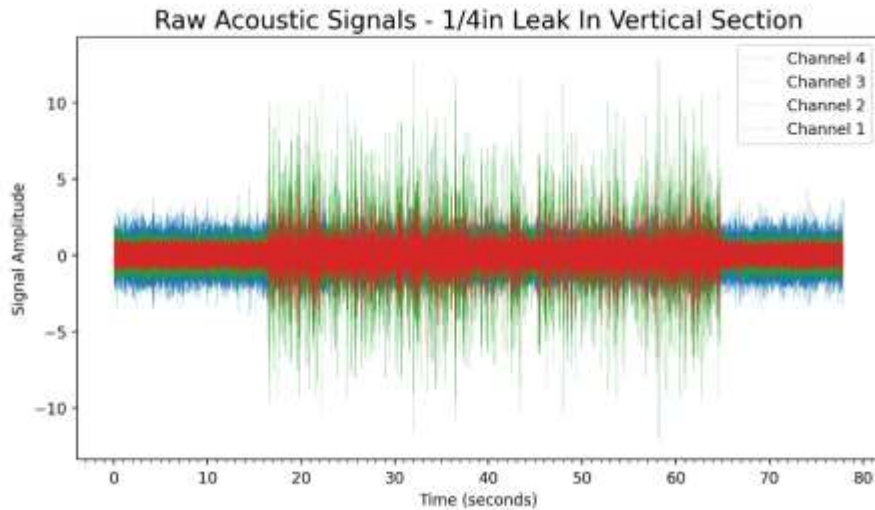
Figure 98. Raw acoustic data from all sensors during ¼" hole leak.

A ¼" hole was opened, allowed to leak for about a minute, and then sealed again while recording signals from the acoustic sensors. In Figure 98 the raw signals show an immediate response, however, the further the sensor from the location of the leak, the less the leak signal stands out from the noise. To test the sensitivity of the leak detection system a smaller hole of 1/8" was

opened between sensors 1 and 2 and left to leak while recording the acoustic signals from the pipe loop. The leak signal was not as prominent as the larger ¼" hole; however, the presence of aberrant behavior in the acoustic signature can be seen in Figure 99. The hole is opened at approximately 35 seconds elapsed and left to leak for the duration of the recording. Fluctuations are primarily seen in channel 1 and instead of the large increase in signal amplitude seen in Figure 98, the leak signal can be characterized as a decrease in amplitudes. This coincides with observations at the time of data collection that witnessed the hole in the pipe expelling water and then pulling in air in a harmonic rhythm. The decrease in amplitudes of the signal may have been caused by the decrease in pressure in the pipe when air was let in near the channel 1 sensor. When the larger ¼" hole was opened, a constant stream of water was present and did not exhibit any noticeable harmonic pressure changes.
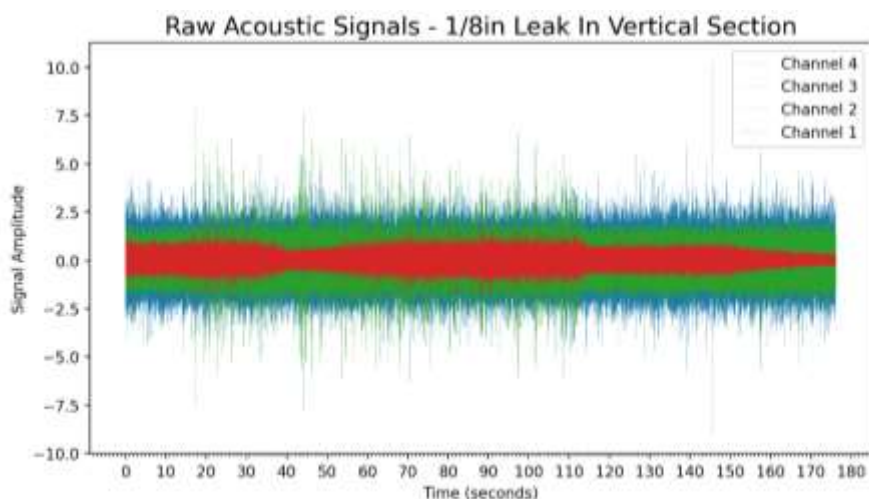
Figure 99. Raw acoustic data from all sensors during 1/8" hole leak.

The signatures of other events were recorded as well and analyzed to determine the method by which the acoustic signature of the pipeline was affected. A pipeline monitoring system should not only be able to detect structural damage such as leaks or physical impacts, but also deliberate actions such as the opening and closing of passages. Valves for stopping or redirecting flow are ubiquitous on pipelines and the more complex the more automated the control systems for these valves can become. Should software malfunction, a worker turns the wrong valve, or a valve fail to open all the way, it is important for a monitoring system to be able to detect these events. To collect data, a bypass valve was open fully that allowed for a shorted return path from the pump to the reservoir tank. The valve to the overhead section of pipe remained open and a small amount of flow was still present while the majority redirected.

The next event included the valve opening and closing. The valve was slowly opened starting at approximately 45 seconds and then closed again after approximately 30 seconds. In Figure 100, it can be seen that the signals from channels 3 and 4 dissipate significantly and channels 1 and 2 dissipate only slightly due to their close proximity to the higher volume of flow.
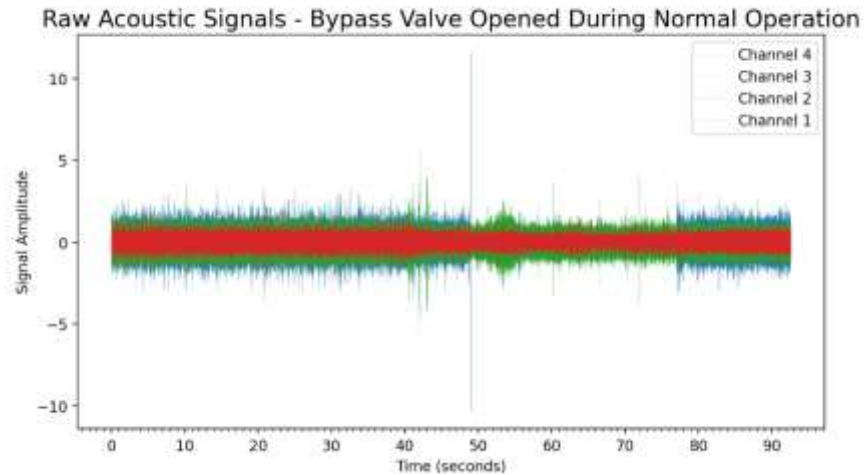
Figure 100. Raw acoustic data from all sensors during bypass valve opening and closing.

Finally, a constant threat to any pipe is damage caused by physical impacts. Buried pipes are always at risk of being struck during excavation projects and in the oil and gas industry vandalism or siphoning occurs on a regular basis. To capture the signature of an impact, the pipeline was struck with a hammer in various locations and exhibited a unique signature, as seen in Figure 101. A massive spike in amplitude across all sensors was witnessed regardless of the location of the strike. The further away from the strike, the amplitude of the signal was lower but still far above the normal operating threshold.
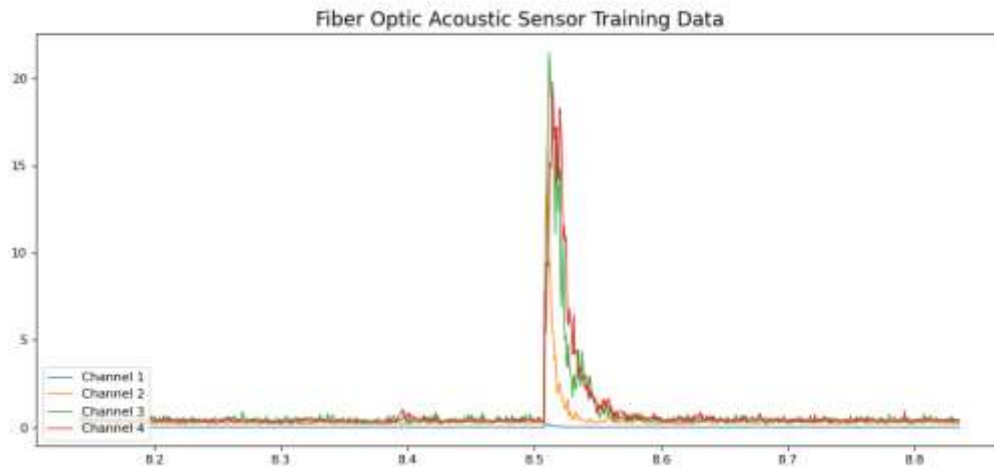
Figure 101. Raw acoustic data from all sensors during hammer strike.

Due to the uniqueness of the signature and the high signal to noise ratio, it was also possible to apply the cross-correlation method to determine the location of the impact. In systems where there is a high level of noise caused by machinery, the increased number of sensors sampling the acoustic signal of the pipeline allows for a higher degree of certainty of any given event and also increases the accuracy when applying the cross-correlation method.

Subtask 19.1: Conclusions

In conclusion, three different sensor systems have been tested this past year for their ability to deal with the challenging structural integrity concerns at various DOE nuclear sites across the country. These systems are the Permasense UT sensors from Emerson Technologies, the fiberoptic sensor systems from Cleveland Electric Limited, and the patented mass loss coupons from SRNL. The Permasense wave-guided UT sensor system for use with pipelines has been previously tested for their precision (0.01 mm), repeatability and reliability of operation. Testing also included the real environmental conditions (temperature and humidity) similar to those at the sites. Based on several tests conducted over a year, it is concluded that the Permasense sensors are a good option to be considered for deployment to the sites for detecting thinning of carbon steel pipe sections. This year's focus was on studying the radiation effects on the sensors. For this, a test plan was developed that included the radiation effects on electronics, in general, and FIU developed radiation testing process customized for the Permasense UT sensors. The test methods of both facility irradiation of the sensors and the use of radiation shields have been suggested. Based on the suggestions from the DOE site contractor WRPS and Hanford and SRNL scientists, a decision will be made in future on the radiation exposure of these sensors for long-term performance.

Current research also verifies and validates the use of the patented SRNL coupons on an engineering scale test bed for their ability to detect pipe wear and erosion on a minute level in real-time. In the previous year, carbon steel coupon testing was initiated in the pipe loop for erosion and corrosion effects. This past year the process was completed and based on the erosion characteristics sensed by the sensor system, the material was changed to detect the erosion in stainless steel. Initial experimental results showed very less change in erosion in stainless steel when compared to the carbons steel coupons. Currently, FIU is troubleshooting and updating the pipe loop to resume testing. This will include addition of flowmeters and pressure gauges as needed. These additional parameters will help characterize the flow and help in accurate erosion measurements. With these added values, more complex models of erosion can also be determined from the quantities extracted from the coupon system. In future, the sand testing will be continued for longer durations. Additionally, a new bench scale loop is being designed and manufactured for the chemical/caustic simulants. SRNL collaborators will provide guidance on simulants to conduct tests at FIU. These experiments will help understand well the effect of actual tank wastes being transferred via the carbon and stainless-steel pipes.

The task also investigated and tested the CEL's fiberoptic electroacoustic sensor system for easily monitoring long sections of pipelines particularly in the waste transfer system. Many experiments were conducted to detect various types of faults including leakage, blockage, hammer strikes, pump and valve dysfunction. This sensor system is capable of registering numerous types of pipeline events in real-time with little to no visible delay. By using 2 in. and 3 in. pipe sections, the bench scale testing documented in this work provides basis for the sensor system's potential implementation in various DOE sites when transferring hazardous materials through a pipeline that requires real-time monitoring. This will ensure that any fault is detected immediately and will reduce the impact. While all analysis of captured data was done by researchers, it can easily be seen that through training a machine-learning model with various types of pipeline fault signatures, an automated real-time monitoring system could be realized. The sensors were successfully able to detect the change in the raw signal during the events when compared to the baseline signal. The baseline signal represented the normal operation of pump while circulating the sand water mixtures. In addition to the fault detection, FIU also developed a method to locate the faults. A

signal cross -correlation and synchronization based on the time of flight has been used to develop the leak location detection method. This is a very useful feature as it can save time, effort and finances and finally conduct safe repair and avoid disasters. In future, the team proposes to deploy the sensor system onsite and check its potential use on a permanent basis as required. Further investigations into applying this same technology to monitoring the storage of static vessels (DST's at Hanford and Savannah River sites) containing hazardous wastes is being explored.

Subtask 19.1: References

1. Aravelli, A., McDaniel, D., Thompson, M., Imrich, K., Wiersma, B., "Erosion-Corrosion Detection in Carbon Steel Pipe Loops using SRNLs Thickness and Mass Loss Measurement Coupons", Waste Management 2020 Conference, Phoenix, AZ, March 2020.

2. Aravelli, A., Thompson, M., McDaniel, D., Krutsch, M., McNeilly, M., Imrich K., Wiersma B., "Advanced Fiber Optic and Ultrasonic Sensor Systems for Structural Health Monitoring of Pipes in Nuclear Waste Sites", IMAPS 52nd International Symposium on Microelectronics (IMAPS), Boston, MA, Sep 30-Oct 3, IMAPS (2019).

3. Aravelli A., McDaniel, D., Davila, C., "Real-time Erosion-Corrosion Detection in Waste Transfer Pipelines using Guided Wave Ultrasonic Sensors", Proceedings of the Waste Management Symposia 2018, Phoenix, AZ, March 18-22, 2018.

4. Aravelli, A., McDaniel, D. and Davila C., "Assessment of Guided Wave Ultrasonic Transducer Systems for Wall Thickness Measurements", Summary Document submitted to DOE –EM under Cooperative Agreement # DE-EM0000598 (FIU-ARC-2016-800006470-04c-242).

5. Aravelli A., D. McDaniel, A. Abrahao, A. Awwad, C. Davila, "Thermal Measurement and Modeling of Nuclear Waste in the Double Shell Tanks at Hanford Nuclear Waste Site Using Miniature Sensors," International Microelectronics Assembly and Packaging Society (IMAPS) 2016, Pasadena, CA, October 11-13, 2016.

6. "Ionizing radiation, health effects and protective measures". World Health Organization. 29 April 2016.

7. Van Lint, V.A.J., T.M. Flanagan, R.E. Leadon, J.A. Naber and V.C. Rogers, 1980. Mechanisms of Radiation Effects in Electronic Materials. Wiley, New York.

8. "Radiation Hardness Testing". The McClellan Nuclear Research Center, U.C. Davis. https://mnrc.ucdavis.edu/radiation-hardness-testing.

9. Leppälä, Kari; Verkasalo, Raimo (17–23 September 1989). Protection of Instrument Control Computers against Soft and Hard Errors and Cosmic Ray Effects. International Seminar on Space Scientific Engineering. CiteSeerX 10.1.1.48.1291.

10. Platteter, Dale G. (October 1980). Protection of LSI Microprocessors using Triple Modular Redundancy. International IEEE Symposium on Fault Tolerant Computing.

11. "Radiation Hardness Assurance", CERN Radiation Working Group RadWG, November 15, 2019.

12. "ATLAS Policy on Radiation Tolerant Electronics: ATLAS Standard Radiation Test Methods", CERN ATLAS Project, ATC-TE-QA-0001, July 21, 2000

13. J. R. Schwank, M. R. Shaneyfelt and P. E. Dodd, "Radiation Hardness Assurance Testing of Microelectronic Devices and Integrated Circuits: Radiation Environments, Physical Mechanisms, and Foundations for Hardness Assurance," in IEEE Transactions on Nuclear Science, vol. 60, no. 3, pp. 2074-2100, June 2013.

14. ASTM F1892-12(2018), Standard Guide for Ionizing Radiation (Total Dose) Effects Testing of Semiconductor Devices, ASTM International, West Conshohocken, PA, 2018, www.astm.org

15. Military Standard MIL-STD750/1, Environmental Test Methods for Semiconductor Devices", revision 1 (DOD, January 2012).

16. https://www.raybar.com/shielding-products/lead-vinyl

17. https://srnl.doe.gov/tech_transfer/tech_briefs/SRNL_TechBriefs_UltrasonicThicknessMassLossMeasurement.pdf

18. https://www.olympus-ims.com/en/shop/item/269-productId.570437480.html

19. http://www.clevelandelectriclabs.com/wp-content/uploads/2016/08/Cleveland-Electric-Labs-Marketing-Pipeline-Monitoring-with-Fiber-Optics.pdf

20. "Radiation Test Plan", SwRI® Project No. 18.24475, Sep 2019.

21. Statistics Solutions, "Correlation (Pearson, Kendall, Spearman)," Statistics Solutions, 2020. https://www.statisticssolutions.com/correlation-pearson-kendall-spearman/.

22. Z. K. Y. Liu, "State of the art review of inspection technologies for condition assessment of water pipes," Measurement, vol. 46, no. 1, pp. 1-15, January 2013.

23. Thompson M., "Structural Health Monitoring of Pipelines in Radioactive Environments through Acoustic Sensing and Machine Learning", M.S. Thesis, Florida International University, Aug 2020.

Subtask 19.2: Evaluation of Nonmetallic Components in the Waste Transfer System

Subtask 19.2: Introduction

Nonmetallic materials are utilized in the waste transfer system at the Hanford tank farms; these include the inner hose of the hose-in-hose transfer lines (HIHTLs), Garlock® gaskets and ethylene propylene diene monomer (EPDM) O-rings. These materials are exposed to simultaneous stressors including β and γ radiation, elevated temperatures, caustic supernatant as well as high pressures during normal use. In 2011, the Defense Nuclear Facilities Safety Board recommended to the U.S. Department of Energy (DOE) to conduct post service examination of HIHTLs to improve the existing technical basis for component service life. Suppliers of the nonmetallic components often provide information regarding the effects of some of the stressors, but limited information is available for simultaneous stressor exposure.

An extensive test plan was developed by Sandia National Laboratories to understand the simultaneous effects of the aforementioned stressors [1]; however, this test plan was never executed. Additional studies conducted by Lieberman provide information on HIHTLs at elevated temperature and pressure, but little information is gained regarding the synergistic effects with the caustic supernatant [2]. Florida International University (FIU) has been tasked with supporting this effort by conducting multi stressor testing on typical nonmetallic materials used at the Hanford tank farms. Previous years' research efforts focused on evaluating the aging behavior of EPDM by exposing samples of HIHTLs as well as EPDM dog bone shaped specimens to a 25% sodium hydroxide (NaOH) solution at (100°F), operating (130°F) and design temperatures (170°F) for 6 months and 12 months. In addition, HIHTL and the EPDM dog bone specimens were also exposed to only hot water at 170°F for a duration of one year. After analyzing the data from the previous phase, it became apparent that the synergistic effects of NaOH with high temperature had a significant effect on the degradation of the specimens. After discussing the findings with the site engineers, it was decided to conduct additional aging of HIHTL and EPDM dog bone specimens at various concentrations of NaOH as well as water only at the elevated temperatures. Four test loops were developed at FIU allowing for the aging of HIHTL as well as dog bone specimens utilizing 6.25%, 12.5% and 25% NaOH and water only at 170°F. This report explains the design, component selection and fabrication of the four test loops.

Subtask 19.2: Objectives

In order to reinforce the findings from the previous phase of testing, HIHTL coupons as was well as EPDM material coupons are used to run additional aging experiments. FIU engineers worked with Hanford personnel to develop the new experimental combinations utilizing sodium hydroxide at concentrations of 6.25%, 12.5% and 25% at 170°F as well as water only at 170°F. Comparing the results of this testing with previous data will provide a better understanding of how the elevated temperature and the sodium hydroxide affect the material properties of the components.

Subtask 19.2: Methodology

In order to perform this research, four aging test loops had to be designed and fabricated utilizing sodium hydroxide at concentrations of 6.25%, 12.5% and 25% at 170°F as well as water only at 170°F as the circulating solution.

Test loop design

Figure 102 shows a schematic of a single aging loop. The main loop components include the pump, pressure transducer, storage tank with heater, flowmeter and thermocouple. In order to withstand the 170°F circulating solutions, each loop was fabricated using schedule 80 CPVC pipe.
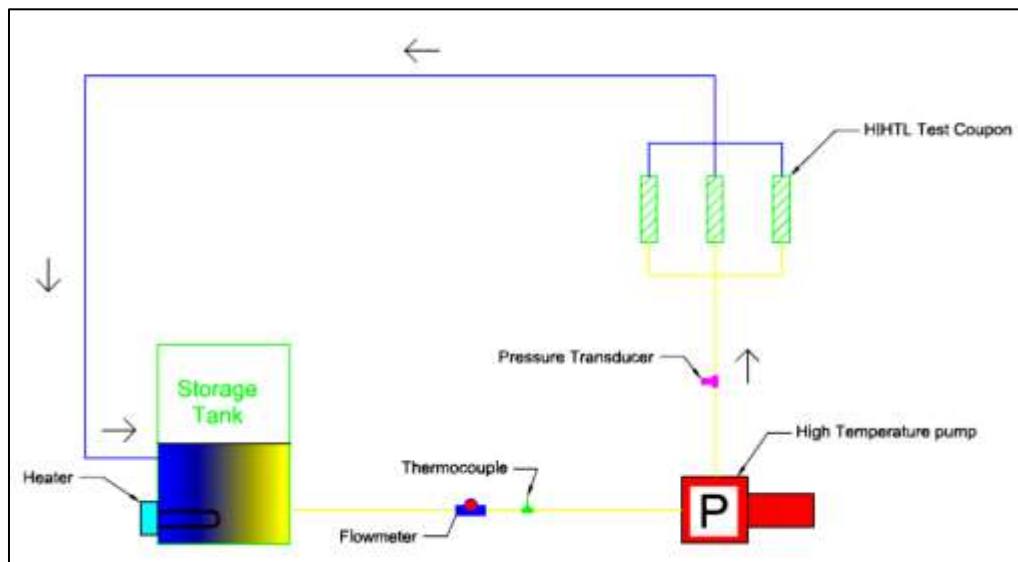
Figure 102. Aging loop schematic.

Primary loop components

During the previous phase of testing, magnetic-drive centrifugal pumps were used that had a chemical resistant plastic body. The plastic body did not withstand the synergetic effects of NaOH at high temperature. This resulted in numerous pump failures during the aging phase. During this phase of testing, FIU decided not to use the same type of pumps and wanted to use a stainless-steel magnetic-drive pump, however it was cost prohibitive. A Finish Thompson AC4 stainless steel pump with a mechanical seal (Figure 103) was then selected for the next phase of testing.

Figure 103. Finish Thompson AC4 stainless steel pump.

Some of the instrumentation elements included a Dwyer model 628CR-08-GH-P1-E1-S1-NIST pressure transducer, which has been proven to withstand the anticipated harsh conditions. In order to maintain the solution temperature at 170°F, a thermostatically controlled immersion heater is installed in each tank. A 1500-watt 120-volt immersion heater with an Incoloy heating element was chosen for the testing. To measure and record the solution flow rate, a model FPR207-PC from Omega Engineering was selected. It has a stainless-steel body that can withstand temperatures up to 225°F with an accuracy of ±1 GPM.

Figure 104. Dwyer pressure transducer, thermostatically controlled immersion heater and flow meter.

The solution temperature is monitored via a thermocouple. Thermocouple model number KQIN-18U-12 from Omega Engineering was selected for the testing. It is a K type thermocouple with a Inconel® 600 sheath. Finally, a 30-gallon 304 stainless-steel drum was selected as the storage tank in order to withstand the hot caustic solution.

Loop fabrication

After receipt of all the components, loop fabrication commenced. Figure 105 shows three of the system's four pumps and tanks with the heaters installed.

Figure 105. Three of the system's four pumps and tanks with heaters installed.

Figure 106 shows the four test loops. Each loop is fabricated from schedule 80 CPVC pipe and contains a set of three hose specimens. There are three sets in the front and one in the right rear. The tank in the front is for the water-only ageing loop. Figure 107 shows the three tanks that will contain the sodium hydroxide solution which are located in the fume hood.

Figure 106. The four ageing loops, three in the front and one in right rear.

Figure 107. Sodium hydroxide tanks.

Sample preparation

In addition to the HIHTL coupons, a total of 24 dog bone specimens were cut out of a sheet of EPBM material (Figure 108). Six specimens were placed in each of the four ageing vessels (Figure 109). An ageing vessel was placed in each loop's storage tank and aged for the same one-year duration as the hose specimens in the same fluid used to age the hose specimens.

Figure 108. Dog bone cut from a sheet of EPDM.

Figure 109. Dog bone aging vessel.

Data collection

A LabVIEW code was written to collect the data from the four loops. Data collected includes the flowrate, pressure, and the temperature. Figure 110 shows the interface screen of the LabVIEW data acquisition program that was written.
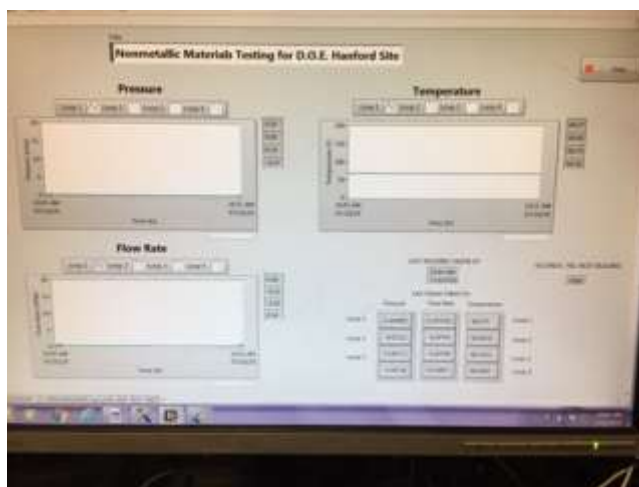
Figure 110. LabVIEW interface screen.

Specimen aging

During the debugging and calibration of the system using only water, a few minor leaks were discovered and repaired. Once the system was debugged and calibrated, the four loops were drained and refilled with 25%, 12.5%, 6.25% sodium hydroxide solution, and water respectively. The aging of the specimens commenced with all four loops operating at 170°F. After operating for approximately two weeks, the flow meters on loops 1 and 2 (25% and 12.5% NaOH, respectively) developed leaks from around their sight glass. All the loops were shut down and the leaks was repaired with a silicone sealant.

Figure 111. Leaking flowmeter (left), repaired flow meter with silicone sealant.

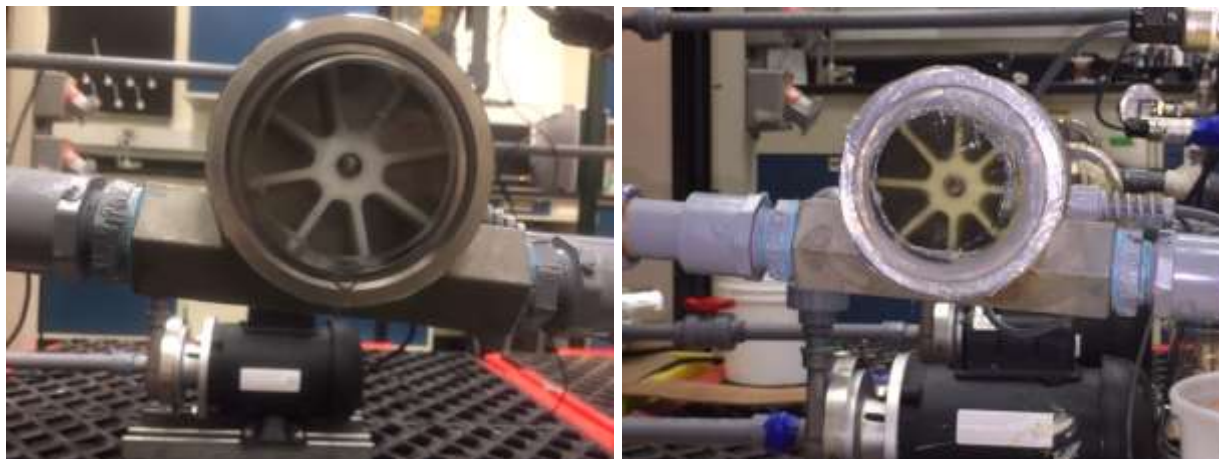After allowing 24 hours for the silicone to cure, all the loops were again restarted and allowed to heat up. After approximately a week of running, the flowmeters on loops 1 and 2 began to leak again. It was decided that since we are measuring the flow pressure in the loop and the exact flow rate was not required for the ageing process, the two leaking flowmeters were removed from loops 1 and 2. Figure 112 shows loop 1 and loop 2 with the flowmeters removed (the loop 3 flowmeter in the background of loop 2). It is believed that the reason the flowmeter on loop 3 has not leaked is because the fluid running in it has a low concentration of NaOH. The concentration of loop 3 is 6.25% NaOH while loops 1 and 2 have concentrations of 25% and 12.5% NaOH, respectively.
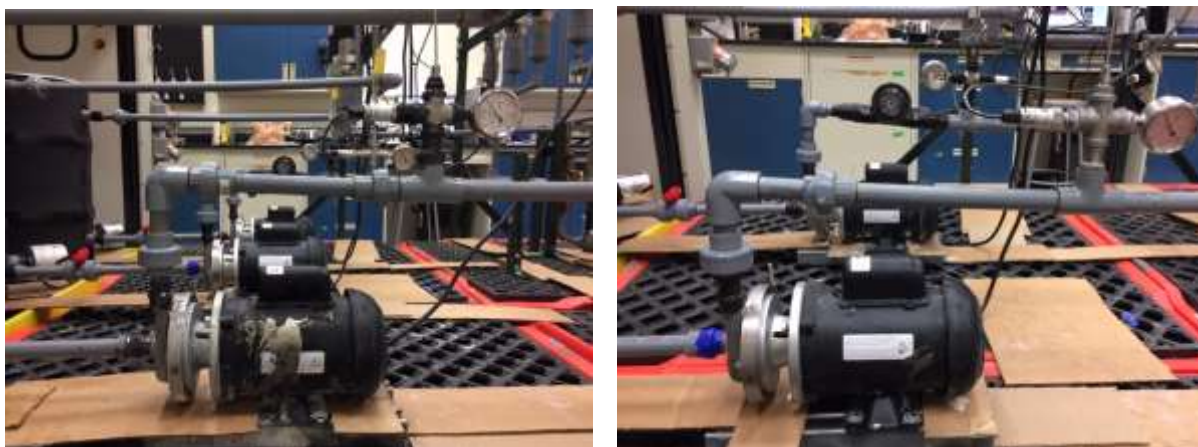

Figure 112. Loop 1 (left) and loop 2 (right) with the flowmeter removed.

After running the loops for approximately two months, a leak developed in the pumps of the three loops circulating NaOH (Figure 113). The leaks appeared to be coming from the mechanical seals on the pumps. After a few days, the leaks appeared to have stopped and the loops continued to run. However, on the afternoon of Labor Day, the pump on loop 3 stopped. After investigating the cause, it was determined that the NaOH had started leaking again and had leaked into the motor of the pump and shorted it out. The following day FIU contacted the manufacturer and advised them of the problem with the pumps. The manufacturer asked FIU to ship them the failed pump in order to examine it and determine the cause of the failure. After examining the pump, the manufacturer determined that the pumps' mechanical seal had failed due to crystal formation that occurs when the NaOH is allowed to cool in the pump. Since the original mechanical seal is comprised of a

carbon and ceramic faces, the NaOH crystal's abrasive properties damage the seal faces. They recommended replacing the seals with ones that have silicon carbide faces that would be able to withstand the abrasion from the crystals longer. The manufacturer agreed to replace the seal with the silicon carbide seal on the pump that was sent to them, as well as replace the shorted-out motor at no cost. FIU did however procure two additional silicon carbide seals for the remaining two pumps and replaced them.

Figure 113. Pump leaking from seal.

FIU repaired the remaining two pumps with the failed mechanical seals. The remaining pumps included pump #1 and pump #2 that circulate 25% and 12.5% NaOH solutions, respectively. Figure 114 shows the backplate of pump #2 where crystalized NaOH can be seen from the location where the mechanical seal resides and where the pump mates up to the motor. In Figure 115, the motor of pump #2 can be seen with its faceplate covered with the crystalized NaOH residue.

Figure 114. Pump #2 backplate showing leakage from mechanical seal location (Seal removed).

Figure 115. Pump #2 motor.

After cleaning the motor, it was observed the NaOH solution had eroded the face of the motor and entered into the motor winding (Figure 116). The motor was bench tested and determined that it was damaged beyond repair. A new motor was ordered to replace the damaged one.

Figure 116. Motor face with eroded hole.

The mechanical seal from pump #2 was cleaned and examined, as can be seen from Figure 117, the white ceramic half of the carbon-ceramic seal had a groove worn into it. Since both surfaces need to be perfectly smooth to seal, this is believed to be the cause of the leak. The same observation was made on the seal of pump #1.

Figure 117. Mechanical seal from pump #2.

After both seals were replaced with a silicon carbide seals and a new motor was installed on pump #2, all four loops were started again, and the aging of the specimens continued.

Subtask 19.2: Conclusions

The pump seal failure on the pumps circulating the NaOH solution was a lesson learned for both FIU as well as the pump manufacturer. Neither party was aware of the issue with crystal formation when NaOH is allowed to cool in a pump. The silicone carbide seals appear to be working and FIU has implemented a policy were the pumps are not shut down unless there is no other option to repair a leak. If the pumps shutdown, it is planned in a way to minimize the pump downtime.

The next phase of testing will include burst and tensile strength testing of the HIHTL specimens and material dog bones that are currently being aged.

Subtask 19.2: References

1. H Brush, C. O. (2013). Test Plan for the Irradiation of Nonmetallic Materials. Albuquerque, New Mexico: Sandia National Laboratories.

2. Lieberman, P. (2004). Banded (Band-It) and Swaged Hose-In-Hose (HIHTL) Assembly Service Life Verification Program. Santa Clarita, California: National Technical Systems.

ACKNOWLEDGEMENTS

CONFERENCE PARTICIPATION, PUBLICATIONS & AWARDS

Peer-reviewed publications

A. Awwad, D. McDaniel, L. Lagos, B. Tansel, "Effects of temperature and exposure duration on nonmetallic components used in caustic liquid waste transfer lines", *Process Safety and Environmental Protection* (submitted 10/20).

Tashakori, S., Abrahao, A., Martin, D., Lagos, L., McDaniel, D., "Miniature Rover for the Inspection of the Hanford High-Level Waste Double Shell Tanks" (In preparation).

Oral presentations (presenter is underlined)

A. Awwad, J. Rivera, D. McDaniel, "Accelerated Aging and Evaluation of Hose-In-Hose Transfer Lines in the Hanford Waste Transfer System - 20312", Proceedings of the Waste Management Symposia 2020, Phoenix, AZ, March 8-12 2020.

A. Aravelli , D. McDaniel, M. Thompson, K. Imrich, B. Wiersma, "Erosion-Corrosion Detection in Carbon Steel Pipe Loops using SRNLs Thickness and Mass Loss Measurement Coupons – 20464", Proceedings of the Waste Management Symposia 2020, Phoenix, AZ, March 8-12 2020.

A. Abrahao, S. Tashakori, C. Excellent, P. Uriarte, D. Martin, L. Lagos, D. McDaniel, "Inspection Tools for Hanford Tanks and Waste Transport Systems - 204", Proceedings of the Waste Management Symposia 2020, Phoenix, AZ, March 8-12 2020.

Poster presentations (presenter is underlined)

A. Baharanchi, E. Nina, D. McDaniel, M. Poirier, "Development of a Testbed for Pipeline Flushing-20425", Proceedings of the Waste Management Symposia 2020, Phoenix, AZ, March 8-12 2020.

M. Boan, A. Abreu, L. Lagos, D. McDaniel, "Aging of Concrete for the Evaluation of Repair Materials to Protect the Walls of the HCAEX Tunnel at Savannah River – 20301", Proceedings of the Waste Management Symposia 2020, Phoenix, AZ, March 8-12 2020.

WM Student Posters

Anilegna Nunez Abreu: Accelerated Aging of Concrete for the Evaluation of Coatings to Protect the HCAEX Tunnel at the Savannah River Site (20588)

Christopher Excellent: Development of a Crawler for the Inspection of the Secondary Liners of The Double Shell Tanks at Hanford (20580)

Daniel Martin: Deployment Updates for Miniature Inspection Tool for Double Shell Tanks at Hanford Site (20583)

Jason Soto: Robotic Mapping and Monitoring of Nuclear Infrastructure (20581)

<u>Jeff Natividad</u>: Robotic System for the Application of Coatings in the Savannah River Site H-Canyon Exhaust Tunnel (20579)

<u>Michael Thompson</u>: Ultrasonic and Fiber Optic Sensors for Pipeline Fault Detection in Hazardous Environments (20586)

Student awards

WM Undergraduate Student Poster Competition

1st Place: Anilegna Nunez Abreu "Accelerated Aging of Concrete for the Evaluation of Coatings to Protect the HCAEX Tunnel at the Savannah River Site"

DOE Fellows Poster Exhibition and Competition

Session I (Undergraduate posters):

2nd Place: Anilegna Nunez Abreu "Accelerated Aging of Concrete for the Evaluation of Coatings to Protect the HCAEX Tunnel at the Savannah River Site"

1st Place: Christopher Excellent "Development of a Crawler for the Inspection of the secondary liners of The Double shell tanks at Hanford"

Session II (Graduate posters):

1st Place: Michael Thompson "Advanced Fiber Optic and Ultrasonic Sensor Systems for Structural Health Monitoring of Pipes in Nuclear Waste Sites"

APPENDIX

The following documents are available at the DOE Research website for the Cooperative Agreement between the U.S. Department of Energy Office of Environmental Management and the Applied Research Center at Florida International University: https://doeresearch.fiu.edu

FIU Year 10 Annual Research Review Presentations:

1. FIU Research Review - Project 1
2. FIU Research Review - Project 2
3. FIU Research Review - Project 3 - DnD
4. FIU Research Review - Project 3 - IT
5. FIU Research Review - Project 4 - 5
6. FIU Research Review - Project 4 - DOE Fellow Derek Gabaldon
7. FIU Research Review - Project 4 - DOE Fellow Gisselle Gutierrez-Zuniga
8. FIU Research Review - Project 4 - DOE Fellow Aurelien Meray
9. FIU Research Review - Project 4 - DOE Fellow Jeff Navidad
10. FIU Research Review - Project 4 - DOE Fellow Silvina De Pietro
11. FIU Research Review - Project 5 - DOE Fellow Olivia Bustillo
12. FIU Research Review - Project 5 - DOE Fellow Eduardo Rojas
13. FIU Research Review - Wrap Up - Project 1
14. FIU Research Review - Wrap Up - Project 2
15. FIU Research Review - Wrap Up - Project 3 - DnD
16. FIU Research Review - Wrap Up - Project 3 - IT
17. FIU Research Review - Wrap Up - Project 4 - 5

In addition, the following documents have been uploaded to OSTI.gov:

Date Submitted to OSTI (mm/dd/yyyy)	OSTI ID	*STI PRODUCT TITLE:	Publication/ Issue Date
09/09/2020	1658912	PROJECT TECHNICAL PLAN - Project 1: Chemical Process Alternatives for Radioactive Waste	12/13/2019
09/09/2020	1658920	Literature Review of Adhesion Mechanisms For Mobile Platforms	4/10/2020
09/15/2020	1660375	Summary of Testing for the Miniature Rover with Integrated UT Sensor	7/24/2020
09/15/2020	1660379	Initial Testing for the H-Canyon Study	8/14/2020
09/15/2020	1660434	FIU PROJECT 1: Chemical Process Alternatives for Radioactive Waste	8/25/2020
09/15/2020	1660389	PROJECT TECHNICAL PLAN - Project 2: Environmental Remediation Science & Technology	12/13/2019

09/15/2020	1660396	FIU PROJECT 2: Environmental Remediation Science & Technology	8/25/2020
09/16/2020	1660534	PROJECT TECHNICAL PLAN - Project 3: Waste and D&D Engineering and Technology Development	12/13/2019
09/16/2020	1660535	EXPERIMENTAL DESIGN: Quantifying / Certifying the Effects of Radiological Fixating Materials & Technologies ISO Source Term Calculations and Open Air Demolition	1/31/2020
09/16/2020	1660536	FIU PROJECT 3: Waste and D&D Engineering and Technology Development	8/25/2020
09/16/2020	1660539	PROJECT TECHNICAL PLAN - Project 4: DOE-FIU Science and Technology Workforce Development Program	12/13/2019
09/16/2020	1660538	Subtle Process Anomalies Detection using Machine Learning Methods	12/20/2019
09/16/2020	1660543	Neptunium (IV) Diffusion through Bentonite Clay	12/20/2019
09/16/2020	1660544	Amplicon Sequencing Assessment to Measure Microbial Community Response from Heavy Metal Contaminated Soils in Savannah River Site, Tims Branch Watershed	12/20/2019
09/16/2020	1660714	An Assessment of Long-Term Monitoring Strategies and Developing Technologies	12/20/2019
09/16/2020	1660717	Mechanical Properties Permanent Foaming Fixatives for D&D Activities	12/20/2019
09/16/2020	1660721	Contributing to the DOE EM 4.1 and 4.12, Office of Groundwater and Subsurface Closure	12/20/2019
09/17/2020	1660918	Double Shelled Tank Visual Inspections	12/20/2019
09/17/2020	1660919	H-6bR Water density Stratification Investigation	12/20/2019
09/17/2020	1660921	2D Dam-Break Analysis of L Lake and PAR Pond Dams Using HEC-RAS	12/20/2019
09/17/2020	1660922	Plutonium Migration from Estuary Sediments (Ravenglass, UK)	12/20/2019
09/17/2020	1660923	FIU PROJECTS 4 & 5: DOE-FIU Science and Technology Workforce Development Program	8/25/2020
09/17/2020	1660925	PROJECT TECHNICAL PLAN - Project 5: DOE-FIU Science and Technology Workforce Development Initiative for Office of Legacy Management (NEW)	12/13/2019

09/17/2020	1660926	DOE-FIU Science and Technology Workforce Development Initiative for Office of Legacy Management	4/30/2020
09/18/2020	1661159	Biotic dissolution of autunite under anaerobic conditions: effect of bicarbonates and Shewanella oneidensis MR1 microbial activity.	Environmental Geochemistry and Health/12/19/2019. https://doi.org/10.1007/s10653-019-00480-7